

Table of Contents

Abstract.....	i
Résumé	iv
Acknowledgements	vii
Table of Contents	ix
List of Figures.....	xii
List of Tables.....	xiv
List of symbols and abbreviations.....	xv
CHAPTER 1 INTRODUCTION.....	1
1.1 Background.....	1
1.2 Statement of the problem.....	4
1.3 Objectives.....	5
1.4 Methodology	5
1.5 Scope.....	6
CHAPTER 2 LITERATURE REVIEW.....	8
2.1 The carbon anode.....	8
2.2 Anode raw materials	9
2.2.1 Coke.....	9
2.2.2 Butts.....	9
2.2.3 Recycled anodes	9
2.2.4 Pitch.....	10
2.3 Impurities in coke and anode	10
2.4 Different methods to estimate Fe, Ni, and V	11
2.4.1 Inductively Coupled Plasma Spectrometry.....	11
2.4.2 X-ray Fluorescence Spectroscopy (XRF).....	12
2.4.3 Colorimetric determination of Fe, Ni, and V.....	12
2.5 Anode properties	19
2.5.1 Density	19

2.5.2	Electrical resistivity	20
2.5.3	CO ₂ /air reactivity	20
2.6	The influence of impurities on CO ₂ and air reactivities.....	23
2.7	Artificial network analysis (ANN).....	27
CHAPTER 3	EXPERIMENTAL SET-UP AND TEST PROCEDURES.....	29
3.1	Materials used	30
3.2	Colorimetric reactions.....	31
3.3	Equipment used.....	32
3.3.1	Datacolor Check II.....	32
3.3.2	Custom set-up using a webcam.....	34
3.3.3	Electrophoresis set-up.....	35
3.3.4	Thermogravimetric analyzer for reactivity measurements	35
3.4	Development of calorimetric methods.....	35
3.4.1	Development of colorimetric methods for the estimation of Fe, Ni, and V in anode samples	35
3.4.2	Study of the effect of impurities on the reactivities of anodes	39
3.4.3	Artificial Neural Network modelling.....	43
CHAPTER 4	RESULTS AND DISCUSSIONS	45
4.1	Development of colorimetric methods for the estimation of Fe, Ni, and V in anode samples.....	45
4.1.1	Identification of conditions for the reaction between the impurity and the reagent using Datacolor	45
4.1.2	Measurement of change in color components using the custom-made set-up with the webcam	47
4.2	Study of the effect of impurity content on anode reactivities	60
4.2.1	Characterization of the green anodes	60
4.2.2	Characterization of cylindrical anode samples used for reactivity studies	61
4.2.3	Reactivities of different anode samples	62
4.2.4	Effect of different impurities on anode reactivities	67
4.3	Results of ANN.....	71

4.3.1 The effect of iron (Fe) concentration on air and CO ₂ reactivities (V, Ni, and S maintained at their typical levels).....	72
4.3.2 The effect of vanadium (V) concentration on air and CO ₂ reactivities (Fe, Ni, and S were maintained at their typical levels).....	74
4.3.3 The effect of nickel (Ni) concentration on air and CO ₂ reactivities (Fe, V, and S were maintained at their typical levels).....	76
4.3.4 The effect of sulfur (S) concentration on air and CO ₂ reactivities (Fe, V, and Ni were maintained at their typical levels).....	78
4.3.5 Remarks	80
CHAPTER 5 CONCLUSIONS AND RECOMMENDATIONS.....	81
5.1 Conclusions.....	81
5.2 Recommendations.....	82
REFERENCES	84
Appendix	95

List of Figures

Figure 2.1. A schematic view of an electrolysis cell with a prebaked anode [1]	8
Figure 2.2. (a) Anode temperature distribution and reactivities in a reduction cell [1, 16], (b) Dust formation during the reaction of air/CO ₂ with anode [53].	23
Figure 2.3. (a) CO ₂ and (b) air reactivities of coke as a function of nickel and sulfur contents [5]	24
Figure 2.4. CO ₂ reactivity of coke as a function of vanadium and sulfur contents [5].	26
Figure 3.1. Summary of the methodology	30
Figure 3.2. Datacolor CheckII	33
Figure 3.3. CIELab color system	33
Figure 3.4. Custom set-up using a webcam	34
Figure 3.5. (a) Core positions in laboratory anodes, (b) Position of samples used for the reactivity tests in anode cores.	42
Figure 4.1. Color components measured with Datacolor during the reaction of 500 ppm pure iron with potassium thiocyanate	46
Figure 4.2. Change in “L” with respect to iron concentration at 300 s	47
Figure 4.3. Change in color components with respect to time for 500 ppm pure iron solution	48
Figure 4.4. Change in color components with respect to concentration of iron solution at 300 s.....	49
Figure 4.5. Colorimetric determination of Fe in anode sample	50
Figure 4.6. Calibration curve for iron concentration measurement determined by the colorimetric method (using electrophoresis and image analysis).....	51
Figure 4.7. Color produced by the reaction of iron with potassium thiocyanate.....	52
Figure 4.8. Calibration curve for iron concentration measurement determined by the colorimetric method (using aqua regia and image analysis) and its validation	53
Figure 4.9. Color produced by the reaction of vanadium with N-benzoyl-N- phenylhydroxylamine	55

Figure 4.10. Calibration curve for vanadium concentration measurement determined using the colorimetric method (aqua regia and image analysis) and its validation.....	56
Figure 4.11. Color produced by the reaction of nickel with dimethylglyoxime.....	57
Figure 4.12. Calibration curve for nickel concentration measurement determined using the colorimetric method (aqua regia, electrophoresis, and image analysis) and its validation ..	58
Figure 4.13. Effect of BAD on CO ₂ reactivity	64
Figure 4.14. Effect of BAD on air reactivity	66
Figure 4.15. CO ₂ and air reactivities of anode samples containing different concentrations of iron.....	68
Figure 4.16. CO ₂ and air reactivities of anode samples containing different concentrations of vanadium	69
Figure 4.17. CO ₂ and air reactivities of anode samples containing different concentrations of nickel	70
Figure 4.18. The effect of iron concentration on air reactivity with different BADs (V, Ni and S were maintained at their typical levels).....	73
Figure 4.19. The effect of iron concentration on CO ₂ reactivity for different BAD (V, Ni, and S were maintained at their typical levels).....	74
Figure 4.20. The effect of vanadium concentration on air reactivity for different BAD (Fe, Ni, and S were maintained at their typical levels).....	75
Figure 4.21. The effect of vanadium concentration on CO ₂ reactivity for different BAD (Fe, Ni, and S were maintained at their typical levels).....	76
Figure 4.22. The effect of nickel concentration on air reactivity for different BAD (Fe, V, and S were maintained at their typical levels).....	77
Figure 4.23. The effect of nickel concentration on CO ₂ reactivity for different BAD (Fe, V, and S were maintained at their typical levels).....	78
Figure 4.24. The effect of sulfur concentration on air reactivity for different BAD (Fe, V and Ni were maintained at their typical levels)	79
Figure 4.25. The effect of sulfur concentration on CO ₂ reactivity for different BAD (Fe, V and Ni were maintained at their typical levels)	80

List of Tables

Table 2.1. Anode impurities [1].....	11
Table 3.1. Samples used for calibration.....	38
Table 3.2. Samples used for validation.....	38
Table 3.3. Percentages of impurities in the six cokes (small size fraction) measured by XRF	39
Table 3.4. Addition of impurities in the ten anodes produced with Coke (6)	40
Table 4.1. Comparison of results obtained by XRF and colorimetry for iron.....	53
Table 4.2. Analysis of coke and anode samples	54
Table 4.3. Comparison of results obtained by XRF and colorimetry for vanadium.....	56
Table 4.4. Analysis of coke and anode samples	57
Table 4.5. Comparison of results obtained by XRF and colorimetry for nickel.....	59
Table 4.6. Analysis of coke and anode samples	59
Table 4.7. Properties of green anodes: (a) anodes produced with different cokes, (b) anodes produced with Coke (6) with addition of impurities.....	60
Table 4.8. Green and baked density of cylindrical samples ($\phi 50 \times 130$ mm) taken from the anodes	62
Table 4.9. CO ₂ reactivity results of anode samples ($\phi 50 \times 50$ mm sample cut from Core 1)	63
Table 4.10. Air reactivity results of anode samples ($\phi 50 \times 50$ mm sample cut from Core 3)	65

List of symbols and abbreviations

V	Volume (cm ³)
I	Current (A)
D	Density (g/cm ³)
GAD	Green anode density (g/cm ³)
BAD	Baked anode density (g/cm ³)
GER	Electrical resistivity of green anode ($\mu\Omega\cdot\text{m}$)
BER	Electrical resistivity of baked anode ($\mu\Omega\cdot\text{m}$)
S	Standard conditions

CHAPTER 1

INTRODUCTION

1.1 Background

The University of Quebec at Chicoutimi/Aluminerie Alouette Inc. (UQAC/AAI) Research Chair on Carbon, under the leadership of Prof. Duygu Kocaefe, has undertaken a research program on the improvement of the quality of carbon anodes used in the production of primary aluminum. The research, in general, focuses on the production of anodes with high density, low electrical resistivity, and low reactivity as well as the effect of the quality of raw materials, granulometry, and all relevant process parameters [1] on anode properties. This project focuses on the detection of metallic impurities (V, Ni, Fe) in coke and carbon anodes and their effect on anode reactivity.

Prebaked carbon anodes are used in the electrolytic alumina reduction process to produce primary aluminum. Prebaked carbon anodes usually consist of approximately 85 % dry aggregates (about 65 % petroleum coke, 20 % recycled anodes and butts) and 15 % coal tar pitch (binder). The production of anodes involves the mixing of raw materials and the compaction of the resulting paste to produce green anodes. These green anodes are baked in furnaces to produce baked anodes with appropriate properties.

During the production of aluminum by the electrolytic reduction of alumina, carbon anodes are consumed according to the following reaction:



CO₂ further reacts with the anode carbon to produce CO. Air also reacts with the exposed anode surface to produce CO₂. These reactions increase anode consumption. Excess carbon consumption due to air burn (air reactivity) and carboxy attack (CO₂ reactivity) increases the cost of aluminum production.

Reaction of oxygen on the exposed surface of the anode (air reactivity) is given by the following equation:



Reaction of CO₂ with the anode carbon (CO₂ reactivity) is given as:



As a result, the excess consumption of carbon increases CO₂ and CO (greenhouse gases) emissions as well as the cost of aluminum production, decreasing the productivity. The excess consumption also depends on the anode recipe and different impurities present in the anode. Usually low electrical resistance, low permeability, low reactivity, high density, high mechanical strength, and high thermal shock resistance are the basic requirements of good quality anodes [1].

Iron, nickel, and vanadium are the common metallic impurities in anodes. The sources of impurities in anodes are the raw materials of the anode. The sources of iron are coke, butts as well as pitch. Vanadium and nickel usually comes from the coke. The source of iron, nickel, and vanadium in coke can come from the crude petroleum and the catalytic processes in the petroleum refinery. Cast iron used in the anode stub holes are the source of iron in the anode butts. These impurities are transition metals and can catalyze the air and CO₂ reactivities. They can bind with a variety of ligands and can form colored complexes.

Due to the presence of partially filled “d” orbitals, the transition metals can form colored compounds.

There are different sophisticated methods for the estimation of impurities in anode materials [2-4]. These methods require costly instruments, ultra-pure reagents, highly trained personnel, and laborious sample preparation. Industries are in need of a simple, fast, and reliable method to estimate the concentrations of impurities in anode raw materials. Colorimetric methods can fulfill the requirement of the industry. Colorimetric determination of different chemical species is based on the color analysis of the product produced by the reaction of the impurity with a reagent. The focus of the project is on the colorimetric detection and the qualitative estimation of the impurities (V, Ni, Fe) in coke and carbon anodes, and their effect on the anode reactivities. There are a large number of colorimetric methods available, which use different reagents for the determination of transition metal impurities (V, Ni, Fe), but these methods have not been applied to cokes and anodes. It is difficult to apply the existing colorimetric methods to estimate Fe, V, and Ni in coke and anodes as these impurities remain bound to the carbon along with other elements, and the color of carbon is black. In this study, methods were developed to extract the impurities in the form of a clear solution from the carbon materials and to analyze their concentrations using the existing colorimetric methods. The methods developed during this investigation are rapid. The knowledge on the impurity level can help understand the effect of each impurity as well as their combinations on anode reactivity. Therefore, the colorimetric methods can be used as tools in choosing or rejecting raw materials.

In order to achieve the goals of this research project, the concentrations of impurities (V, Ni, Fe) were determined with different colorimetric methods. It is well known that the transition elements like V, Ni, and Fe can form colored complexes with chelating compounds. Once the color is formed, a digital-camera (with a custom-made image analysis software) or the Datacolor equipment was used to analyze the color. The method is simple, quick, repeatable, and environment-friendly. The air and CO₂ reactivities of the anode samples, with different levels of V, Ni, and Fe, were studied. The experimental results were analyzed to understand the effect of different impurities on the CO₂ and air reactivities of the anode samples. In addition, an artificial neural network model was used to analyse and clarify the trends.

1.2 Statement of the problem

Some of the common impurities found in cokes and anodes are transition metals such as vanadium (V), nickel (Ni), iron (Fe), etc. They affect the air/CO₂ reactivity of anodes in the electrolytic cell during aluminum production; consequently, they increase the anode consumption, emission of greenhouse gases, and the energy consumption and thus decrease the productivity. Generally, these impurities are analyzed by inductively-coupled plasma spectroscopy-optical emission spectroscopy (ICP-OES), inductively-coupled plasma spectroscopy-atomic emission spectroscopy (ICP-AES), inductively-coupled plasma mass spectroscopy (ICP-MS), X-ray fluorescence spectroscopy (XRF), atomic absorption spectroscopy (AAS), x-ray photoelectron spectroscopy (XPS), and combustion techniques. However, all these methods are costly and require a lot of time, precision instruments, and well-trained operators. Thus, the industry is in need of developing new

techniques that are easy to apply, rapid, and economical to determine the level of impurities in carbon materials. It is also important for the industry to understand the effect of different impurities on anode reactivities to control the quality of anodes in spite of the variations in the properties of raw materials. The density and electrical resistivity of the anode samples influence the reactivities. However, the anodes are always nonhomogeneous, and this affects the anode properties. Thus, the density and the resistivity of the samples were also measured to see if the anode quality remained relatively similar during the tests.

1.3 Objectives

The global objective of the project is to develop a simple, quick, and inexpensive method for the quantification of Ni, V, and Fe (transition metals) present in coke, butt particles, dry aggregates, and anodes as well as to study the effect of different impurities on anode reactivity.

The specific objectives are:

- a. to estimate the level of different impurities (V, Ni, and Fe) in carbon materials using colorimetric methods;
- b. to reduce the time for sample preparation and measurement;
- c. to facilitate the implementation of the method in an industrial environment;
- d. to study the effect of V, Ni, and Fe on the air and CO₂ reactivities of anodes.

1.4 Methodology

In this study, colorimetric methods were developed to determine the level of impurities (Fe, V, Ni) in cokes and anodes. In this method, the metallic impurities were

extracted from the carbon sample by acids and/or electrophoresis. The solution of the extracted metal was treated with a reagent to produce a color. The picture of the colored solution in a plastic container was taken using a camera, and the color of the picture was analyzed after a certain time with a custom-made image analysis software. A calibration curve was prepared by plotting a color component (red, green or blue) as a function of the known concentration (measured by XRF) of the impurity. The calibration curve was later used to determine the concentration of the metallic impurity of a sample with an unknown concentration. The method was validated in the presence of interfering ions.

Two sets of anodes were produced. In one set, the amount of one impurity (Fe, Ni, and V) was changed for the same coke. In the other set, the anodes were fabricated using cokes with different impurity contents. The green anodes were baked under conditions similar to those typically used in industry. The properties of the green and baked anodes were measured (density, electrical resistivity for both anodes; air and CO₂ reactivities for baked anodes). The experimental results were analyzed in order to determine the effects of the impurities on the reactivities of anodes. Also, an artificial neural network (ANN) model was used to complete the analysis.

1.5 Scope

The thesis contains five chapters and one appendix. Chapter 1 introduces the general subject, the background, the statement of the problem, the objectives and the scope.

Chapter 2 presents the previous works reported on colorimetric estimation of metallic impurities and the effects of the impurities on coke and anode properties.

Chapter 3 provides information on the chemical reagents, the methodology, and chemical reactions taking place during the experiments. It also gives a description of the equipment used for the determination of color. The development of the colorimetric method is also described in this chapter.

Chapter 4 presents the results and discussion of the determination of metallic impurities and the effect of impurity contents on anode and coke samples. The results of the investigation of the laboratory anode properties (density, air/CO₂ reactivities, and electrical resistivity) are given. In this section, the results for two sets of anodes were presented. In one set, the amount of one impurity was changed for the same coke by adding different chemicals to that coke. In the other set, cokes with different impurity contents were used. Anodes were prepared for both sets and the properties of these anodes were measured. In addition, the artificial neural network (ANN) method was used in order to study the intricate relationship between impurities and anode reactivities using the results of all anode samples. The main ANN results are presented in this chapter. The rest of the results are given in appendix.

Chapter 5 gives the conclusions of the current study and the recommendations for future work.

CHAPTER 2

LITERATURE REVIEW

2.1 The carbon anode

The production of aluminum is carried out in the electrolytic cells. Alumina (Al_2O_3) is dissolved in a bath of molten cryolite (Na_3AlF_6) at approximately 960°C , and aluminum (produced through the electrolysis of alumina) is collected on the cathode below the bath (see Figure 2.1). Carbon anodes, immersed in the molten electrolyte, are used in the reduction process and thus are consumed during the electrolysis. This electrolytic process is represented by the following reaction:

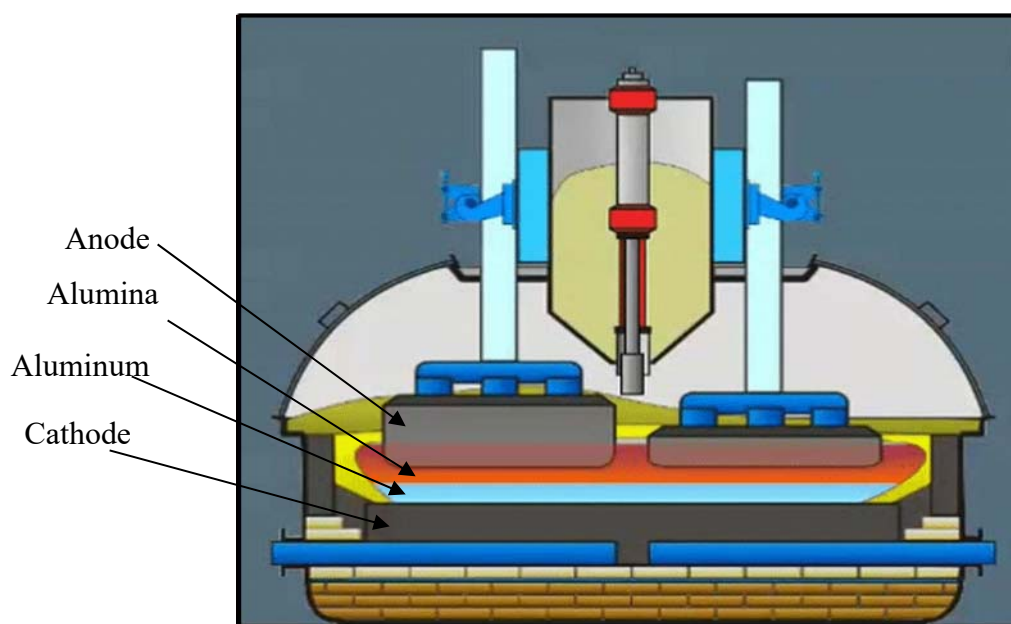


Figure 2.1. A schematic view of an electrolysis cell with a prebaked anode [1]

A carbon anode consists of approximately 65% petroleum coke, 15 % coal tar pitch, and 20% recycled anodes and butts. Coal tar pitch is produced as a byproduct during the metallurgical coke production [1].

In spite of various practical and economic constraints, the overall objective of the industry is to determine the appropriate conditions to produce carbon anodes with a high density, low CO₂ and air reactivities, and a low electrical resistivity.

2.2 Anode raw materials

2.2.1 Coke

One of the raw materials of carbon anodes is calcined petroleum coke, which is produced from the heavy residual fractions of crude oil. The source of crude oil, processes within the refinery, and calcination conditions determine its quality and composition. The calcined coke contains different impurities such as sulfur and metals including Ni, V, and Fe. In recent years, the impurity content of the coke has increased [1].

2.2.2 Butts

Butts are the remaining section of the anode after electrolysis. They contain large amounts of sodium coming from the electrolytic bath. Butts are cleaned and recycled [1].

2.2.3 Recycled anodes

Recycled anodes are usually generated from start-up and shutdown operations, process variations and reject formed during anode manufacturing. Green recycled anodes can have different pitch contents. The baked recycled anode is usually processed with the butt fraction [1].

2.2.4 Pitch

The role of binder pitch is to cover the coke particle surface, penetrate into the pores, and fill the void space between the particles. During baking, pitch carbonizes and binds the particles together. Good wetting of coke by pitch helps better coat and bind coke particles and improves the filling of the pores. Pitch is obtained as a residue during the distillation of coal tar in a coke oven at about 1100 °C. The chemical compounds in pitch have a broad molecular weight distribution [1].

2.3 Impurities in coke and anode

The impurities present in raw materials, especially in petroleum coke and coal tar pitch used for anode production, influence significantly the reactivity of carbon anodes. Petroleum coke is produced from heavy residual fractions of crude oil. Iron, nickel, vanadium, and other impurities become concentrated in these heavy fractions. Coal tar pitch does not contain any nickel or vanadium. It is found that vanadium present in heavy petroleum product diffuses inside the pores of the petroleum coke during heat treatment. Vanadium is found in the pores as V_2O_3 whereas nickel stays in the metallic form [2]. Typical concentrations of metallic impurities in anodes are presented in Table 2.1.

Table 2.1. Anode impurities [1]

Elements	Units	Typical Range	Typical 2 σ Range
Sulphur (S)	%	0.5-3.2	0.1-0.8
Vanadium (V)	ppm	30-320	10-60
Nickel (Ni)	ppm	40-200	10-40
Silicon (Si)	ppm	50-300	100-400
Iron (Fe)	ppm	100-500	100-500
Aluminum (Al)	ppm	150-600	100-600
Sodium (Na)	ppm	150-600	100-800
Calcium (Ca)	ppm	50-200	50-100
Potassium (K)	ppm	5-30	5-10
Magnesium (Mg)	ppm	10-50	10-30
Fluorine (F)	ppm	150-600	100-500
Chlorine (Cl)	ppm	10-50	10-20
Zinc (Zn)	ppm	10-50	10-20
Lead (Pb)	ppm	10-50	10-20

2.4 Different methods to estimate Fe, Ni, and V

2.4.1 Inductively Coupled Plasma Spectrometry

Inductively Coupled Plasma Mass Spectrometry (ICP-MS) is widely used in the determination of impurities in crude oil, fuel oil, naphtha, residual oil, asphalt, and coke. The method is also used in the analysis of monomers, natural gas, and oil products [5]. Another report describes the determination of vanadium in petroleum and petroleum products using ICP-MS techniques [6]. Inductively Coupled Plasma Atomic Emission Spectroscopy (ICP-AES) was used to measure the catalytic performance of NiMo catalysts supported on tailored activated carbon (AC) [7].

2.4.2 X-ray Fluorescence Spectroscopy (XRF)

Verma [8] described the application of X-ray Fluorescence (XRF) technique in the fields of industry, medicine, biology, environmental studies, archaeology, and geology. Atomic Absorption Spectrometry (AAS)

Some researchers used atomic fluorescence spectrometry as a standard method for Hg determination in green coke and oily sludge samples [9]. Atomic adsorption spectrometric analysis (AAS) was used to characterize monometallic oil-soluble Mo or Ni catalyst [10].

2.4.3 Colorimetric determination of Fe, Ni, and V

Colorimetric analysis carried out using a smartphone camera was reported in the literature [11-15]. These studies show the possibility of using a high-resolution camera to determine the quantity of phosphorus, chlorine, and methamphetamine. Moonrungsee et al. [11] found that the ambient light intensity seriously affected the color of a picture. The results were more precise in the cabinet using a single LED light. An analysis based on red (R), green (G), blue (B) [11, 14, 15], and intensity [14, 15] values of color showed good correlations with the results obtained by sophisticated techniques. Published articles demonstrated the potential for the development of accurate, rapid, quantitative, and real-time determination methods using the digital camera of smartphone [14, 15].

It was reported that Matlab software can be used to analyse the R, G, B values for the colorimetric determination of iron content. The results showed greater accuracy compared to UV-visible spectrophotometry [16].

As can be seen from the above literature review, even though articles have been published on the determination of transition metal content using colorimetric methods in a number of fields, no study was found on the application of such methods to carbon anodes or carbon materials.

a) Colorimetric determination of nickel

Gazda et al. [17] reported a method for the estimation of nickel using dimethylglyoxime. The reagent formed a pink colored complex and precipitated as colored sediment on the surface of an extraction membrane and was analyzed by diffused reflectance spectroscopy.

Chilton [18] reported the colorimetric determination of nickel by complexation with diethyldithiocarbamates. He found that it is easier to extract the metal-diethyldithiocarbamate complex from slightly basic solution. The efficiency of the extraction process was reduced in the presence of ammonium ions. He suggested that sodium carbonate is a better choice instead of ammonium hydroxide to make the solution alkaline.

Lingane and Kerlinger [19] and Flora and Nieboer [20] reported a polarographic method using dimethylglyoxime for the estimation of nickel. Tartarotti et al. [21] reported a method for the estimation of nickel in ethanol using an electrode modified with carbon paste containing dimethylglyoxime. It was found that 1-nitroso-2-naphthol is effective for both nickel and iron. It acts as a color-forming chelating reagent and forms complexes which are sparingly soluble in water. The stability and the amount of the complex formed

can be improved by adjusting the pH level. Adjusting pH to a certain value or adding masking agents such as NH_3 or oxalate can reduce the interfering effects of other ions [14].

b) Colorimetric determination of iron

Different researchers used the colorimetric method for the estimation of iron. Muir and Andersen [15] developed such a method for the determination of ferrous iron in a copper-process metallurgical solution using o-phenanthroline as the chromogenic agent.

Braunschweig et al. [16] compared the use of ferrozine and o-phenanthroline reagents for the colorimetric estimation of iron in geomicrobiological studies. He compared the results with those obtained using ICP-AES. The results obtained using o-phenanthroline was more accurate compared to that for ferrozine. Saywell and Cunningham [22] used an o-phenanthroline method for a quick and reliable determination of iron (5-20 ppm) in plant tissues and their extracts. He mentioned that this method can also work for the analysis of inorganic substances such as industrial products and dilute salt solutions. The presence of copper, aluminum, and magnesium did not affect the accuracy of the measurement within a certain range of concentrations.

Baumann [23] published a method for the determination of relative amounts of Fe^{2+} and Fe^{3+} in glass. He dissolved the glass sample with a sulfuric acid-hydrofluoric acid mixture. Ammonium metavanadate was used to preserve the Fe^{3+} ions. At pH 5, magenta Fe II–Ferrozine complex was formed to estimate Fe^{2+} . Fe^{2+} content was determined from the absorbance at 562 nm, and the total Fe was determined from the absorbance of the same solution after ascorbic acid was added to reduce Fe^{3+} to Fe^{2+} . Kitson [24] used a spectrophotometric technique for the estimation of iron using thiocyanate-acetone which

formed a colored complex. The method was simple, rapid, and free of interferences. Beyer et al. [25] described a combination of DC and AC polarographic methods for the estimation of iron. Van den Berg et al. [26] used cathodic stripping voltammetry for the determination of iron using hanging mercury drop electrode.

Fe^{2+} was estimated spectrophotometrically in flow-injection systems [27-30] using 1,10-phenanthroline as the chromogenic reagent [31]. Ascorbic acid was used to reduce Fe^{3+} and the total iron content was estimated [32,33] using 1,10-phenanthroline. The method could measure total iron in the range of 0.1-30 mgL^{-1} . Dieker and Linden [30] measured Fe^{2+} and Fe^{3+} in rock samples by a flow injection system using an amperometric detector. Another report published the use of a spectrophotometric method to determine the quantity of Fe^{2+} and Fe^{3+} by synchronized sample injection into two parallel flow systems [34-36]. They used 1, 10-phenanthroline and thiocyanate as chromogenic agents to determine the iron content [28]. Some researchers [29] used a similar system, but they used the same detector for two parallel flow systems. The system described above has been applied to the simultaneous determination of species that does not produce color at the same rate [30]. Masoom and Townshend developed a similar method for the simultaneous enzymatic determination of sucrose and glucose [34].

Apilux et al. [35] developed a lab-on-paper device combining electrochemical and colorimetric detection for the quick determination of Au and Fe contents. The limit of this detection (LOD) of the proposed method was 1 ppm. The results were in line with those obtained from ICP-AES.

Kawakubo [36] developed a simple on-site technique for the colorimetric determination of chromium, iron, and copper in electroplating bath solutions. He used a portable colorimeter (containing red-green-blue light emitting diode) to measure the absorbance. Copper and iron amounts were determined from the chelating form of Cu(I)-bathocuproindisulfonate and Fe(III)-thiocyanate, respectively. Analytical results agreed with those obtained by AAS.

Usually, iron exists with other ions. It was reported that EDTA is effective to reduce the influence of other impurities on iron. Goto et al. [37] published a rapid photometric method for the estimation of manganese content in presence of iron using formaldoxime. Formaldoxime worked as a colorimetric agent to develop color with manganese. The iron formaldoxime formation was controlled by adding EDTA and hydroxylamine.

Another effective way to eliminate the interference is to control the pH values. Yun and Choi [14] described a colorimetric method for the estimation of iron, nickel, and cobalt quantity using 1-nitroso-2-naphthol to form chelating complexes. The effect of other ions was eliminated by controlling the pH. A colorimetric method for the estimation of Fe³⁺ content under physiological pH conditions (pH 7.0) [38] using 4-(4-hydroxy-1-naphthylazo) benzenesulfonic acid (HNABA) has been reported. The color of the solution varied from brick red to light red and was stable under acidic or neutral conditions. Under these pH conditions, there was less effect of the solvent and the coexisting metal ions.

c) Colorimetric determination of vanadium

There are also numerous colorimetric methods to determine the vanadium content. It may be noted that vanadium is always present together with other ions.

HCl is an appropriate chemical to extract vanadium from coke and anode. It is reported that a minimum of 10 ppm of vanadium can be detected with a few drops of concentrated sulfuric acid and one drop of sodium metavanadate solution [39] by a spot test. Sulfuric acid can also be used to extract impurities from coke and anode when developing quantitative methods for the determination of impurities.

Dispersive liquid-liquid microextraction (DLLME)-digital colorimetry (DC) was used to determine trace amount of vanadium in water. N-benzoyl-N-phenylhydroxylamine was used as chromogenic agent, and ethanol and chloroform were used as dispersive solvent and extractant to test vanadium in an acidic environment. This produced a purplish red chelate complex. The picture of the color was taken by a digital camera [40] and analyzed. This method involved less time and lower cost than those required for XPS, AAS, XRF, etc. In addition, it was rapid and highly sensitive. This method has not been used with cokes and anodes.

The first use of N-benzoyl-N-phenylhydroxylamine (BPHA) was reported by Bamberger [41]. He used this reagent to estimate copper, iron, aluminum, and titanium contents. Shome [42] also used the same reagent, and it produced orange-red color sediments with vanadate ions. The sediments were hardly soluble in organic solvents such as ethanol and acetic acid. It is possible to determine vanadium content using this reagent because the chelate complex produced stays in the colloidal state and does not pass through the filter paper easily. Thus, it can easily be separated. It was reported that in the absence of air, the chelating complexes would not be formed and there would be no color. In an open environment, it was easy to form the colored chelate complex. It was revealed from

different experiments that BPHA is a chelating ligand that preferably reacts with V^{5+} compared to V^{4+} [43].

Priyadarshini and Tandon [44] also adopted BPHA as a highly specific reagent for vanadium. It was found that, under strongly acidic conditions, vanadium formed a deep violet water-insoluble chelating complex. Chloroform was used to extract the violet chelating complexes, and then the extracts were used for the spectrophotometric estimation of vanadium quantity. This method could also be used for anodes to eliminate the effect of the interfering ions. A report was published which described a fast and sensitive determination method for vanadium. Less than $0.06 \mu\text{g}$ of total vanadium was collected from airborne particles in a filter bag attached to an air sampler. This method utilized nitric, sulfuric, and perchloric acids to dissolve the samples, then decompose the suspended silicate residue in a sulfuric-hydrofluoric acid mixture, followed by the addition of BPHA to form a vanadium-N-benzoyl-N-phenylhydroxylamine complex. Later, chloroform was used to extract the complex for spectrophotometric measurement [45].

As a reagent, the advantage of BPHA is that it is easy to handle and sensitive to vanadium for its colorimetric estimation. It is possible to preserve BPHA for a long time. Even if there was interferences of cobalt and copper, it was possible to estimate vanadium content quite efficiently [43].

To eliminate the interference of other ions with vanadium, Sandell [46] used a colorimetric method to separate vanadium from chromium using 8-hydroxyquinoline and chloroform. Vanadium was first reacted with 8-hydroxyquinoline in neutral or slightly acidic solutions and then it was extracted using chloroform.

Belitskus and Danka [47] obtained the correlation between the reactivity of cokes and the vanadium content of coke.

2.5 Anode properties

Two types of anodes (Soderberg and prebaked) are used in the electrolytic cells [1]. Raw material is continuously fed when Soderberg anode is used, and this produces lots of volatile gases containing PAH (polycyclic aromatic hydrocarbons). On the other hand, prebaked anodes need to be replaced at regular time intervals. The advantage of prebaked anodes is that they are compacted and it is easy to maintain their quality (compared to Soderberg anodes). This leads to lower carbon consumption as well as makes it easier to control the fumes produced during the baking of anodes [1]. Due to technical and environmental reasons, prebaked anodes are commonly used in the aluminum reduction process, especially in modern smelters. High density and consistent quality anodes are important in the electrolytic process.

2.5.1 Density

Typical industrial anodes have a green density (GAD) in the range of 1.55-1.65 g/cm³, a baked density (BAD) between 1.50-1.60 g/cm³, and a baking loss or volatile loss of around 4.5-6 % during baking [1, 48].

Low baked density implies high porosity which leads to low mechanical strength, high elasticity, low thermal conductivity, and high permeability [1, 48]. It is well known that high gas permeability results in high anode consumption. Thus, high porosity increases the air and CO₂ reactivities and the electrical resistivity [1, 48].

High baked density reduces air permeability and extends anode life [1, 48]. However, extremely high density leads to thermal shock problem. The optimum baked density depends on the raw materials, aggregate granulometry, mixing and forming conditions, process parameters, and pitch content.

Anode quality improves when the baked anode density stays in the optimal range. Apparent density of anode samples (cores) are measured using the ASTM D5502-00 standard [49].

2.5.2 Electrical resistivity

High electrical resistivity results in high energy consumption and reduces efficiency and economy of the electrolytic process. Typical industrial anodes have electrical resistivities of around 50-60 $\mu\Omega\cdot\text{m}$ [1, 48]. The electrical resistivity of baked anodes is much lower compared to that of green anodes. A decrease in electrical resistivity of a baked anode results in an increase in its thermal conductivity. However, too high a thermal conductivity increases the anode surface temperature, causing excess carbon consumption (air-burn, dust formation) [1, 48]. The electrical resistivity is related to both anode density and cracks in the anode. Denser anodes have fewer cracks and thus lower electrical resistivity as dense anodes contain low porosity. The ASTM D6120-97 standard is used to measure the electrical resistivity of anode samples (cores) [50].

2.5.3 CO₂/air reactivity

During the production of aluminium by the electrolytic reduction of alumina, carbon anodes are predominantly consumed according to Equation (1-1) [1, 48]. A certain quantity of CO is also produced when CO₂ further reacts with anode carbon; this increases anode

consumption. Also, air diffuses through the alumina layer covering the top of the anode and reacts with the carbon anode; this is another cause of anode over-consumption. Excess carbon consumption occurs due to (a) air burn (air reactivity); (b) carboxy attack (CO_2 reactivity); and (c) dusting (selective oxidation). These are also grouped into chemical consumption and physical consumption. In chemical consumption, air and CO_2 react with the anode, and carbon is consumed due to the reaction [1, 48]. During physical consumption, a part of the coke or pitch detaches from the anode and falls into the electrolytic cell. The inherent cause of physical consumption can be due to the deterioration of anode structure since air/ CO_2 gases react with carbonized pitch and coke present in anode to different extents. This reactivity imbalance weakens the structure, and the physical loss of carbonized pitch and coke occurs. This process is called dusting.

Air reactivity depends on the permeability and the porosity of anode and is favored at temperatures above $450\text{ }^\circ\text{C}$. It is reported that the air reactivity is reduced with increasing calcination temperature of coke [51]. Reaction of oxygen on the anode surfaces exposed to air is called air burn (see Equation 1.2).

CO_2 reactivity is also permeability-dependent (permeability is intimately linked to porosity) and favoured at bath temperatures of $950\text{-}970\text{ }^\circ\text{C}$ [51]. Permeability is an index that indicates the ease with which a fluid flows through a porous solid [52]. This also explains the importance of the effect of porosity on the reactivities [1]. Reaction of CO_2 with the anode carbon (also called carboxy attack) is given by equation 1.3.

As a result, the excess consumption of carbon increases the cost of aluminum production as well as the CO_2 and CO (greenhouse gas) emissions. The excess

consumption is also dependent on the chemical composition and the structure of raw materials used in the anode production as well as the anode production parameters and the baking conditions [1, 48].

Figure 2.2 (a) shows the temperature distribution in a relatively new anode in the electrolysis cell and the regions where air and CO₂ reactions take place. The CO₂ reactivity is selective and reacts with carbon atoms in reactive sites [51]. The CO₂ bubbles produced according to the reaction 1.1 can increase the resistance between the anode and the electrolyte. Diffusion of the gas into the anode body can lead to an internal reaction occurring in the pores. Raw material properties, production process, pitch content, and baking parameters are the important factors that can have an influence on the gas permeability of the carbon anode; and this, in turn, has an impact on anode reactivity [1, 53]. Figure 2.2 (b) shows dust formation during air/CO₂ reactivity [51]. Researchers have [1, 14] studied the subsurface carboxy reactivity and used macroscopic analysis of anode butts to confirm that internal attack is selective, and air and CO₂ preferentially attack the regions of pitch-coke and coke fines rather than the larger coke particles (Figure 2.2 (b)) [1, 48].

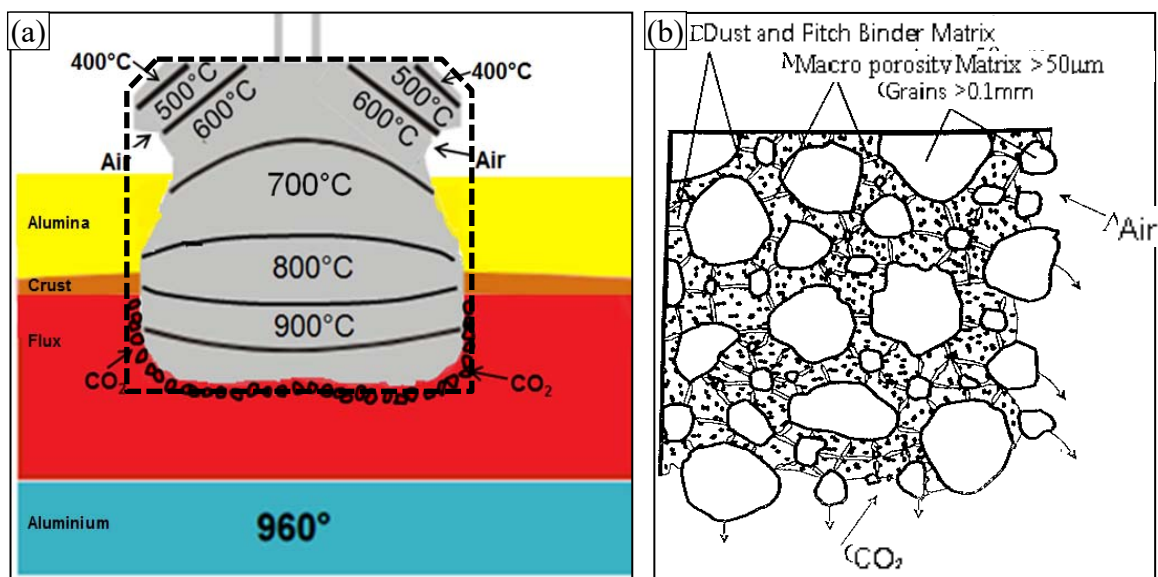


Figure 2.2. (a) Anode temperature distribution and reactivities in a reduction cell [1, 48],
 (b) Dust formation during the reaction of air/CO₂ with anode [51].

ASTM-D6558-00a [54] for CO₂ reactivity and ASTM-D6559-00a [55] for air reactivity are the standard test methods for baked carbon anode samples.

2.6 The influence of impurities on CO₂ and air reactivities

Carbon anodes contribute significantly to the cost of primary aluminum production. The oxidation of anodes by air and CO₂ causes extra carbon consumption. A study described that air and CO₂ reactivities have a medium to strong positive correlation with the level of metallic impurities such as nickel, iron, and vanadium [3].

A number of researchers found that nickel does not have any significant effect on the air and CO₂ reactivities [4]. On the other hand, some researchers reported that it can

catalyze both CO₂ and air reactivities [56-58]. In spite of the variations in the opinions of various researchers regarding the effect of nickel, they always observed that, as seen in Figure 2.3, an increase in sulfur content can reduce the effect of nickel [56, 57] in the range of nickel concentrations studied.

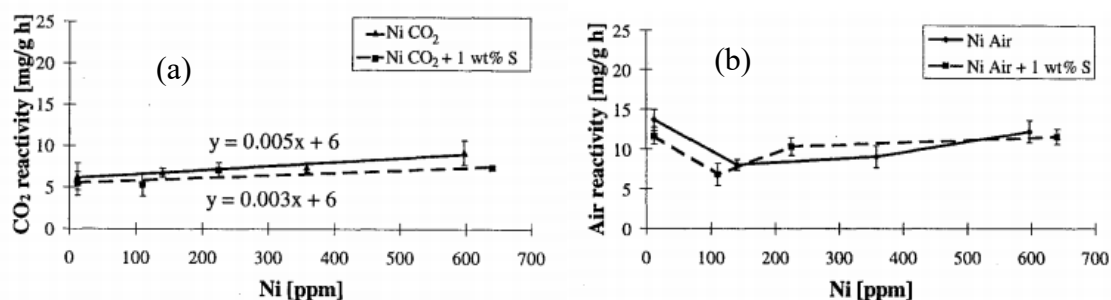


Figure 2.3. (a) CO₂ and (b) air reactivities of coke as a function of nickel and sulfur contents [56]

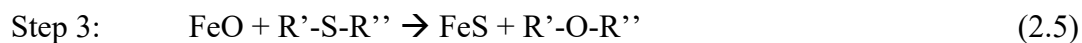
Casada et al. [4] found that nickel alone does not affect the air/CO₂ reactivities of anode, but it can increase CO₂ reactivity in the presence of butt particles [58].

It is difficult to judge the effect of nickel on anode reactivity as the nickel content of coke is highly related to the vanadium content. Recently, Nian-Bing et al. [59] found that the presence of the right amount of Ni (between (210~710 ppm) can inhibit the reactivity and reduce the mass loss rate and dusting of carbon anode by CO₂ or air reactivities. It is difficult to study the effect of nickel only due to the presence of other impurities. The conflict of different views on effects of Ni is probably due to the presence of other impurities and their quantities.

Sulfur concentration can influence the effect of nickel. In low-sulphur anodes, it was found that the CO₂ reactivity increases with increasing baking temperature [60]. The

reason for this increase is that nickel and nitrogen can form nickel nitrides and stay in anodes, and these nitrides decompose at elevated temperatures in carbon dioxide environment. In this process, nickel compounds are reduced and form metallic nickel, which may catalyze the CO₂ reactivity.

It is reported that salts of iron and coke deposits cause the corrosion and fouling of the preheater tubes of the crude oil at high temperature. This may lead to the formation of iron sulfide [61] and contaminate the petroleum coke. Sulfur compounds (such as sulfates or organic sulfur compounds) and iron can also react. The possible reactions are shown below:



where R' and R'' represent aliphatic or aromatic functional groups.

By these pathways, sulfur can reduce the effect of iron as a catalyst for air reactivity. The iron sulfide is not catalytically active during the initially, but can be converted to the active metallic state after a certain time [3].

Vanadium usually stays chemically-bonded to hydrocarbons. It is known that vanadium is not only a strong CO₂ reactivity catalyst, but also a strong air burn catalyst for carbon anodes. The vanadium content can increase the CO₂ reactivity as a catalyst, but the effect of vanadium is reduced with the increasing sulfur content (Figure 2.4) [56].

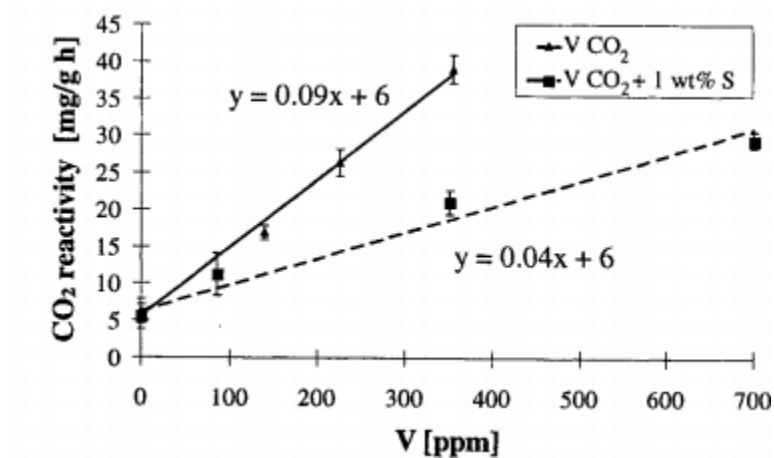


Figure 2.4. CO₂ reactivity of coke as a function of vanadium and sulfur contents [56]

It is stated in the literature that high amounts of vanadium in coke increases the air reactivity of anodes. However, the correlation for these trends is usually not good due to the difficulty of separating the effect of vanadium from other impurities present [48].

There is also one report which states that a certain amount of vanadium (480~1480 ppm) can help make better anodes, but the quality can deteriorate when more vanadium [59] is present. This finding needs to be verified.

Fukasawa et al. [45] re-calcined several coke samples to study the effect of variation in the thermal history of cokes and observed that there was an increase in the reactivity of low impurity cokes as the content of vanadium is increased. However, the sulfur content was not reported. Houston and Oye [57] found that the presence of metallic impurities can catalyze the reactivities of anodes. They stated that it is difficult to find a universal correlation between the vanadium content and the CO₂ reactivity of anodes.

The catalytic effect of the impurities (V, Ni, and Fe) can be reduced by sulfur as it can form inactive metal-sulfur complexes. At high temperatures, the effects of these

metallic impurities usually increase in the absence of sulfur. The catalytic activities of these metallic impurities are influenced by their physical state, chemical form, and type of interactions with other compounds [40].

As it can be seen from the previous works, the effect of impurities on the anode reactivity has not been well understood. There are conflicts between the results of different studies. This is most probably due to differences in the concentration of impurities other than the one being studied. The present study addresses this issue.

2.7 Artificial neural network analysis (ANN)

Artificial neural network (ANN) is an important tool in predicting the values of dependent parameters when there is no known relation that exists [62, 63]. Neural networks are inspired by biological nervous systems [64]. They are used to find patterns, to express an output parameter as a function of a number of input parameters, and to predict the value of an output parameter for a set of input parameters.

It contains different interconnected layers (input layer, hidden layers and the output layer). Construction of the artificial neural network model, training, validation and prediction of output for a desired set of input parameters are the main steps of an artificial neural network model development.

Artificial neural network models have been used in a diverse range of chemical engineering applications. In one study, it has been used to show the effect of pitch percentage and coke porosity on the CO₂ reactivity of anodes [65]. Another research used ANN to reveal that hardness increased with total alloy loading, whilst the corrosion rates

did not show any clear relationship with alloy loading. ANN results contributed to an understanding of compositional effects on the corrosion of Mg, and can predict corrosion resistance of Mg alloys [66].

Although these models were used in different fields as explained above, they were rarely applied to carbon anodes used in aluminum industry [67]. Different ANN models were developed for anodes and cokes within the frame of the UQAC/AAI Chair on carbon. [68-70] . In the current study, an ANN model is applied in order to predict the effect of metallic impurities on anode reactivity.

CHAPTER 3

EXPERIMENTAL SET-UP AND TEST PROCEDURES

The methodology is summarized in Figure 3.1. It is broadly classified into two sections: a) colorimetric estimation of iron, vanadium, and nickel contents in coke/anode samples; and b) investigation of the effect of different impurities on anode air/CO₂ reactivities.

In this project, based on the information published in the literature and some preliminary studies, methods for colorimetric analysis were developed using a web-cam to determine the concentration of metallic impurities (Fe, V, Ni). These methods have never been applied to carbonaceous materials before. The methods are fast, precise, economical, and can be used easily in industrial applications to analyse the metallic impurities. The impurities were extracted from the carbon materials by chemical reaction and electrophoresis techniques. Calibration curves were prepared using samples having known amounts of impurities. The results were validated using other samples with known impurity contents. Finally, the calibration curves were used to measure the impurity concentrations in different carbon samples for which the impurity contents were not known.

Anodes were fabricated using: a) different cokes with known amounts of impurities or b) the same coke and adding predetermined amounts of impurities. The densities and electrical resistivities of the anodes were measured. The reactivities depend on the quality of the cores. Even though all the raw materials were the same, the quality of anodes may

vary due to non-homogeneity of the raw materials. The density and resistivity measurements showed the quality of the cores. The air/CO₂ reactivities of the anode samples were measured using the standard ASTM methods. The results were analyzed to understand the effect of the impurities on anode reactivities. The artificial neural network (ANN) method was used for the analysis due to the complexity of the data.

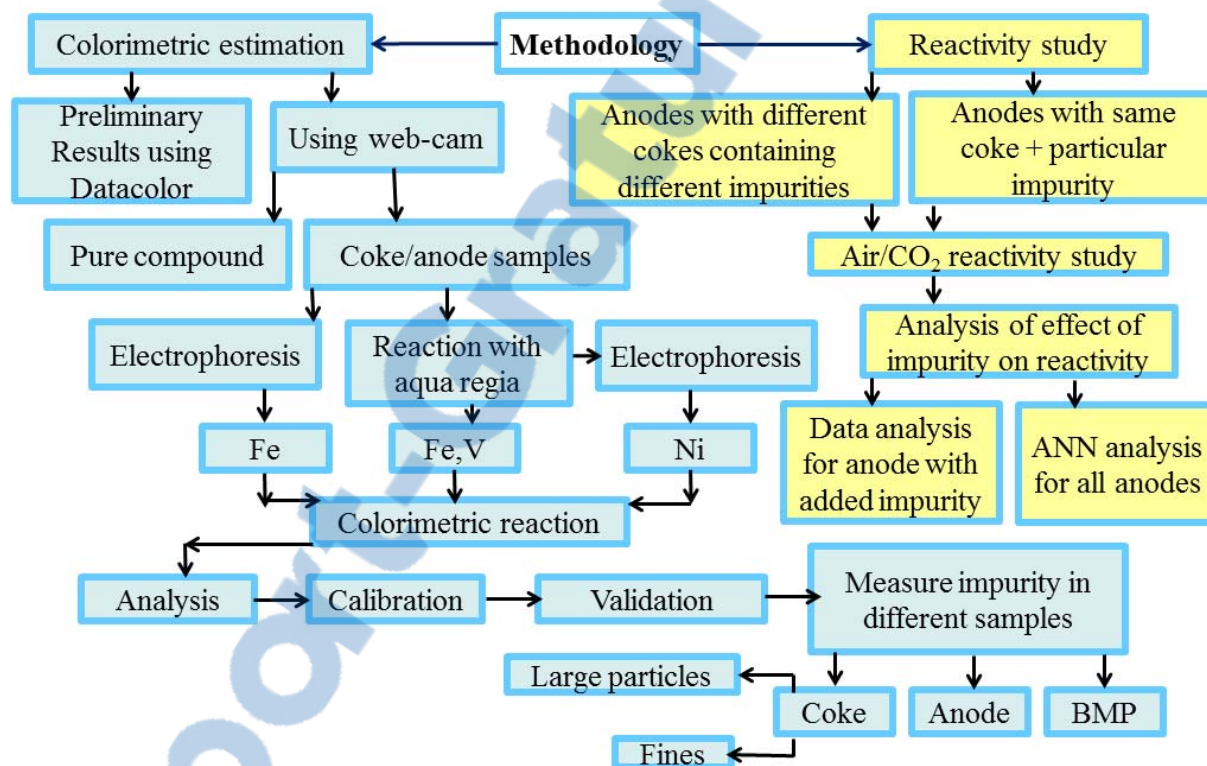


Figure 3.1. Summary of the methodology

3.1 Materials used

Colorimetric methods for the estimation of iron, nickel, and vanadium were developed using potassium thiocyanate, dimethylglyoxime, and N-benzoyl-N-phenylhydroxylamine, respectively, as reagents. The reagents form colored complexes

reacting with the transition metal ions. The methods were validated by comparing the results with the XRF measurements carried out independently using the same samples.

Two groups of anodes were produced. For the first group, six different commercially available calcined petroleum cokes of known impurity levels and a coal tar pitch were used for the fabrication of anodes. These cokes contain different amounts of a number of impurities. It is not possible to have different cokes where only the amount of one impurity is different while the others are the same. Samples from these anodes were used to study the effect of different impurities, present in different coke samples, on anode reactivities.

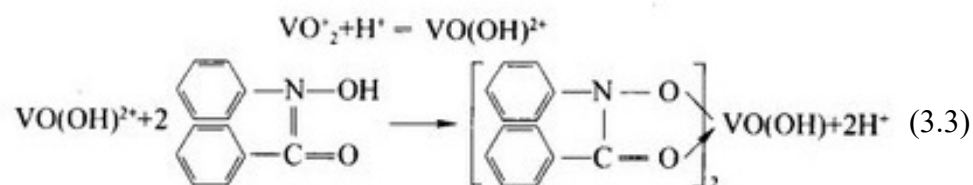
For the second group, different chemicals (impurities) were added to a particular calcined petroleum coke (one of the six cokes mentioned above), and anodes were produced to study the effect of a particular impurity on the anode reactivities. This method was used to change the level of one impurity without affecting others. The chemicals were chosen based on the possible forms of the specific impurity present in anode. Iron, nickel, and vanadium were added in the form of ferrous sulfate, nickel chloride, and vanadium chloride, respectively.

3.2 Colorimetric reactions

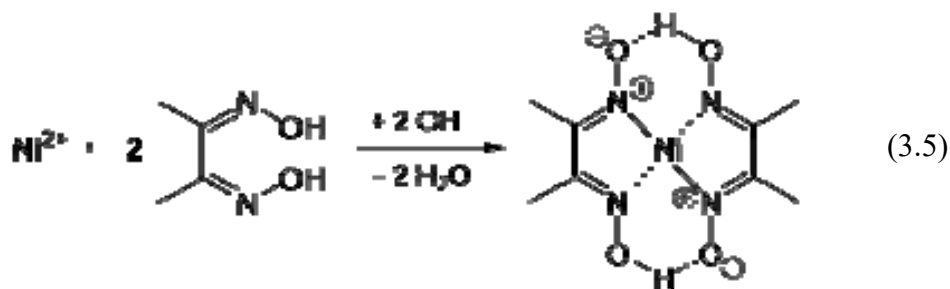
Iron salts react with potassium thiocyanate to produce ferric thiocyanate salts (Equation 3.1) under acidic conditions. Their color varies from red to reddish-brown.



Vanadium salts react with N-benzoyl-N-phenylhydroxylamine to produce a colored complex (Equation 3.2). The color of the complex varies from purple to brown depending on pH and the type of acids used.



Nickel salts react with dimethylglyoxime to produce a pink colored complex (Equation 3.4).



3.3 Equipment used

3.3.1 Datacolor Check II

It is a multi-gonio-spectrophotometer widely used to obtain the color values of solid samples (see Figure 3.2) [72]. It uses CIE Lab color system (see Figure 3.3) which is a model for the representation of surface colors adopted in 1976 by the International Commission on Illumination (CIE). The component “L” is clarity, which ranges from 0 (black) to 100 (white). The component “a” represents a range of 600 levels on the axis red

(positive value 299) to green (negative value -300). Component “b” represents a range of 600 levels on the axis yellow (positive value 299) to blue (negative value -300). The Datacolor equipment was used for the preliminary study of the colorimetric methods.



Figure 3.2. Datacolor CheckII

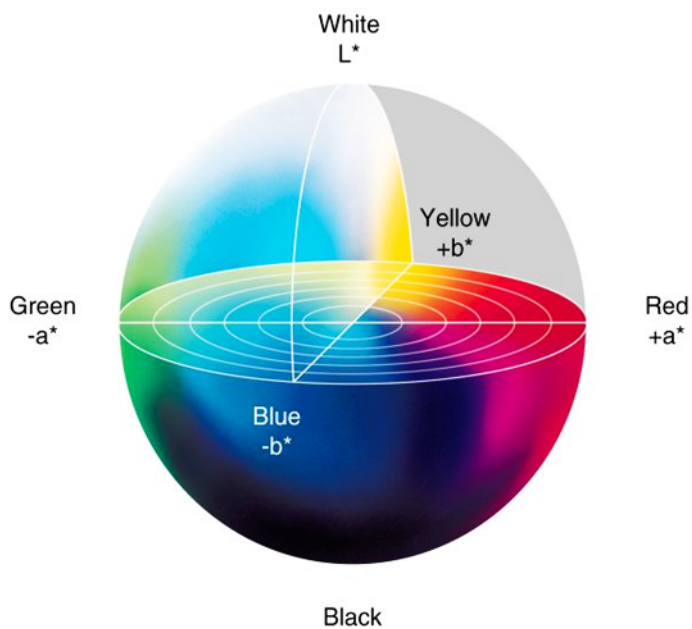


Figure 3.3. CIE Lab color system

3.3.2 Custom set-up using a webcam

A set-up was developed using a webcam (Microsoft Lifecam 3000) and a small tube light (Figure 3.4). They were placed in a box so that external lights and shadows could not interfere with the color measurements. The camera was connected to a computer, and a custom-made image analysis software was used to capture the image of the sample at a predefined time interval and to analyze the red, green, blue, and intensity components of the color of a certain region of the images. The software plotted the components of color with respect to time. This equipment was used to replace the Datacolor equipment with a low-cost version. This set-up was capable of analyzing colors of solid as well as liquid samples.

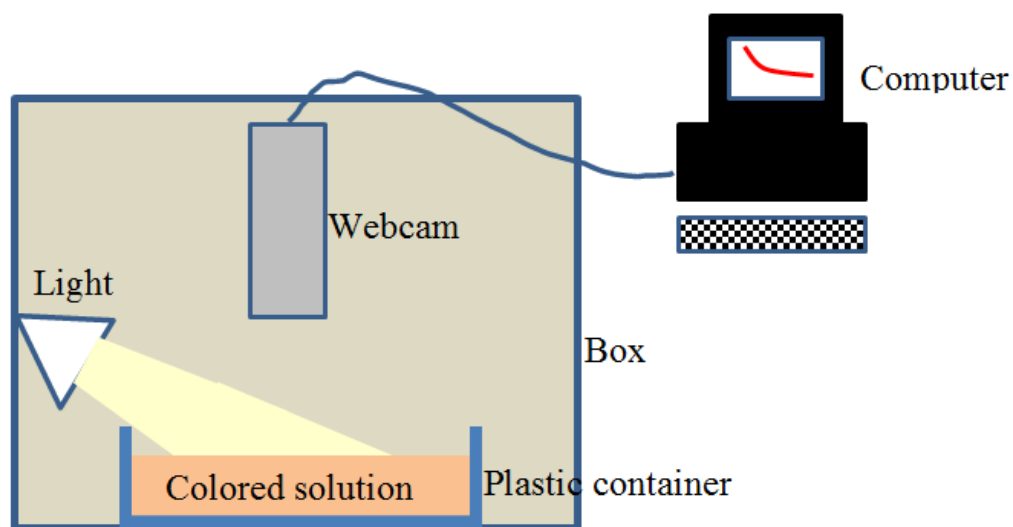


Figure 3.4. Custom set-up using a webcam

3.3.3 Electrophoresis set-up

An electrophoresis set-up was fabricated where a measured quantity of carbon samples were placed in a porous conducting container adjacent to a positive electrode. A negative electrode was placed at a distance. The system was filled with dilute HCl solution. Current was passed through the system for a certain time. The cations from the carbon materials moved to the HCl solution as they moved towards the negative electrode. This served to separate the impurities from coke or anode.

3.3.4 Thermogravimetric analyzer for reactivity measurements

Air and CO₂ reactivities of the anode samples were measured according to the standards ASTM D 6559 (at 525°C for 3 h) and ASTM D 6558 (at 960°C for 7 h), respectively, using a thermogravimetric analyzer available at the laboratory of UQAC/AAI Research Chair on Carbon. The change in weight was recorded every minute during the experiments. The dimensions and the weight of the samples were also measured before the experiment. The weight of the dust formed due to the reaction was measured at the end of each experiment.

3.4 Development of calorimetric methods

3.4.1 Development of colorimetric methods for the estimation of Fe, Ni, and V in anode samples

a) Identification of the conditions of reaction between the impurity and the reagent

A filter paper was soaked with a measured quantity of a solution containing a specific amount of reagent. A measured quantity of an aqueous solution of the impurity

(known concentration) was added on the filter paper. The colors of the filter papers were analyzed at different times (2, 5, and 10 min) using the Datacolor equipment. The “L”, “a”, and “b” values of the color were noted. The values of “L”, “a”, and “b” corresponding to different times were plotted against the concentrations of the impurities. A linear plot giving a high R^2 (close to 1) value showed which parameter (L, a, b) change can be correlated with the concentration of that impurity. It also gave an idea of the waiting time required for the color development before the analysis. The pH of the reagent solution was adjusted to generate the color without interferences caused by other impurities.

b) Measurement of the change in color components using the custom-made set-up with the webcam

A measured quantity of a reagent solution was taken in a white plastic container. Then, a measured quantity of an aqueous solution of the impurity (using pure compound) was added to the reagent solution. The change in color was monitored with respect to time. The changes in red (R), green (G), blue (B), and intensity ($0.3R+0.59G+0.11B$) of the color produced by the reaction of the pure compound containing known concentrations of the impurities were plotted. The objective was to identify the parameter that varied linearly with the concentration of the impurity. The color of the pure compounds can also influence the calibration.

The calibrations using pure compounds cannot work for carbon samples as they are black and the impurities are bound to the matrix. Thus, different methods were used to extract the impurities from coke/anode samples. These methods are:

- i) The reaction of coke/anode samples with aqua regia: The sample was treated with a measured quantity of aqua regia for a fixed time. The sample was then filtered and the filtrate was used for colorimetric analysis.
- ii) The use of electrophoresis: The coke/anode samples were placed in a porous container adjacent to the anode. The impurity cations moved to the negatively charged electrode of the electrophoresis equipment. Time needed to move the ions from the carbon matrix to the aqueous solution was determined. The solution at the cathode was used for colorimetric analysis.

These two methods were tried separately as well as in conjunction with one another.

Initially different samples were used arbitrarily to test the method. The preliminary tests were conducted for iron estimation as it is easy to see a color change. The solution containing impurities was added to the reagent solution in a plastic container. The color of the resulting mixture was analysed using the custom-made set-up. During the preliminary trials (using only electrophoresis) calibration curves were prepared with different samples (see Table 3.1). Once the final protocol has been established, a calibration curve was prepared using different carbon samples (butts, and anodes) with known concentrations of the impurities and the color values (see Table 3.1). This calibration curve was used for the estimation of an impurity of unknown concentration in a carbon sample.

Table 3.1. Samples used for calibration

Calibration for	Sample name	Type	Concentrations measured by XRF		
			Iron, ppm	Vanadium, ppm	Nickel, ppm
Iron (only electrophoresis)	Calibration (2)	Anode	300	360	170
	Calibration (3)	Anode	490	360	180
	Calibration (9)	Butt	1080	330	160
Iron (Final calibration)	Calibration (5)	Anode	50	410	190
	Calibration (2)	Anode	300	360	170
	Calibration (3)	Anode	490	360	180
Vanadium	Calibration (4)	Anode	620	310	150
	Calibration (3)	Anode	490	360	180
	Calibration (5)	Anode	50	410	190
Nickel	Calibration (6)	Anode	310	155	75
	Calibration (7)	Anode	375	190	90
	Calibration (8)	Anode	500	250	120
	Calibration (3)	Anode	490	360	180
	Calibration (1)	Anode	50	390	190

For the final method, the calibration was validated using samples with known concentrations of the impurities. These samples were not used for the calibration.

Table 3.2 lists the samples used for validation. The Fe, V, and Ni contents in these samples were also measured using XRF.

Table 3.2. Samples used for validation

Validation for	Sample name	Type	Concentrations measured by XRF		
			Iron, ppm	Vanadium, ppm	Nickel, ppm
Iron	Validation (1)	Anode	100	320	170
	Validation (2)	Anode	260	360	170
Vanadium	Validation (3)	Butt	1080	330	160
	Validation (4)	Anode	50	390	190
Nickel	Validation (1)	Anode	100	320	170
	Validation (3)	Butt	1080	330	160
	Validation (5)	Anode	620	310	150

The method was applied to measure the concentrations of different impurities (Fe, V, and Ni) in coke/anode samples.

3.4.2 Study of the effect of impurities on the reactivities of anodes

a) Fabrication of green anodes

Fresh coke (around 60% of dry aggregate), green and baked rejects of certain granulometry were preheated and mixed with a measured amount of molten pitch in a mixer. After mixing for a certain time, the paste produced was transferred to the mould of the vibrocompactor. The paste was compacted in the vibrocompactor. After cooling the mould below the softening point of pitch, the green anode was taken out of the mould.

i. Fabrication of anodes using six different cokes and one pitch using the same recipe

Six anodes were fabricated using different calcined petroleum cokes. The impurity contents in the cokes were given by the supplier. The granulometry, pitch, and fabrication conditions were kept the same. No butt particles were added. This was done to isolate the effect of the coke impurities on the reactivities of anodes. Table 3.3 lists the concentrations of different impurities in the coke samples measured with XRF.

Table 3.3. Percentages of impurities in the six cokes (small size fraction) measured by XRF

Coke Name	Anode	Nickel, ppm	Iron, ppm	Vanadium, ppm	Sulfur, %
Coke (1)	Anode (1)	184	196	217	1.82
Coke (2)	Anode (2)	189	93	301	1.91
Coke (3)	Anode (3)	176	114	368	3.55
Coke (4)	Anode (4)	190	470	506	4.79
Coke (5)	Anode (5)	163	161	426	5.42
Coke (6)	Standard	200	200	320	2.00

ii. *Fabrication of anodes using Coke (6) with the addition of different chemical compounds containing iron, nickel, and vanadium*

Ten different anodes were fabricated using the same recipe and fabrication conditions. Coke (6) was used in all of these cases. A measured amount of chemical compounds was added during the mixing phase to change the impurity level in the anode. Different impurities added to the anodes are listed in Table 3.4. The ppm levels were calculated based on the amount of coke used.

Table 3.4. Addition of impurities in the ten anodes produced with Coke (6)

Anode Name	Chemical compound added	Iron added, ppm	Vanadium added, ppm	Nickel added, ppm
Standard	-	-	-	-
Fe(1)	FeSO ₄	50	-	-
Fe(2)		150	-	-
Fe(3)		250	-	-
V(1)	VCl ₃	-	10	-
V(2)		-	20	-
V(3)		-	30	-
Ni(1)	NiCl ₂	-	-	20
Ni(2)		-	-	60
Ni(3)		-	-	100

b) *Characterization of the green anodes*

The densities and the electrical resistivities of the green anodes were measured. The volumes of the anodes were calculated with a program developed using Solidworks, which

represents the precise anode geometry. The densities were calculated by dividing the mass with the calculated volume. The electrical resistivities were measured using SERMA (Specific Electrical Resistivity Measurement of Anodes) developed by the UQAC/AAI Research Chair on Carbon.

i. Sample characterization and preparation for the study of air and CO₂ reactivities

Cylindrical samples of 50 mm diameter and 130 mm length were cored from the anodes. The density and the electrical resistivity of the samples were measured. The samples were baked in a furnace using baking conditions similar to those used in industry. The density and the electrical resistivity of the samples were again measured after baking. The aim in measuring the densities and resistivities of green and baked anode cores was to make sure that the anode quality is within the acceptable range since the anode properties also affect the reactivities. Then, samples of 50-mm height were cut for the reactivity tests. The densities of these samples were re-measured to be able to correlate better the reactivity data to the core density. The positions of the samples are shown in Figure 3.5. Core 1 and Core 3 were used for CO₂ and air reactivity tests, respectively.

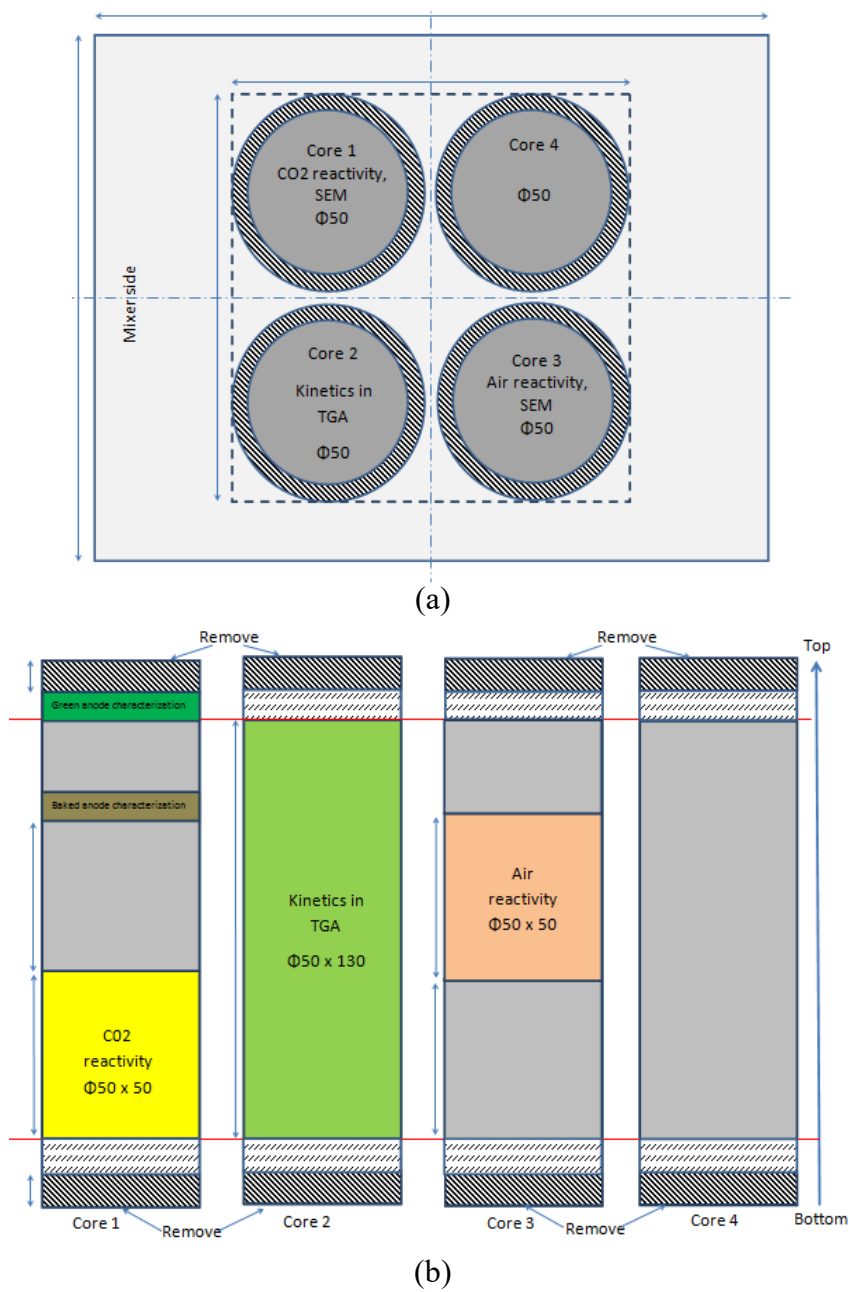


Figure 3.5. (a) Core positions in laboratory anodes, (b) Position of samples used for the reactivity tests in anode cores.



c) Air and CO₂ reactivity studies

The experiments were performed in a thermogravimetric analyzer following the ASTM standards, and the weight loss was recorded every minute. After the experiment, the amount of dust collected was also measured. The reactivities were expressed as the rate of weight loss per unit exposed surface area.

d) Analysis of the effect of different impurities on anode reactivities

The effect of different impurities on anode reactivities were studied for the anodes prepared using Coke (6) with the addition of different impurities. Ideally, the effect of the impurities can be seen if the densities of the baked samples are the same. It is difficult to have identical baked anode densities (BAD) due to the non-homogeneity of the raw materials and anodes. However, the effects can be seen, at least to some extent, by plotting the impurity content against the reactivities of the anodes.

Due to the variations of different impurities at the same time, it is difficult to study the effect of a particular impurity on reactivity for the anodes prepared using different commercial cokes. Thus, the artificial neural network (ANN) method was used to study the effect of different impurities and BAD on anode reactivities. The ANN analysis is a useful mathematical tool to study such patterns of data.

3.4.3 Artificial Neural Network modelling

The reactivities of the anode samples were predicted using artificial neural network (ANN). The basic structure of the ANN models was similar. It consisted of an input layer, a hidden layer and an output layer. Five input parameters were used: concentrations of V, Fe, Ni and S, and baked anode density. The output parameter was the air or CO₂ reactivity.

Sigmoidal and linear transfer functions were associated to the hidden layer. The models were trained by the experimental data leaving three data for validation of the final model. Feed-forward ANN with error back-propagation was used for the ANN model. The model was developed using Matlab R2015a software. Levenberg-Marquardt back-propagation algorithm was used for training, i.e., to set the values of weights and biases used in the model. Gradient descent weight and bias learning function was used for learning. Learning refers to identification of patterns in the data. The number of neurons associated to the hidden layer was adjusted by trial and error. Once the prediction of the model was found to be in the acceptable range, the effect of different input parameters on the reactivity was determined.

CHAPTER 4

RESULTS AND DISCUSSIONS

4.1 Development of colorimetric methods for the estimation of Fe, Ni, and V in anode samples

4.1.1 Identification of conditions for the reaction between the impurity and the reagent using Datacolor

Pure metal salts were used for the analysis to identify the relation between color components and impurities. In these experiments, only one impurity was present. Therefore, no interaction with other impurities was possible. Figure 4.1 shows the “L”, “a”, and “b” values measured by the Datacolor equipment corresponding to the color generated by the reaction of aqueous solution of 500 ppm ferric chloride and potassium thiocyanate solution. The reaction produced a red color. The components of the color changed with time. The “L” value changed more with respect to time compared to the change in “a” and “b” values. It also gave the highest R^2 value indicating the best correlation among the three data sets. Thus, the “L” value was used to correlate the concentration of this impurity at different times. The problem with this method was that, at low pH, the color of the filter paper changed. It was also difficult to monitor the color change continuously with time.

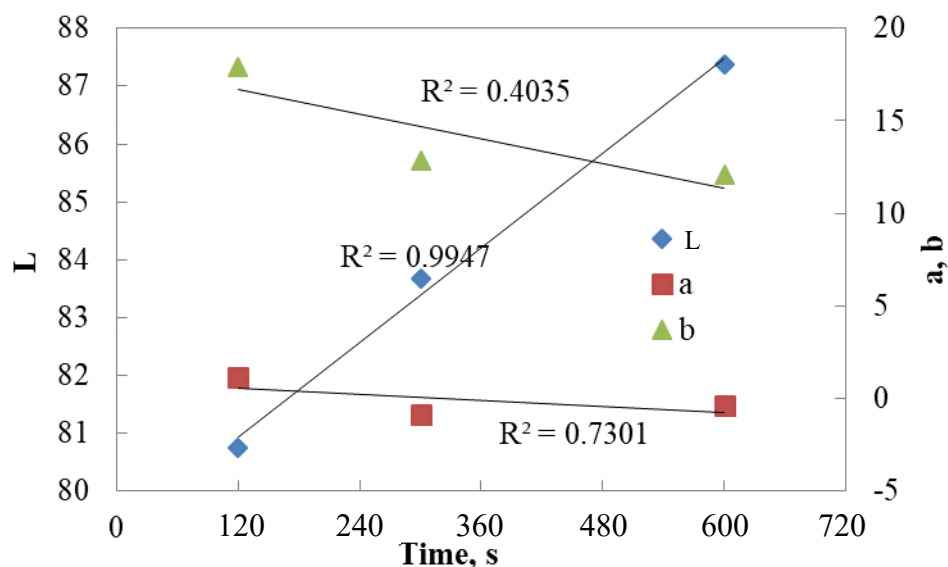


Figure 4.1. Color components measured with Datacolor during the reaction of 500 ppm pure iron with potassium thiocyanate

Figure 4.2 shows the plot of “L” value at different concentrations of iron in aqueous solution 300 s after the addition of the sample on the filter paper soaked with potassium thiocyanate solution. The “L” value decreased with increase in concentration, which shows that the color became darker with increasing concentration of iron. The plots corresponding to different times were tried. It was found that linearity of the change of “L” with concentration was the best ($R^2 = 0.9868$) at 300 s. Thus, for the following experiments, 300 s was used as the waiting time before any color measurement. The concentrations of iron (using pure iron salt) were chosen based on its level in different carbon samples.

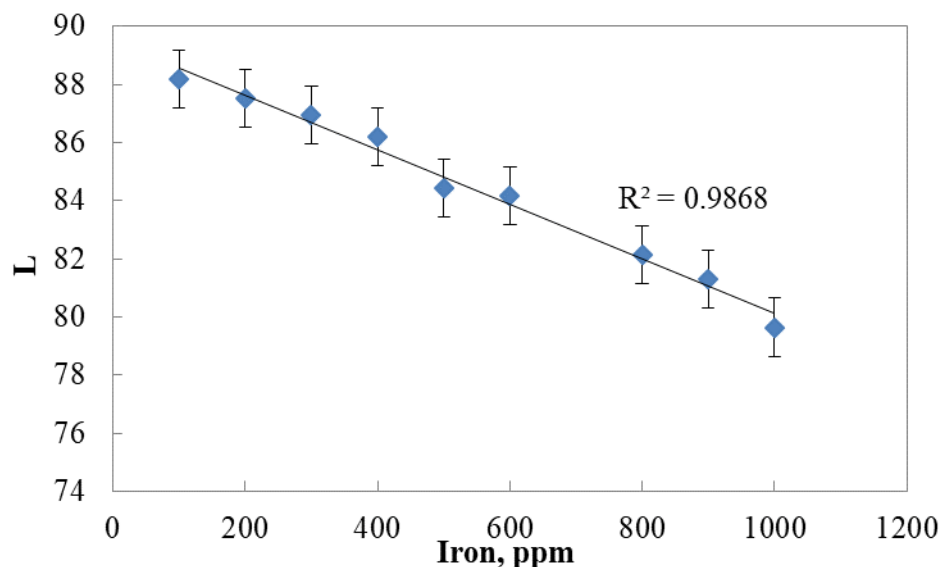


Figure 4.2. Change in “L” with respect to iron concentration at 300 s

The Datacolor equipment is costly and was difficult to use for some samples. Thus, there was a need to simplify the method by replacing it with image analysis using a digital web camera and a software developed for this purpose.

4.1.2 Measurement of change in color components using the custom-made set-up with the webcam

a) Iron

One impurity at a time was investigated also in this part of the study. Figure 4.3 shows the change in different color components (red (R), green (G), blue (B), and intensity) of the color obtained by the reaction of ferric chloride and potassium thiocyanate with respect to time. The advantage of this set-up was the use of solution. As the container was made of plastic, there was no significant change in color due to pH of the solution. All the parameters showed some noise in the first 150 s and became stable after that. However,

300 s was chosen for the following experiments based on the results obtained previously with the Datacolor equipment.

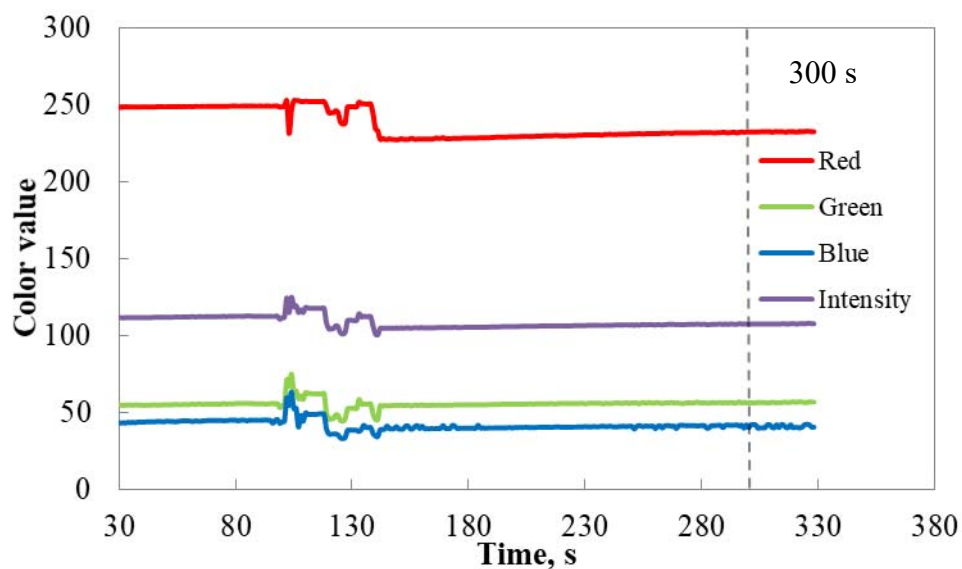


Figure 4.3. Change in color components with respect to time for 500 ppm pure iron solution

Figure 4.4 shows the change in different color components as a function of the change in iron concentration obtained using the image analysis method developed. The figure shows that R, B, and intensity components varied linearly with the concentration of iron.

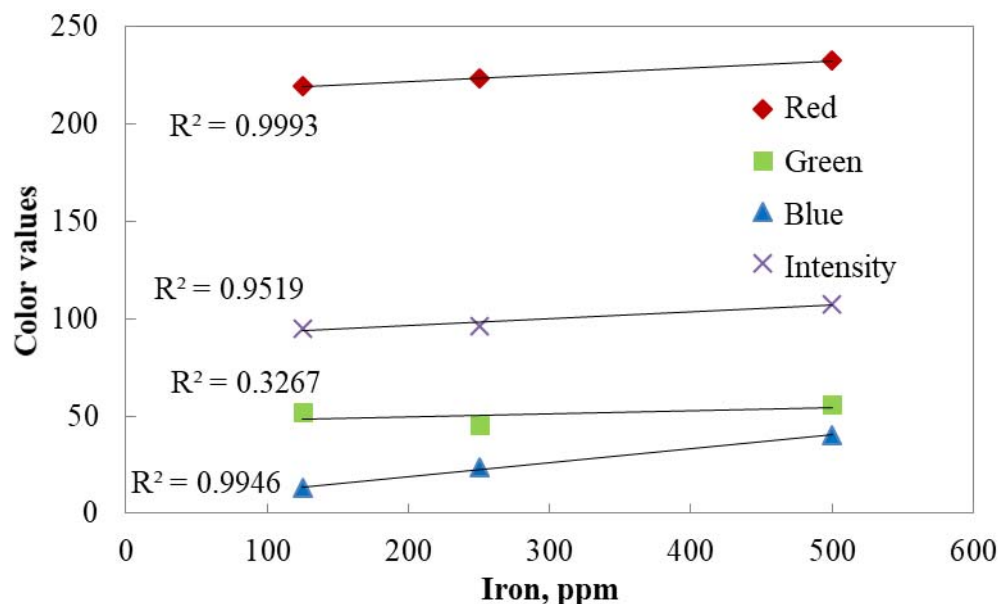


Figure 4.4. Change in color components with respect to concentration of iron solution at 300 s

Figure 4.5 shows the color change taking place during the reaction of iron extracted from an anode sample using the electrophoresis set-up and potassium thiocyanate. This was a preliminary experiment to test if only electrophoresis was enough to extract iron from the carbon samples (see Figure 3.1 for iron (only electrophoresis)). Anode sample contains a number of impurities together. It can be seen that the color changed significantly up to 210 s. After this time, the color became stable. It means that the impurity ions reacted with thiocyanate during this time, and it is better to study the color after 210 s. Then, 300 s was chosen based on the earlier studies. In this case, the results had more noise compared to those for the pure compounds. This might be due to the presence of other smaller ions which migrated together with iron even after the desired impurity was separated from the anode sample using electrophoresis.

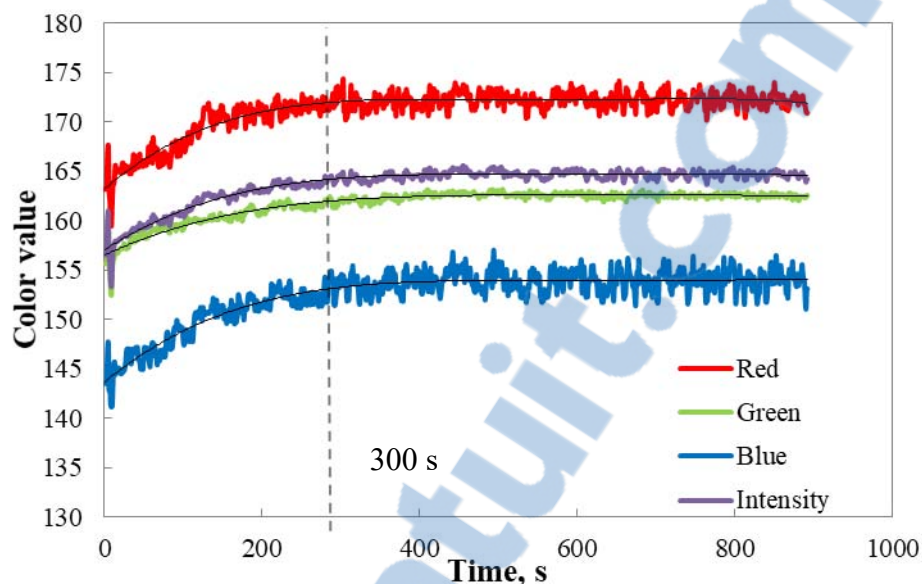


Figure 4.5. Colorimetric determination of Fe in anode sample

Figure 4.6 shows the calibration corresponding to the preliminary study using four samples (three calibration samples shown in Table 3.1 and one repetition) with known iron concentrations. Two of the four samples had a similar concentration of iron. The concentrations of different impurities (iron, nickel, and vanadium) were previously determined using XRF. The blue (B) component of the color showed a good correlation with different concentrations of iron as it was the case for the pure impurity compounds. The B component also gave similar values for the two samples with similar levels of iron. The other color components had lower R^2 value, possibly due to the presence of other impurities. The difference in the color of the solution obtained by electrophoresis (transparent) and that of the pure compound (light brown) can also cause a shift in the values of the color components after the reaction with the reagent (potassium thiocyanate).

The iron concentration of an unknown sample can be measured using the curve for the B component (calibration curve) given in this figure.

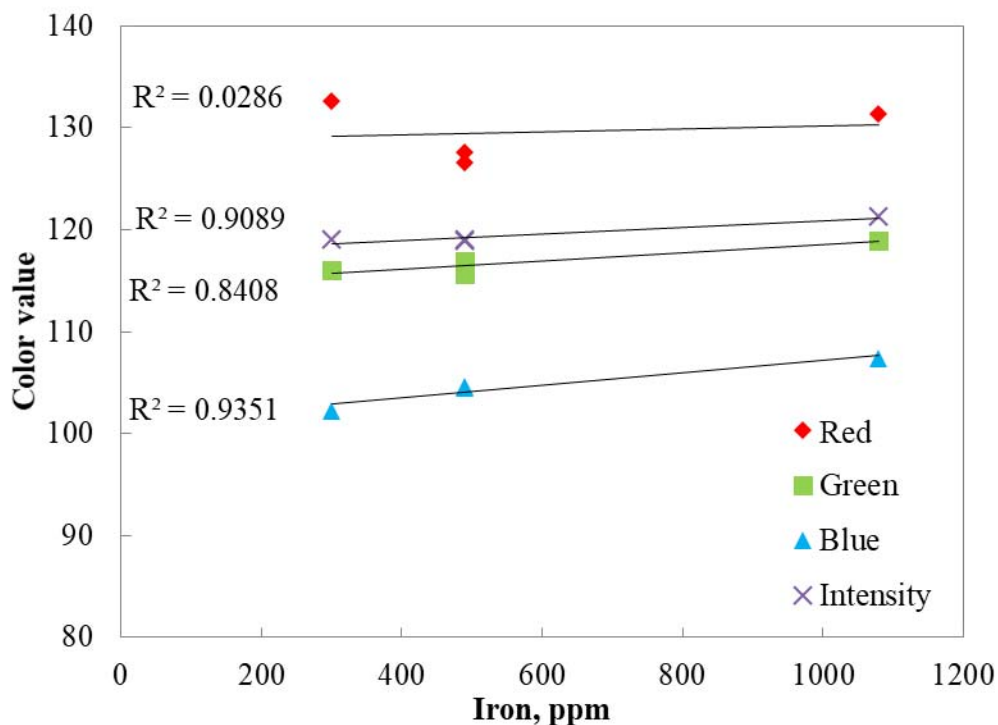


Figure 4.6. Calibration curve for iron concentration measurement determined by the colorimetric method (using electrophoresis and image analysis)

As the change in blue color was small with variation in the concentration of iron, extraction of iron was done using aqua regia. Aqua regia is a strong acid capable of dissolving even noble metals. Thus, aqua regia was used to react with the metals/metal salts to produce water soluble salts. This reaction helped extract the metallic impurities present in the carbon samples. Electrophoresis was avoided to reduce the complexity of the analysis. Figure 4.7 shows the color produced by the reaction of iron with potassium thiocyanate.



Figure 4.7. Color produced by the reaction of iron with potassium thiocyanate.

Figure 4.8 shows the calibration curve obtained using this method. The number of points used for calibration was limited due to the availability of samples with known concentrations of iron (see Table 3.1 for iron (final calibration)). The calibration curve was used for the measurement of two samples for which the concentrations of iron (see Table 3.2) was known to validate the method. The validation points on the calibration line show that the method is reliable. Figure shows a different trend compared to that observed in Figure . It is possible that the presence of aqua regia and the pH of the solution influenced the trend of the blue color component.

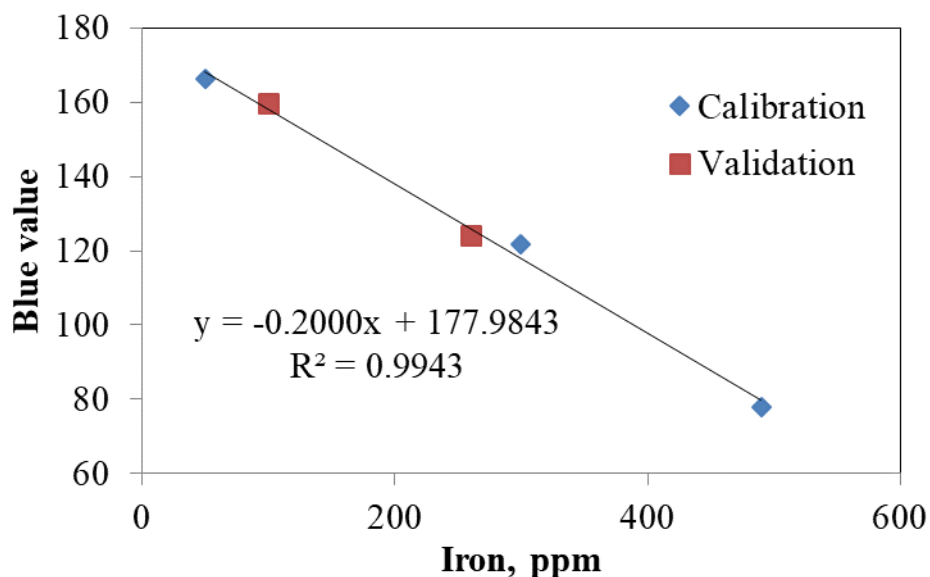


Figure 4.8. Calibration curve for iron concentration measurement determined by the colorimetric method (using aqua regia and image analysis) and its validation

Table 4.1 shows that the colorimetric and XRF measurements of iron in the coke samples were close. The variation might be due to the non-homogeneity of the samples.

Table 4.1. Comparison of results obtained by XRF and colorimetry for iron

Sample	Concentration of iron, ppm	
	XRF	Colorimetry based on blue
Validation (1)*	100	92
Validation (2)*	260	270
Coke (6)**	200 (supplier data)	210 (in pan)

* See Table 3.2, **See Table 3.3

The method was applied to measure the concentrations of iron in different anode and coke samples (see Table 4.2). The impurity level in anode samples (e.g. Anode (4)) was less than that of fresh coke (Coke (4)) as around 60% of fresh coke was present in the dry aggregate. It may also be seen that Coke (6) contains less impurity (Fe 121 ppm in large size fraction according to Table 4.2) in large size fractions compared to that in small size fractions (Fe 210 ppm in pan according to Table 4.1). Thus, it may also be noted that the impurity percentage in anode may vary with granulometry and non-homogeneity. This applies to all the metallic impurities (Fe, V, and Ni) (see Tables 4.1- 4.6).

Table 4.2. Analysis of coke and anode samples

Sample	Remarks	Concentration of iron by colorimetry, ppm
Anode (4)*	Coke (4) was used	297
Fe(1) **	Coke (6) + 50 ppm Fe added	232
Fe(3) **	Coke (6) + 250 ppm Fe added	345
Coke (6)* (large particle size)	-	121
BMP	-	172

*See Table 3.3, **See Table 3.4

b) Vanadium

Vanadium was estimated by analyzing the color developed due to the reaction of vanadium with N-benzoyl-N-phenylhydroxylamine. Vanadium was also extracted from

samples using aqua regia. Figure 4.9 shows the color produced by the reaction of vanadium with N-benzoyl-N-phenylhydroxylamine.

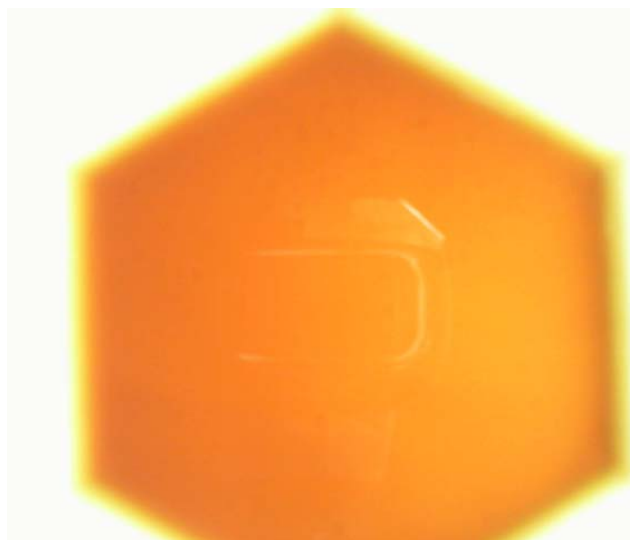


Figure 4.9. Color produced by the reaction of vanadium with N-benzoyl-N-phenylhydroxylamine

Figure 4.10 shows the calibration curve obtained using this method. The number of points used for calibration was limited due to the availability of samples with known concentrations of vanadium. The calibration curve was used for the measurement of two samples for which the concentrations of vanadium were known to validate the method. The validation points are also given on the calibration line showing that the method is reliable.

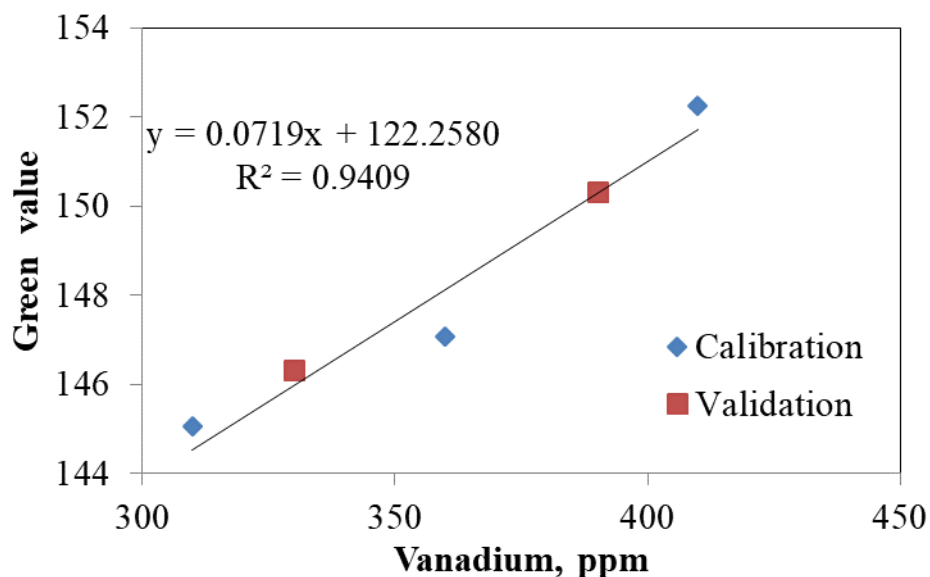


Figure 4.10. Calibration curve for vanadium concentration measurement determined using the colorimetric method (aqua regia and image analysis) and its validation

Table 4.3 shows that the colorimetric and XRF measurements of vanadium in the same samples are close. The variation might be due to the non-homogeneity of the samples.

Table 4.3. Comparison of results obtained by XRF and colorimetry for vanadium

Sample	Concentration of vanadium, ppm	
	XRF	Colorimetry
Validation (3)*	330	335
Validation (4)*	390	390
Coke (6)**	320 (supplier data)	318 (in pan)

*See Table 3.2, **See Table 3.3

The method was applied to measure the concentrations of vanadium in different anode and coke samples (Table 4.4).

Table 4.4. Analysis of coke and anode samples

Sample	Remarks	Concentration of vanadium by colorimetry, ppm
Anode (4)*	Coke (4) was used	317
V(1)**	Coke (6) + 10 ppm V added	306
V(3)**	Coke (6) + 30 ppm V added	342
Coke (6)* (large particle size)	-	126
BMP	-	280

*See Table 3.3, **See Table 3.4

c) *Nickel*

Nickel usually stays as metal in anode. It does not react rapidly with acids. Thus, nickel was first treated with aqua regia. Then, it was extracted from the mixture using the electrophoresis set-up while the electrophoresis was not used for iron and vanadium. Nickel was estimated by analyzing the color developed due to its reaction with dimethylglyoxime. Figure 4.11 shows the color produced by the reaction of nickel with this reagent.



Figure 4.11. Color produced by the reaction of nickel with dimethylglyoxime.

Figure 4.12 shows the calibration curve obtained using this method. The number of points used for calibration was limited due to the availability of samples with known concentrations of nickel. The calibration curve was used for the measurement of two samples for which the concentrations of nickel was known to validate the method. The validation points are also presented on the calibration line showing that the method is reliable.

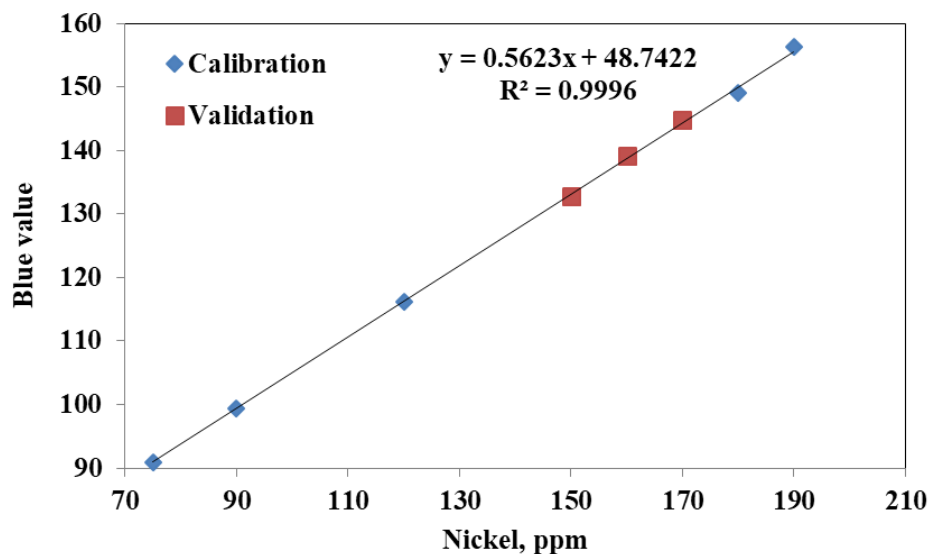


Figure 4.12. Calibration curve for nickel concentration measurement determined using the colorimetric method (aqua regia, electrophoresis, and image analysis) and its validation

Table 4.5 shows that the colorimetric and XRF measurements of nickel in the same samples were close. The variation might be due to the non-homogeneity of the samples.

Table 4.5. Comparison of results obtained by XRF and colorimetry for nickel

Sample	Concentration of nickel, ppm	
	XRF	Colorimetry
Validation (1)*	170	171
Validation (3)*	160	161
Validation (5)*	150	149
Coke (6)**	200 (supplier data)	201 (in pan)

*See Table 3.2, **See Table 3.3

The method was applied to measure the concentrations of nickel in different anode and coke samples. Results are given in Table 4.6.

Table 4.6. Analysis of coke and anode samples

Sample	Remarks	Concentration of nickel by colorimetry, ppm
Anode (4)*	Coke (4) was used	70
Ni(1)**	Coke (6) + 20 ppm Ni added	81
Ni(3)**	Coke (6) + 100 ppm Ni added	130
Coke (6)* (large particle size)	-	124
BMP	-	150

*See Table 3.3, **See Table 3.4

4.2 Study of the effect of impurity content on anode reactivities

4.2.1 Characterization of the green anodes

The density and electrical resistivities of the anodes were measured. Table 4.7 summarizes the results. Table 4.7 (a) shows that the anodes produced with different coke have different densities and electrical resistivities. This indicates that coke has a significant effect on the properties of green anodes. The densities and resistivities of entire anodes were measured to make sure that they have acceptable properties (see Section 3.4.2.b). The anode properties and the quantity of impurities added to each anode are given in Table 4.7 (b). The differences in density observed for anodes with V addition are likely due to the anode fabrication parameters. The resistivity variations in the anodes are probably due to differences in pitch distribution and non-homogeneity.

Table 4.7. Properties of green anodes: (a) anodes produced with different coke, (b) anodes produced with Coke (6) and with addition of impurities

(a)

Anode	Coke	In coke				Green anode	
		Nickel, ppm	Iron, ppm	Vanadium, ppm	Sulfur, %	Density, g/cc	Electrical resistivity, $\mu\Omega.m$
Anode (1)	Coke (1)	184	196	217	1.82	1.376	9147
Anode (2)	Coke (2)	189	93	301	1.91	1.536	6760
Anode (3)	Coke (3)	176	114	368	3.55	1.354	8443
Anode (4)	Coke (4)	190	470	506	4.79	1.425	5140
Anode (5)	Coke (5)	163	161	426	5.42	1.460	4282
Std*	Coke (6)	200	200	320	2.00	1.519	8235

(b)

Anode	Impurity addition	Green anode density, g/cc	Green anode electrical resistivity, $\mu\Omega.m$
Std*	0	1.519	8235
Ni (1)	Ni 20 ppm	1.520	6903
Ni (2)	Ni 60 ppm	1.514	7538
Ni (3)	Ni 100 ppm	1.516	4835
Fe (1)	Fe 50 ppm	1.524	4145
Fe (2)	Fe 150 ppm	1.527	4130
Fe (3)	Fe 250 ppm	1.523	8215
V (1)	V 10 ppm	1.463	6799
V (2)	V 20 ppm	1.543	7408
V (3)	V 30 ppm	1.519	4814

*Std: The same anode produced using standard conditions.

4.2.2 Characterization of cylindrical anode samples used for reactivity studies

Table 4.8 summarizes the densities of the cores (50 mm diameter x 130 mm length) (see Figure 3.5b) before and after baking (see Section 3.4.2.c). It can be seen that the green core densities are not the same as those of the parent anodes (see table 4.7) due to the non-homogeneity of the anodes.

The properties of coke, which is usually nonhomogeneous, influenced the green and baked densities of the anodes. It is known that the porosity, real density, apparent density, bulk density, shape factors, etc. of coke influences the density of the anode before and after baking. In this study, no butt particles or anode rejects were used since their metallic impurity contents were unknown. This also could have influenced the density of the anodes.

Table 4.8. Green and baked density of cylindrical samples ($\phi 50 \times 130$ mm) taken from the anodes

Anode	Coke	Core 1 (for CO ₂ reactivity tests)		Core 3 (for air reactivity tests)	
		GAD, g/cc	BAD, g/cc	GAD, g/cc	BAD, g/cc
Std	Coke (6)	1.557	1.507	1.612	1.521
Ni(1)		1.553	1.504	1.606	1.525
Ni(2)		1.559	1.509	1.601	1.517
Ni(3)		1.563	1.511	1.615	1.525
Fe(1)		1.571	1.537	1.609	1.534
Fe(2)		1.574	1.520	1.615	1.535
Fe(3)		1.557	1.524	1.607	1.516
V(1)		1.572	1.529	1.616	1.529
V(2)		1.586	1.537	1.625	1.526
V(3)		1.576	1.526	1.618	1.525
Anode (1)		Coke (1)	1.424	1.376	1.435
Anode (2)	Coke (2)	1.584	1.528	1.590	1.536
Anode (3)	Coke (3)	1.394	1.359	1.407	1.361
Anode (4)	Coke (4)	1.476	1.433	1.474	1.427
Anode (5)	Coke (5)	1.493	1.456	1.503	1.457

4.2.3 Reactivities of different anode samples

Table 4.9 summarizes the CO₂ reactivities of the different anode samples (50 mm diameter x 50 mm height) (see Figure 3.5b). The densities of the cores used for the

reactivities are not exactly the same as those of the parent cores because the densities of the cores cut for the reactivity tests were re-measured as explained in Section 3.4.2.c. The results show that the CO₂ reactivity is significantly different for different cokes. However, for the same coke, the reactivity change is less in spite of the addition of impurities. Also, in general, increasing S concentration seems to reduce the CO₂ reactivity (see Anodes 1-5 and Std. in Table 4.9).

Table 4.9. CO₂ reactivity results of anode samples (φ50 x 50 mm sample cut from Core 1)

Anode	Nickel, ppm	Iron, ppm	Vanadium, ppm	Sulfur, %	BAD, g/cc	CO ₂ reactivity, mg/cm ² h
Std	200	200	320	2.00	1.499	16.93
Ni(1)	220	200	320	2.00	1.498	16.95
Ni(2)	260	200	320	2.00	1.511	14.68
Ni(3)	300	200	320	2.00	1.506	16.24
Fe(1)	200	250	320	2.02	1.536	14.92
Fe(2)	200	350	320	2.03	1.489	16.29
Fe(3)	200	450	320	2.38	1.511	17.25
V(1)	200	200	330	2.00	1.523	13.52
V(2)	200	200	340	2.00	1.532	12.18
V(3)	200	200	350	2.00	1.518	14.16
Anode (1)	184	196	217	1.82	1.365	34.95
Anode (2)	189	93	301	1.91	1.516	23.60
Anode (3)	176	114	368	3.55	1.359	27.37
Anode (4)	190	470	506	4.79	1.429	23.71
Anode (5)	163	161	426	5.42	1.464	18.86

Figure 4.13 shows that the CO₂ reactivity generally decreases with increase in anode density as expected since it cannot easily diffuse into the anode as the density increases and the porosity decreases. Some scattering is also observed due to the non-homogeneous nature of anodes.

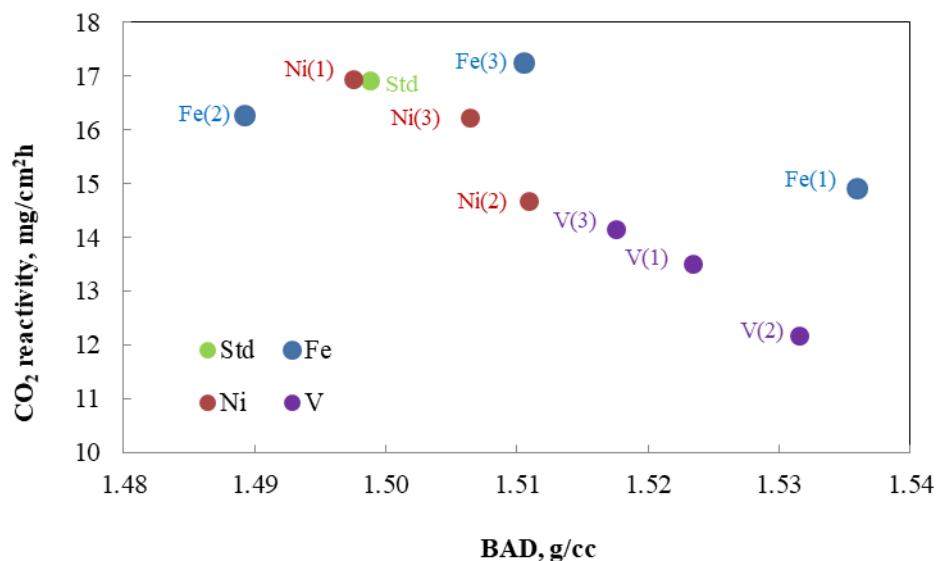


Figure 4.13. Effect of BAD on CO₂ reactivity

It is difficult to see a trend concerning the impact of S concentration on air reactivity; however, if only the anodes with S concentrations up to 3.55% are considered, a decrease in air reactivity is observed with increasing S concentration (see Anodes 1-5 and Std. in Table 4.10).

Table 4.10 summarizes the air reactivities of the different anode samples (50 mm diameter x 50 mm height) (see Figure 3.5b). The results show that the air reactivity is influenced not only by the type of coke, but also by the presence of different impurities.

It is difficult to see a trend concerning the impact of S concentration on air reactivity; however, if only the anodes with S concentrations up to 3.55% are considered, a decrease in air reactivity is observed with increasing S concentration (see Anodes 1-5 and Std. in Table 4.10).

Table 4.10. Air reactivity results of anode samples ($\phi 50 \times 50$ mm sample cut from Core 3)

Anode	Nickel, ppm	Iron, ppm	Vanadium, ppm	Sulfur, %	BAD, g/cc	Air reactivity, mg/cm ² h
Std	200	200	320	2.00	1.517	62.15
Ni(1)	220	200	320	2.00	1.528	60.12
Ni(2)	260	200	320	2.00	1.514	56.21
Ni(3)	300	200	320	2.00	1.518	51.50
Fe(1)	200	250	320	2.02	1.533	54.90
Fe(2)	200	350	320	2.03	1.529	56.34
Fe(3)	200	450	320	2.38	1.525	55.29
V(1)	200	200	330	2.00	1.519	60.04
V(2)	200	200	340	2.00	1.536	52.42
V(3)	200	200	350	2.00	1.534	57.52
Anode (1)	184	196	217	1.82	1.399	71.66
Anode (2)	189	93	301	1.91	1.548	64.83
Anode (3)	176	114	368	3.55	1.372	58.42
Anode (4)	190	470	506	4.79	1.439	70.40
Anode (5)	163	161	426	5.42	1.461	68.24

The reactivity results show that air reactivity values are higher compared to the CO₂ reactivity values for the same anodes. The reason is that the rate of reaction in the case of air reactivity is much faster compared to that of the CO₂ reactivity.

Figure 4.14 shows that no definite trend could be found for the effect of BAD on air reactivity. This is probably due to the non-homogeneous nature of anodes, which affects the concentration and the distribution of impurities in samples taken from these anodes.

In the current project, the effect of a single parameter on the reactivity was difficult to analyze experimentally, as there were variations of more than one parameter. Thus, the artificial neural network (ANN) analysis was used to understand the effect of each parameter on reactivity since, with ANN, it is possible to vary only one parameter while keeping others constant and predict the reactivity. This analysis is presented in Section 4.3.

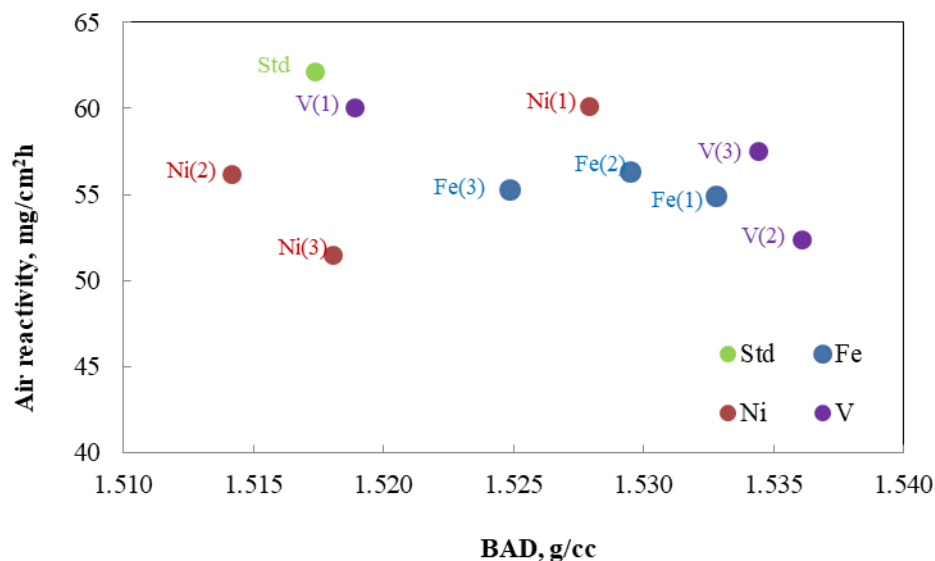


Figure 4.14. Effect of BAD on air reactivity

4.2.4 Effect of different impurities on anode reactivities

The effect of different impurities on reactivities were studied by plotting the concentration of the total impurities against the reactivity values. This study was done for the anodes produced using Coke (6). The trends are also influenced by the densities of the baked anode samples (BAD). ANN can help understand the effect of different impurities on the air and CO₂ reactivities. The ANN analysis results are presented in the next section (Section 4.3).

There are different parameters that can influence the reactivity. It should be noted that the densities of anodes are slightly different (see Tables 4.9 and 4.10). The density of anode controls the diffusion of gas and the kinetics of the reaction. The transition metal impurities can catalyze the reaction. The gases may also react with the impurities to produce volatile compounds. The distribution of impurities in different size fractions of coke can influence the contact of the impurities with the reacting gas. The non-homogeneity of coke and anode can also influence the reactivity. Thus, the reactivity of anode is complex and is influenced by a number of different parameters. It is difficult to maintain all other parameters identical to study the effect of a single parameter experimentally. In this study, different chemical compounds were added to study the effect of a particular impurity. The following results show their effect on reactivity. However, it was not possible to have samples with similar baked anode densities.

Figure 4.15 shows the effect of iron on the CO₂ and air reactivities. If all four results are considered, it can be seen that the CO₂ reactivity decreased initially, and then increased with increase in iron content. The air reactivity also decreased initially, then it did not

change significantly with increase in iron concentration. It must be noted that the addition of a chemical may not match with the form of metal already present in coke. Thus, the initial decrease in CO₂ reactivity may not be the result of only iron. For the same iron concentration, the reactivities might differ due to the densities of the samples.

If the samples with Fe addition are considered, the results showed that increase in iron content increased the CO₂ reactivities, but did not significantly affect the air reactivity. Perhaps the effect of iron has been partially masked by the differences in BAD.

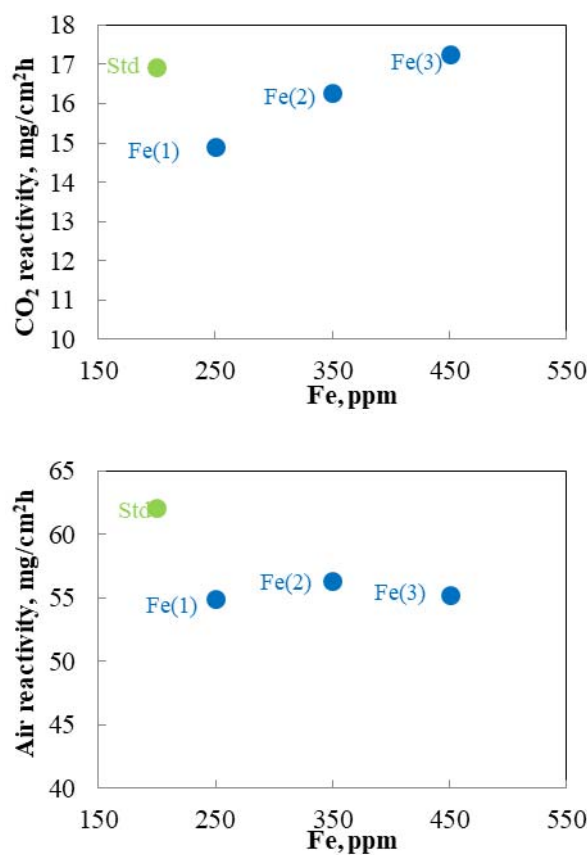


Figure 4.15. CO₂ and air reactivities of anode samples containing different concentrations of iron

Figure 4.16 shows the effect of vanadium on the CO₂ and air reactivities. Considering all samples, the results show that both CO₂ and air reactivities decreased initially, then increased with further increase in vanadium content. If only the three samples with vanadium addition are compared, the same trend is observed. For the same vanadium concentration, the reactivities might have differed due to the differences in densities of the samples.

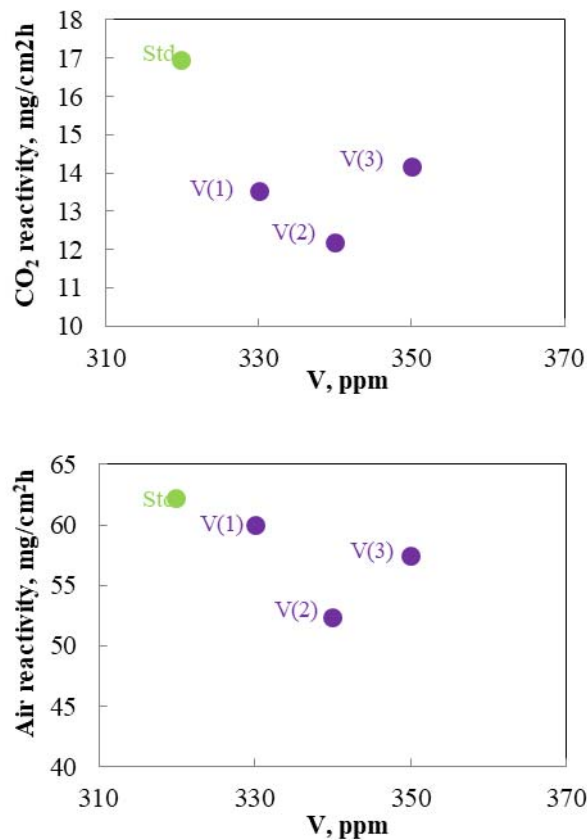


Figure 4.16. CO₂ and air reactivities of anode samples containing different concentrations of vanadium

Figure 4.17 shows the effect of nickel on the CO₂ and air reactivities. The CO₂ reactivity decreased initially, and then increased with increase in nickel content. The results also show that the air reactivity decreased with increase in nickel content. The differences in sample densities may have affected the results as well. It is difficult to distinguish the impact of such factors on the reactivities based on experimental work.

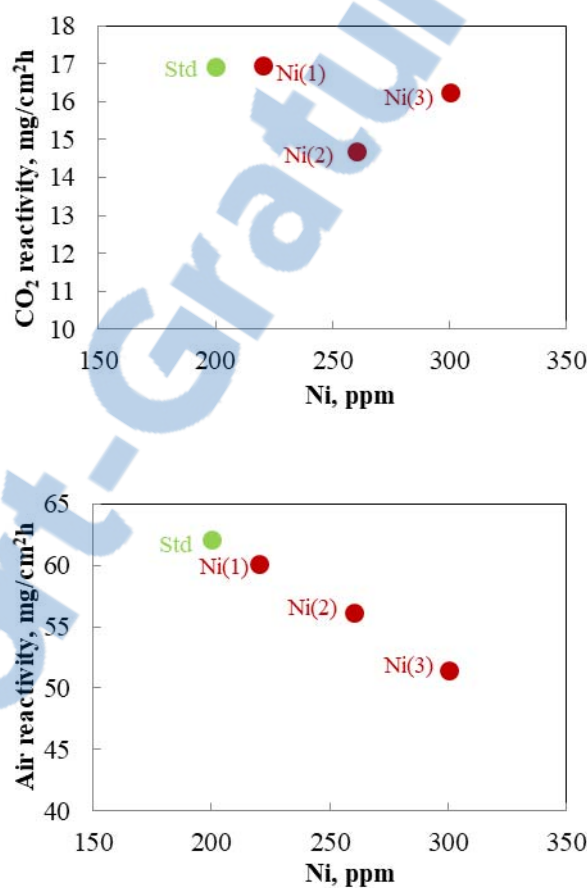


Figure 4.17. CO₂ and air reactivities of anode samples containing different concentrations of nickel

It is worth mentioning that the trends observed might be valid only for the cases studied. For the anodes prepared using different cokes, it was difficult to find some

relationships among the CO₂/ air reactivity and impurity contents by conventional methods. The reason was that concentrations of different impurities in the cokes changed at the same time. The densities of the anodes also differed significantly. The artificial neural network (ANN) method was used for the analysis in order to understand the effect of each parameter keeping all other parameters constant and the results of this analysis is presented in the next section.

4.3 Results of ANN

In this study, multilayer custom feedforward ANN models, which were previously developed by the UQAC/AAI Chair personnel, were applied to explain the effect of different impurities on anode reactivities. The data related to all the anodes (using additives with Coke (6) and different cokes) were used. The models were trained using 80% of the experimental results. The predictions of the models were validated using the rest of the results (20% of the experimental results), which were not used for training. The models were used to predict the effect of different parameters on the reactivities. In each of the figures, the concentration of a particular impurity was varied for different BAD keeping the concentrations of all other impurities constant (Figures 4.18-4.25). The constant level of each impurity can be high, low or in the range typically found in industry. The effects of a particular impurity on the air or CO₂ reactivity keeping other impurity concentrations in their typical ranges have been presented in this section. The effect of the concentration of metallic impurities (Fe, V, Ni) as well as that of sulfur was studied. As the reactivities may be controlled by the anode density, the effects of density (changing one impurity while

maintaining other impurities at their typical levels) have also been presented in appendix I (Figures A1.1-A1.4). The effect of a particular impurity on reactivity might be influenced by the presence of other impurities. Thus, the effects of the level of an impurity in conjunction with the levels (high and low) of another impurity on anode reactivities keeping the remaining impurities at their typical levels for different BAD were presented in appendix (Figures A1.5-A1.26). These results also show the effect of density on anode reactivities for different levels of impurities. Thus, the results in appendix give an idea about the combined effect of two impurities as well as baked anode density on reactivities. Usually such reactions are controlled by two factors: kinetics and diffusion. If the rate of reaction decreases with increase in density, the reaction is diffusion controlled. On the other hand, if the reaction rate increases with density, the reaction is kinetically controlled. Both mechanisms are possible in these reactions. The ANN study can help understand the reaction mechanism under different conditions. Further experiments are necessary to explain and validate the results obtained by ANN since the precision of ANN models is improved by increasing the number of data available to train the model.

4.3.1 The effect of iron (Fe) concentration on air and CO₂ reactivities (V, Ni, and S maintained at their typical levels)

Figure 4.18 shows the effect of iron concentration on air reactivity for different BAD. V, Ni, and S were maintained at the levels typically used in the industry. As shown in this figure, at the lowest BAD, iron increases air reactivity. At higher BAD, addition of iron decreases air reactivity. The combined effect of BAD, impurity concentration and

distribution, and interaction of impurity with the gas might have influenced the reactivities.

Further studies are required to understand the detailed mechanism.

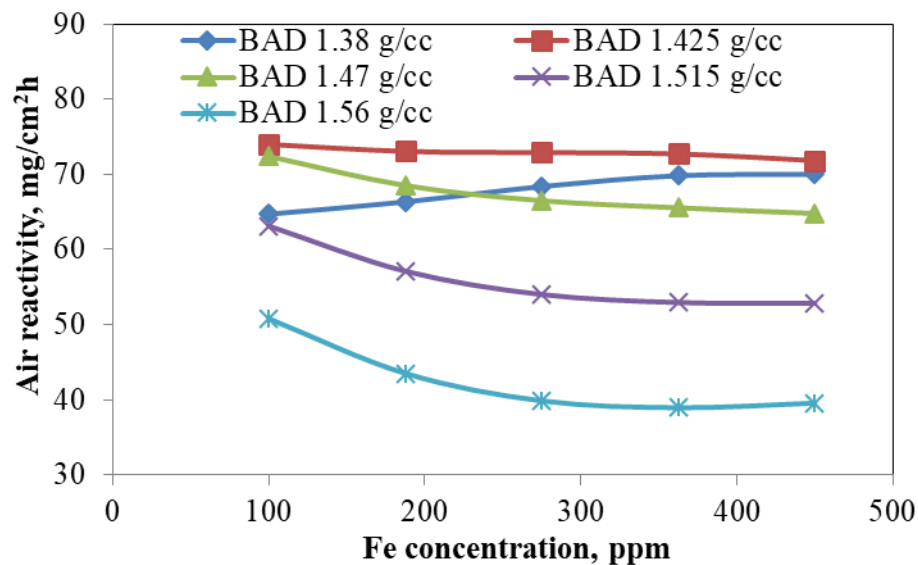


Figure 4.18. The effect of iron concentration on air reactivity with different BADs (V, Ni and S were maintained at their typical levels)

Figure 4. shows the effect of iron concentration on CO_2 reactivity for different BADs. V, Ni, and S were maintained at their usual levels. CO_2 reactivity decreases with increase in iron concentration up to a certain limit. At the lowest BAD, the reactivity stays almost constant after this limit. However, at higher BAD, iron catalyzes CO_2 reactivity once the limit is exceeded and the CO_2 reactivity increases with increasing iron concentration. As reaction with CO_2 is mostly diffusion controlled, low anode density results in higher reactivity. It can be found that increasing the concentration of Fe reduces the difference in CO_2 reactivity for different densities.

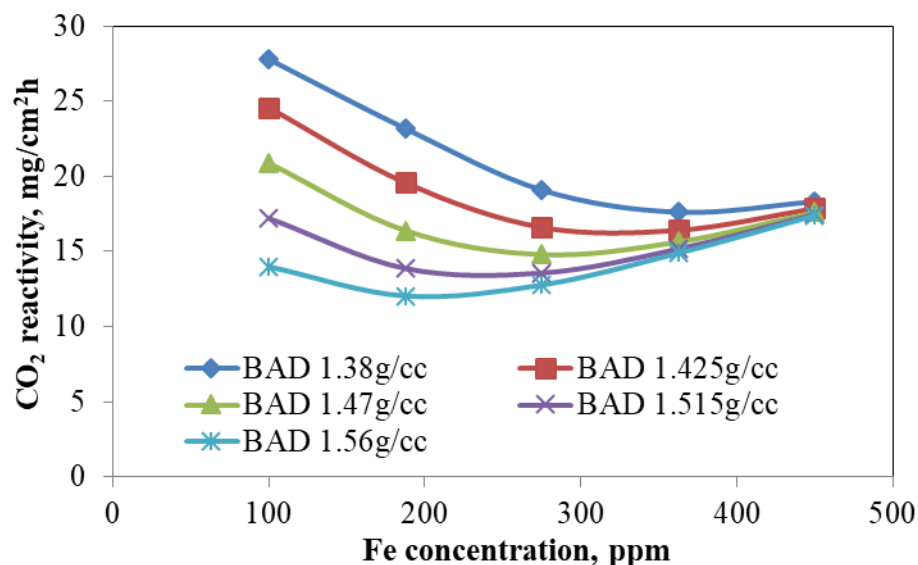


Figure 4.19. The effect of iron concentration on CO₂ reactivity for different BAD (V, Ni, and S were maintained at their typical levels)

4.3.2 The effect of vanadium (V) concentration on air and CO₂ reactivities (Fe, Ni, and S were maintained at their typical levels)

Figure 4.20 shows the effect of vanadium concentration on air reactivity for different BAD. Fe, Ni, and S were maintained at their typical levels. At high BAD, addition of vanadium decreases air reactivity, however, it increases with increasing vanadium concentration at low BAD. As discussed earlier, the combined effect of BAD, impurity concentration and distribution, and reaction of impurity with the gas might have influenced the air reactivity. Increasing anode density leads to decreasing porosity which might decrease air reactivity.

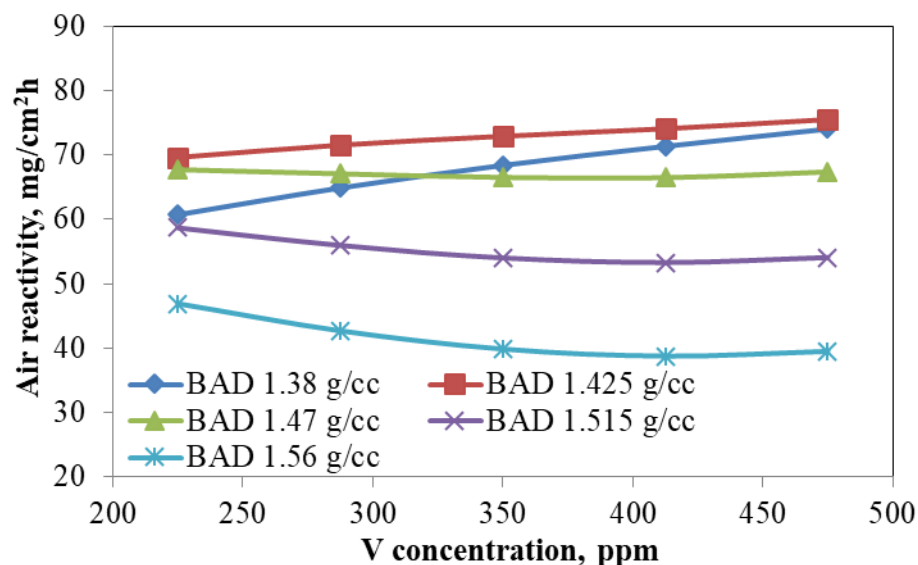


Figure 4.20. The effect of vanadium concentration on air reactivity for different BAD (Fe, Ni, and S were maintained at their typical levels)

Figure 4.21 shows the effect of vanadium concentration on CO₂ reactivity for different BAD. It can be seen from this figure that CO₂ reactivity decreases with increasing BAD as well as increase in V content. Increase in density reduces porosity and in turn reduces the diffusion of CO₂ in anode matrix. It appears that the reaction is diffusion controlled. It can also be seen from the figure that the CO₂ reactivity becomes independent of density at high V concentrations.

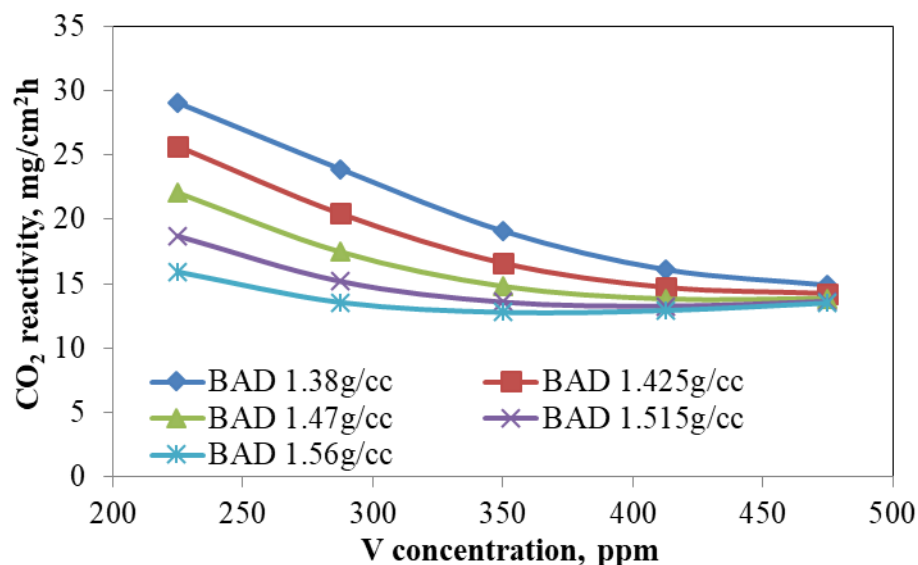


Figure 4.21. The effect of vanadium concentration on CO₂ reactivity for different BAD (Fe, Ni, and S were maintained at their typical levels)

4.3.3 The effect of nickel (Ni) concentration on air and CO₂ reactivities (Fe, V, and S were maintained at their typical levels)

Figure 4.22 shows the effect of nickel concentration on air reactivity for different BAD. It can be seen from this figure that air reactivity increases initially and then decreases with increasing BAD at constant Ni concentration up to around 275 ppm. After this point air reactivity is not affected significantly at lower BAD values. However, it decreases with increasing BAD at higher BAD values for a given Ni concentration. For a particular BAD, air reactivity decreases up to a certain nickel concentration. At higher nickel concentrations, air reactivity increases with increase in the amount of nickel.

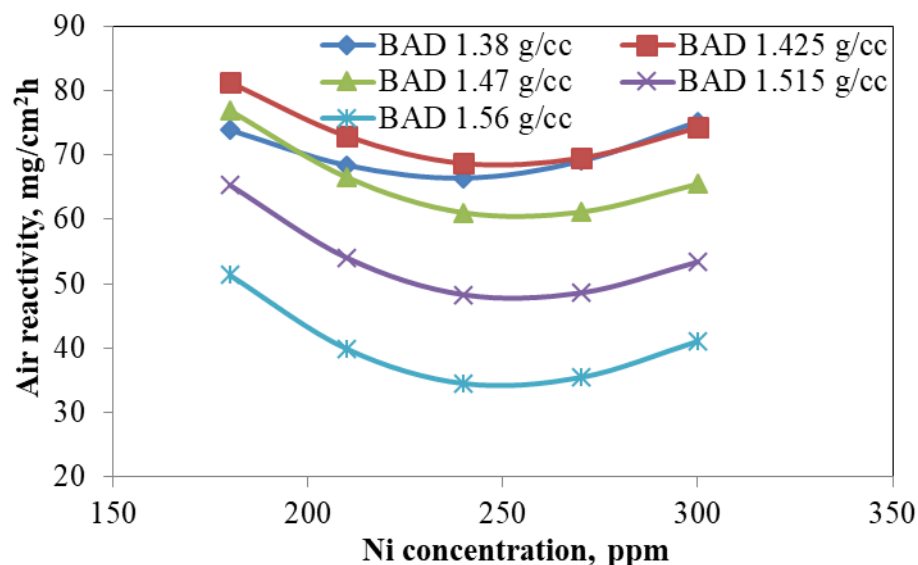


Figure 4.22. The effect of nickel concentration on air reactivity for different BAD (Fe, V, and S were maintained at their typical levels)

The effect of nickel concentration on CO_2 reactivity for different BAD is shown in Figure 4.23. This figure shows that CO_2 reactivity decreases with increasing BAD because CO_2 reactivity is mainly diffusion-controlled. For a given BAD, CO_2 reactivity decreases with increase in the concentration of nickel. However, at high Ni level, the change in reactivity is small.

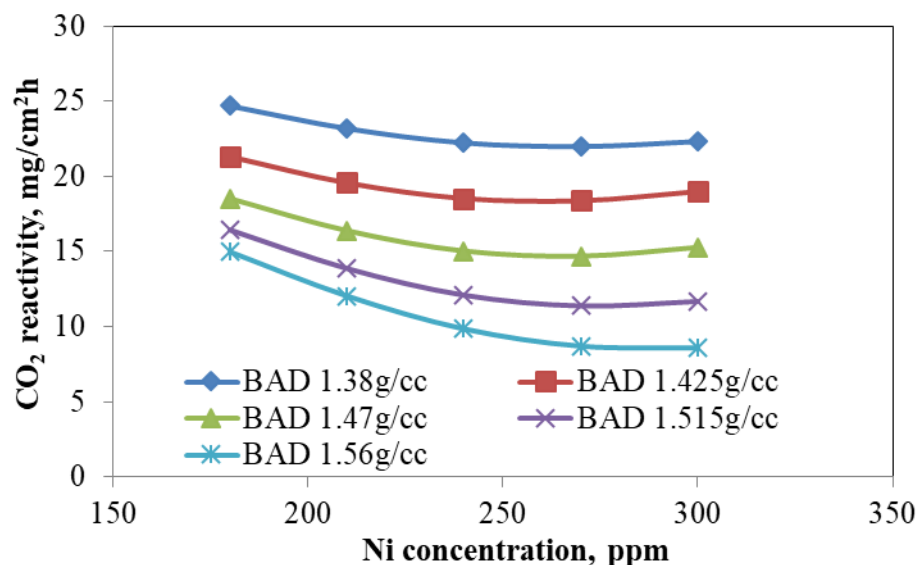


Figure 4.23. The effect of nickel concentration on CO₂ reactivity for different BAD (Fe, V, and S were maintained at their typical levels)

4.3.4 The effect of sulfur (S) concentration on air and CO₂ reactivities (Fe, V, and Ni were maintained at their typical levels)

Sulfur can poison transition metal catalysts by forming strong covalent bonds, hence decreases their catalytic effect on reactivity. On the other hand, it can react with air to produce SO₂. Figure 4.24 shows the effect of sulfur concentration on air reactivity for different BAD. Fe, V, and Ni were maintained at their typical levels. As it can be seen from the results, air reactivity increases initially and later decreases with increasing BAD at constant S concentration. The figure shows that for constant BAD, air reactivity decreases with increase in S content for the range studied.

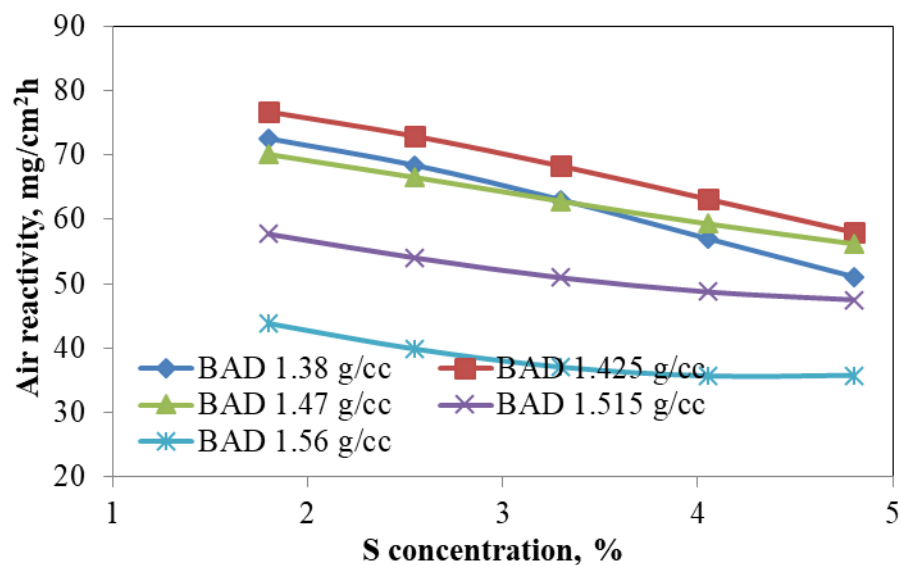


Figure 4.24. The effect of sulfur concentration on air reactivity for different BAD (Fe, V and Ni were maintained at their typical levels)

Figure 4.25 shows the effect of sulfur concentration on CO_2 reactivity for different BAD. The CO_2 reactivity decreases with increasing BAD because high density reduces porosity. It can be observed that at low BAD, increase in sulfur content reduces reactivity. On the other hand at high BAD, increase in sulfur content shows the opposite trend. It can be seen from the figure that increasing concentration of S reduces the difference in CO_2 reactivity among the anodes with different BAD.

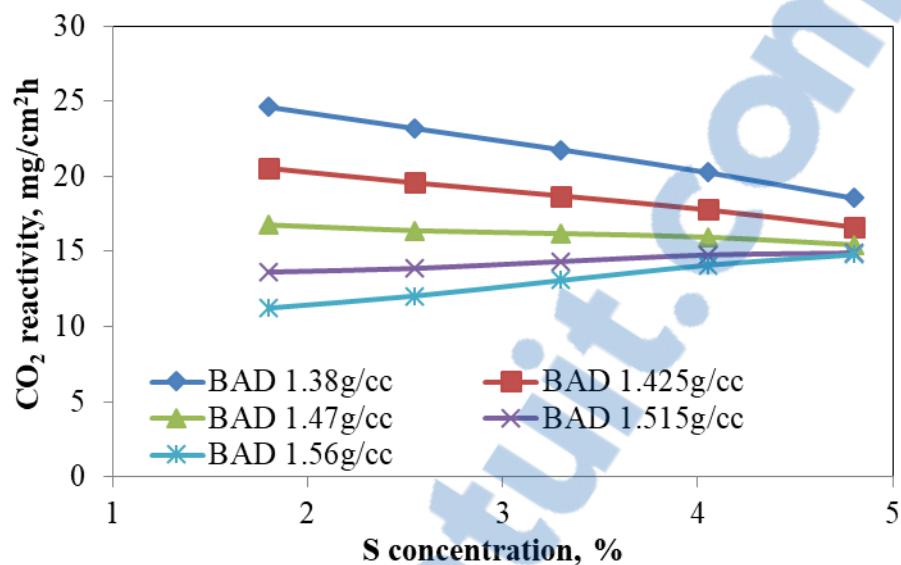


Figure 4.25. The effect of sulfur concentration on CO₂ reactivity for different BAD (Fe, V and Ni were maintained at their typical levels)

4.3.5 Remarks

The results obtained with the ANN analysis depend on the number of input data available. More tests should be done on the reactivities using a greater number of samples, and the analysis with ANN should be revised using the additional data to verify the trends obtained with the limited number of samples. There are many factors that affect the reactivities. Increasing the number of samples will also help better identify the relationship between different parameters and the combined effect on the reactivities.

CHAPTER 5

CONCLUSIONS AND RECOMMENDATIONS

5.1 Conclusions

A simple, quick, and inexpensive method for the determination of the transition metal impurities present in anodes was developed. The calibration curves for the determination of iron, vanadium, and nickel present in carbon samples were prepared. The impurities were extracted from the carbon samples using different methods (aqua regia and electrophoresis). This type of analyses was never applied to the measurement of impurity content in carbonaceous materials (coke, anode, etc.). The results were validated using samples with known concentrations of the impurities. It was found that the developed methods work as well as the sophisticated methods such as XRF. In addition, they are less costly and simple to use.

Also, a number of anodes with different cokes as well as with one coke and the addition of impurities were fabricated. The green anodes and the green and baked samples from these anodes were characterized. Air and CO₂ reactivities of the baked samples were measured. The CO₂ reactivity showed a reasonably good correlation with BAD and decreased with increasing BAD. However, no relation was observed between the air reactivity and BAD. Also, increase in sulfur concentration seemed to generally decrease the reactivities.

Due to the variation in densities of the samples, especially for the anodes produced using different cokes, it was difficult to analyze the effect of different impurities on anode reactivities only from the experimental data. This was also seen in literature. Different authors reported different trends for the same impurity. The possible reason is that the effect of each impurity changes depending on the presence and the amount of other impurities. Artificial neural network method was used to analyze the effect of different metallic impurities (Fe, V, Ni) and S as well as the baked anode density (BAD) on the anode reactivities. If the anode density is high, the contact of the gas with carbon is more limited due to less porous nature of the anode even if the impurities are present. The results showed that, in general, CO₂ reactivity usually decreases with increase in BAD. Air reactivity increases up to a certain density of the anode; then, it shows some decrease. The effects of the impurities on the reactivities depend on the BAD as well as the presence of other impurities.

5.2 Recommendations

The effects of different impurities on anode reactivities need to be further studied in more detail in order to determine the underlying mechanisms.

The efficiency of an ANN model can be enhanced by increasing the number of input data. A large number of experiments carried out under different conditions can help develop improved ANN models which will allow a better prediction of the effect of different impurities on anode reactivities.

Incorporation of detailed chemical compositions of coke and other raw materials can help improve the prediction ability of the ANN models.

REFERENCES

1. Hulse, K.L, Anode manufacture : Raw materials, formulation and processing parameters (Sierre [Suisse]: R & D Carbon Ltd., 2000), xxxv, p. 416.
2. Bonnamy, S. and A. Oberlin, Carbon, 1982. 20(6): p. 499-504.
3. Eidet, T., M. Sorlie, and J. Thonstad, Effects of iron and sulphur on the air and CO₂ reactivity of cokes, Light Metals, 1997: p.511-517.
4. Casada, M. R., J. Rolle, A.J. Edmond, S. Romero, D. Hester, Z. DeMori, J. Turpial, J. Mora, E. Epstein, D. Pirolo, and J. Velasco, Quantification of the influence of nickel on reduction cell anodes, Light Metals, 1997: p. 489-495.
5. Song, Y., Li, X., Huang,W., and Zhang, Y., Application of ICP-MS in petrochemical industry, Shiyou Huagong/Petrochemical Technology, 2016. 45(10): p.1279-1287.
6. Poirier, L., J. Nelson, D. Leong, L. Berhane, P. Hajdu, and F. Lopez-Linares, Application of ICP-MS and ICP-OES on the Determination of Nickel, Vanadium, Iron, and Calcium in Petroleum Crude Oils via Direct Dilution, Energy and Fuels, 2016. 30(5) : p. 3783-3790.
7. Hita, I., R. Palos, J.M. Arandes, J.M. Hill, and P. Castaño, Petcoke-derived functionalized activated carbon as support in a bifunctional catalyst for tire oil hydroprocessing, Fuel Processing Technology, 2016. 144: p. 239-247.

8. Verma, S.P., T. Besch, M. Guevara, and B. Schulz-Dobrich, Determination of twelve trace elements in twenty-seven and ten major elements in twenty-three geochemical reference samples by x-ray fluorescence spectrometry, *Geostandards Newsletter*, 1992. 16(2): p. 301-309.
9. Camera, A.S., T.A. Maranhão, F.J.S. Oliveira, J.S.A. Silva, and V.L.A. Frescuraa, Total mercury determination in petroleum green coke and oily sludge samples by cold vapor atomic fluorescence spectrometry, *Journal of the Brazilian Chemical Society*, 2015. 26(10): p. 2116-2124.
10. Yang, T., C. Huang and W. Deng, Hydrogenation activity and coke restraining ability of oil-soluble catalysts for residue slurry-bed hydrocracking, *Petroleum Processing and Petrochemicals*, 2016. 47(5): p. 51-56.
11. Moonrungsee, N., S. Pancharee, and J. Jakmunee, Colorimetric analyzer based on mobile phone camera for determination of available phosphorus in soil. *Talanta*, 2015. 136: p. 204-209.
12. Kehoe, E. and R.L. Penn, Introducing colorimetric analysis with camera phones and digital cameras: An activity for high school or general chemistry. *Journal of Chemical Education*, 2013. 90(9): p. 1191-1195.

13. Sumriddetchkajorn, S., K. Chaitavon, and Y. Intaravanne, Mobile device-based self-referencing colorimeter for monitoring chlorine concentration in water. *Sensors and Actuators B: Chemical*, 2013. 182: p. 592-597.
14. Yun, J. and H. Choi, Micellar colorimetric determination of iron, cobalt, nickel and copper using 1-nitroso-2-naphthol, *Talanta*, 2000. 52(5): p. 893-902.
15. Muir, M.K. and T.N. Andersen, Determination of ferrous iron in copper-process metallurgical solutions by the o-phenanthroline colorimetric method, *Metallurgical Transactions B*, 1977. 8(2): p. 517-518.
16. Braunschweig, J., J. Bosch, K. Heister, C. Kuebeck, and R.U. Meckenstock, Reevaluation of colorimetric iron determination methods commonly used in geomicrobiology, *Journal of Microbiological Methods*, 2012. 89(1): p. 41-48.
17. Gazda, D. B., J. S. Fritz, and M. D. Porter, Determination of nickel(II) as the nickel dimethylglyoxime complex using colorimetric solid phase extraction, *Analytica Chimica Acta*, 2004.508(1): p. 53-59.
18. Chilton, J. M, Simultaneous Colorimetric Determination of Copper, Cobalt, and Nickel as Diethyldithiocarbamates, *Anal.Chem*, 1953. 25(8): p. 1274-1275.
19. Lingane, J.J. and H. Kerlinger, Polarographic determination of nickel and cobalt: Simultaneous determination in presence of iron, copper, chromium, and manganese, and determination of small amounts of nickel in cobalt compounds, *Industrial and Engineering Chemistry*, 1941. 13(2): p. 77-80.

20. Flora, C.J. and E. Nieboer, Determination of nickel by differential pulse polarography at a dropping mercury electrode, *Analytical Chemistry*, 1980. 52(7): p. 1013-1020.
21. Tartarotti, F.O., M.F. De Oliveira, V.R. Balbo, and N.R. Stradiotto, Determination of nickel in fuel ethanol using a carbon paste modified electrode containing dimethylglyoxime, *Microchimica Acta*, 2006. 155(3-4): p. 397-401.
22. Saywell, L.G. and B.B. Cunningham, Determination of iron :Colorimetric o-phenanthroline method, *Industrial and Engineering Chemistry*, 1937. 9(2): p. 67-69.
23. Baumann, E.W., Colorimetric determination of iron(II) and iron(III) in glass, *The Analyst*, 1992. 117(5): p. 913-916.
24. Kitson, R.E., Simultaneous spectrophotometric determination cobalt, copper, and iron, *Analytical Chemistry*, 1950. 22(5): p. 664-667.
25. Beyer, M.E., A.M. Bond, and R.J.W. McLaughlin, Simultaneous polarographic determination of ferrous, ferric, and total iron in standard rocks, *Analytical Chemistry*, 1975. 47(3): p. 479-482.
26. Van den Berg, C.M.G. and Z.Q. Huang, Determination of iron in seawater using cathodic stripping voltammetry preceded by adsorptive collection with the hanging mercury drop electrode, *Journal of Electroanalytical Chemistry*, 1984. 177(1-2): p. 269-280.

27. Krasiejko, M. and Z. Marczenko, Separation and spectrophotometric determination of trace elements in high-purity cadmium, *Mikrochimica Acta*, 1975. 63(5-6): p. 585-596.
28. Mortatti, J., F.J. Krug, L. C. R. Pessenda, E. A. G. Zagatto and S. S. Jorgensen, Determination of iron in natural waters and plant material with 1,10-phenanthroline by flow injection analysis, *The Analyst*, 1982. 107: p. 659-663.
29. Adams, A. N., J.P. Mathews, and H.H. Schobert, The use of image analysis for the optimization of pre-baked anode formulation, *Light Metals*, 2002: p. 545-552.
30. Dieker, J.W. and W.E. Van Der Linden, Determination of iron(II) and iron(III) by flow injection and amperometric detection with a glassy carbon electrode, *Analytica Chimica Acta*, 1980. 114(C): p. 267-274.
31. Lynch, T. P., N. J. Kernoghan and J. N. Wilson., Speciation of metals in solution by flow injection analysis: Part 2. Determination of iron(III) and iron(II) in mineral process liquors by simultaneous injection into parallel streams, *Analyst*, 1984. 109: p. 843-846.
32. Kagenow, H. and A. Jensen, Differential kinetic analysis and flow injection analysis. Part 3. The (2.2.2) Cryptates of Magnesium, Calcium and Strontium, *Analytica Chimica Acta*, 1980. 114: p. 227-234.
33. Fernandez, A., M.A. Gomes-Nieto, M. D. Luque de Castro, and M. Valcarcel, A flow-injection manifold based on splitting the sample zone and a confluence point before a single detector unit, *Anal. Chim. Acta*, 1984. 165: p. 217-226.

34. Masoom, M., and A. Townshend, Determination of glucose in blood by flow injection analysis and an immobilized glucose oxidase column, *Anal. Chim. Acta*, 1985. 166: p. 111-118.
35. Apilux, A., W. Dungchai, W. Siangproh, N. Praphairaksit, C.S. Henry, and O. Chailapakul, Lab-on-paper with dual electrochemical/ colorimetric detection for simultaneous determination of gold and iron, *Analytical Chemistry*, 2010. 82(5): p. 1727-1732.
36. Kawakubo, S., K. Shimada, Y. Suzuki, and K. Hattori, An on-site colorimetric technique for routine determination of chromium, iron and copper in bath solutions for chromium(III) conversion coating, *Analytical Sciences*, 2011. 27(3): p. 341-344.
37. Goto, K., T. Komatsu, and T. Furukawa, Rapid colorimetric determination of manganese in waters containing iron. A modification of the formaldoxime method, *Analytica Chimica Acta*, 1962. 27(C): p. 335-338.
38. Hu, L., L. Nie, G. Xu, H. Shi, X. Xu, X. Zhang, and Z. Yan, Spectral properties of 4-(4-hydroxy-1-naphthylazo) benzenesulfonic acid and its application for colorimetric determination of trace Fe^{3+} , *RSC Advances*, 2014. 4(37): p. 19370-19374.
39. Rocha, V.G., C. Blanco, R. Santamaría, E.I. Diestre, R. Menéndez, and M. Granda, "An insight into pitch/substrate wetting behaviour. The effect of the substrate processing temperature on pitch wetting capacity," *Fuel*. 86(7-8), 2007, p. 1046-1052.

40. Tran, K.N., A.J. Berkovich, A. Tomsett, and S.K. Influence of sulfur and metal microconstituents on the reactivity of carbon anodes, *Bhatia, Energy and Fuels*, 2009. 23(4): p. 1909-1924.
41. Bamberger, E., Bel., Wasserstoffsuperoxyd als Lösungsmittel, *Monatshefte für Chemie*, 1919. 40(8-10): p. 411-416.
42. Shome, S.C., Gravimetric determination of copper, iron, aluminium and titanium with n-benzoylphenylhydroxylamine, *Analyst*, 1950. 75: p. 27-32.
43. Shome, S.C., Colorimetric determination of vanadium with benzoylphenylhydroxylamine, *Analytical Chemistry*, 1951. 23(8): p. 1186-1188.
44. Priyadarshini, U. and S.G. Tandon, Spectrophotometric determination of vanadium(V) with N-benzoyl-N-phenylhydroxylamine, *Analytical Chemistry*, 1961. 33(3): p. 435-438.
45. Fukasawa, T., S. Miyata, and S. Matsunaga, Rapid and sensitive determination of total vanadium in airborne particulates by an extraction-spectrometric method with N-benzoyl-N-phenylhydroxylamine, *Analytica Chimica Acta*, 1981. 130(2): p. 353-360.
46. Sandell, E.B., Determination of chromium, vanadium, and molybdenum in silicate rocks, *Industrial and Engineering Chemistry*, 1936. 8(5): p. 336-341.

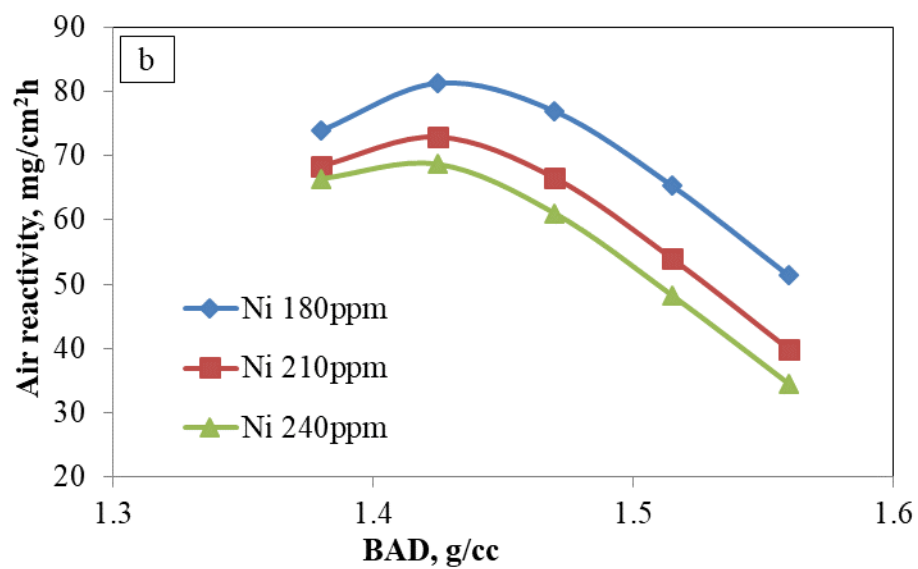
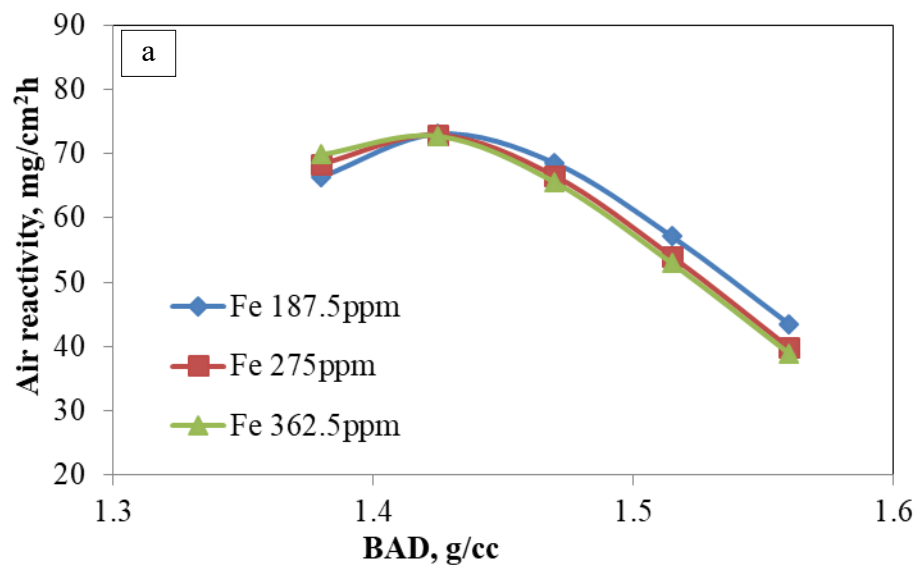
47. Belitskus, D. and D.J. Danka, Comprehensive determination of effects of calcined petroleum coke properties on aluminum reduction cell anode properties, *Light Metals*, 1989. p. 429-439.
48. Hume, S. M., Anode reactivity : Influence of raw material properties (Sierre [Suisse]: R & D Carbon Ltd., 1999), xi, p. 433.
49. An American National Standard, ASTM D5502-00 (Reapproved 2005), Standard test method for apparent density by physical measurements of manufactured anode and cathode carbon used by the aluminum industry, 2010.
50. An American National Standard, ASTM D6120-97 (Reapproved 2007), Standard test method for electrical resistivity of anode and cathode carbon material at room temperature, 2010.
51. Fischer W. K. and R. Perruchoud, Determining prebaked anode properties for aluminum production, *JOM*, 1987.39(11): p. 43-45.
52. Marsh, H., Introduction to carbon science, Butterworth-Heinemann, 1989.
53. Sadler, B.A. and S.H.Algie, Sub-surface carboxy reactivity testing of anode carbon, *Light Metals*, 1992: p. 649-658.
54. An American National Standard, ASTM D6558 - 00a, Standard Test Method for Determination of TGA CO₂ Reactivity of Baked Carbon Anodes and Cathode Blocks, 2010.

55. An American National Standard, ASTM D6559 - 00a, Standard Test Method for Determination of TGA Air Reactivity of Baked Carbon Anodes and Cathode Blocks, 2010.
56. Eidet, T., M. Sørli, and J. Thonstad, Effects of Sulfur, Nickel and Vanadium on the Air and CO₂ Reactivity of Cokes. *Light Metals*, 1997: p. 436-437.
57. Houston, G. J. and H.A. Oye, Reactivity testing of anode carbon materials, *Light Metals*, 1985: p. 885-899.
58. Lee, J.M., J.J. Baker, J.G. Rolle, and R. Llerena, Characterization of green and calcined coke properties used for aluminum anode-grade carbon, ACS Division of Fuel Chemistry, Preprints, 1998. 43(2): p. 271-275.
59. Nian-Bing, Z., L. Zhi-Ying, L. Shi-Yong, H. Peng, and L. Wei, Effect of Trace Nickel Element on Carbon Anode Reactivity, *Nonferrous Metals (Extractive Metallurgy)*, 2013. 5: p. 24-26.
60. Ugarković, D. and M. Legin, Alteration of metallic microconstituents in petroleum coke by high temperature treatment, *Carbon*, 1986. 24(2): p. 195-201.
61. Wang, W and A.P. Watkinson, Iron Sulphid and Coke Fouling from Sour Oils: Review and Initial Experiments, Proceedings of International Conference on Heat Exchanger Fouling and Cleaning, Crete Island, Greece, June 5-10 2011: p. 23- 30.

62. Parthiban, T., R. Ravi, and N. Kalaiselvi, Exploration of artificial neural network [ANN] to predict the electrochemical characteristics of lithium-ion cells, *Electrochimica Acta*, 2007. 53(4): p. 1877-1882.
63. Milewski, J. and K. Świrski, Modelling the SOFC behaviours by artificial neural network, *International Journal of Hydrogen Energy*, 2009. 34(13): p. 5546-5553.
64. Madić M.J. and V.J. Marinković, Assessing the sensitivity of the artificial neural network to experimental noise: a case study. *FME Transactions*, 2010. 38: p. 189-195.
65. Bhattacharyay, D., D. Kocaefe, Y. Kocaefe, and B. Morais, An artificial neural network model for predicting the CO₂ reactivity of carbon anodes used in the primary aluminum production, *Neural computing and Applications*, 2017. 28(3): p. 553-563.
66. Simanjuntak, S., M. K.Cavanaugh, D. S.Gandel, M. A.Easton, M. A.Gibson, and N.Biribilis. The influence of iron, manganese, and zirconium on the corrosion of magnesium: An artificial neural network approach, *Corrosion*, 2015. 71(2): p. 199-208.
67. Berezin A. I., P. V. Polaykov, O. O.Rodnov, V. A. Klykov, and V. L., Krylov, Improvement of green anodes quality on the basis of the neural network model of the carbon plant workshop, *Light Metals*, 2002: p. 605–608.
68. Sarkar, A., D. Kocaefe, Y. Kocaefe, D. Bhattacharyay, B. Morais, and P. Coulombe, Effect of coke granulometry on the properties of carbon anodes based on

- experimental study and ANN analysis, *Journal of Materials Science Research (JMSR)*, 2016. 5(4): p. 63-78.
69. Chamam, Y., D. Kocaefe, Y. Kocaefe, D. Bhattacharyay, and B. Morais, Effect of heating rate during baking on the properties of industrial carbon anodes used in aluminum industry, *Light Metals*, 2016: p. 947-951.
70. Bhattacharyay D, D. Kocaefe, Y. Kocaefe, and B. Morrais, Comparison of linear multivariable, partial least square regression, and artificial neural network analyses to study the effect of different parameters on anode properties, *Light Metals*, 2015: p. 1129-1134.
71. Bhattacharyay, D., D. Kocaefe, Y. Kocaefe, B. Morrais, and m. Gagnon, Application of the artificial neural network (ANN) in predicting anode properties, *Light Metals*, 2013: p. 1189-1194.
72. Perales, E., E. Chorro, V. Viqueira, and F.M. Martínez-Verdú, Reproducibility comparison among multiangle spectrophotometers, *Color Research and Application*, 2013. 38(3): p. 160-167.

Appendix



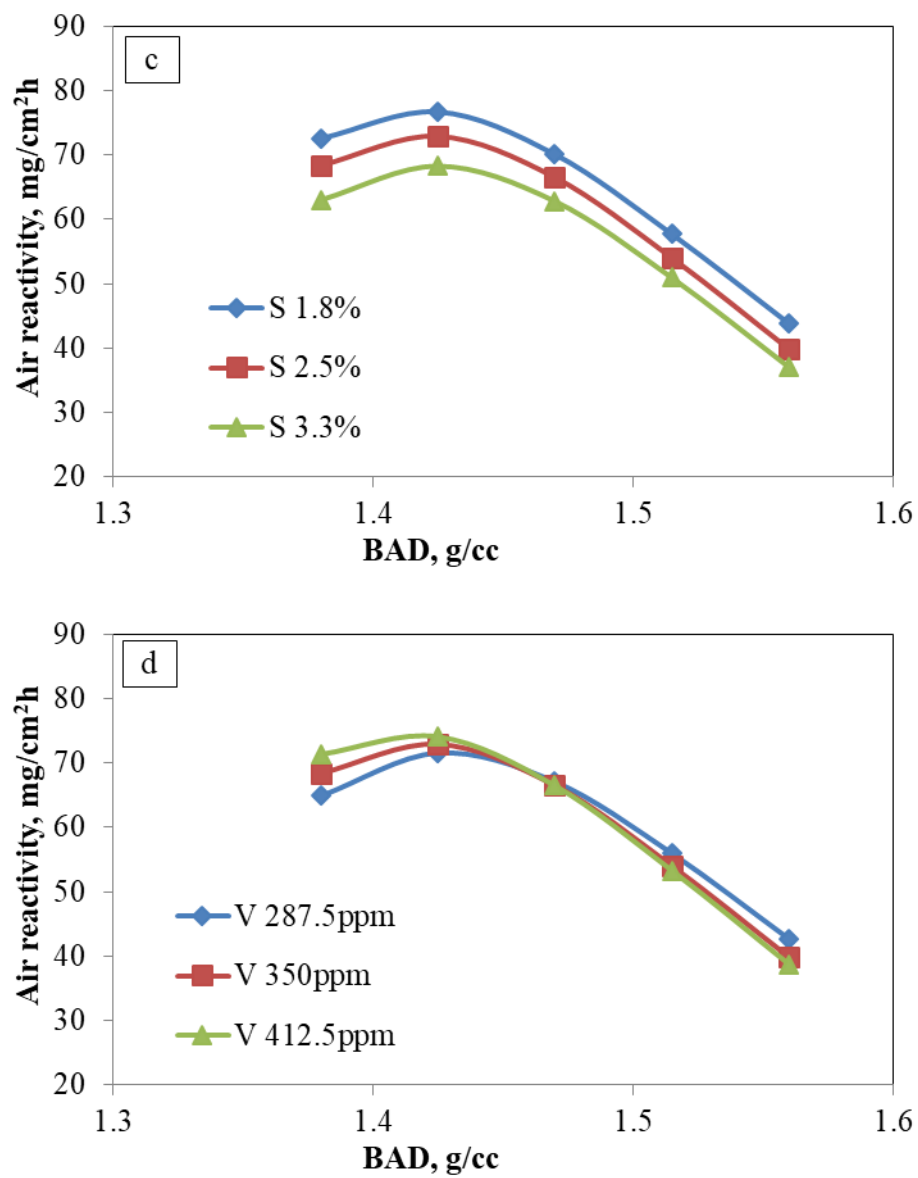
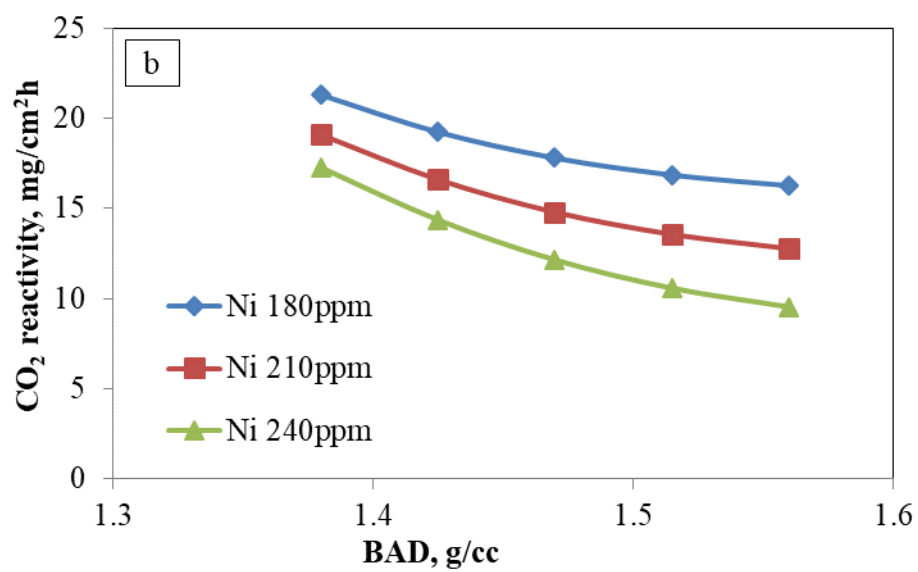
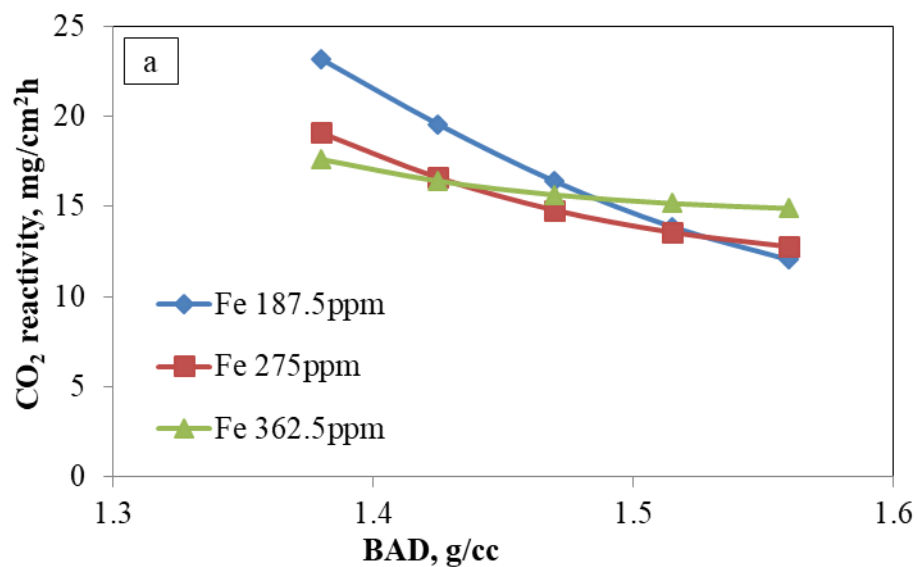


Figure A.1: The effect of BAD on air reactivity at different concentrations of (a) iron, (b) nickel, (c) sulfur, (d) vanadium (one impurity has been varied while others were maintained at their typical levels)



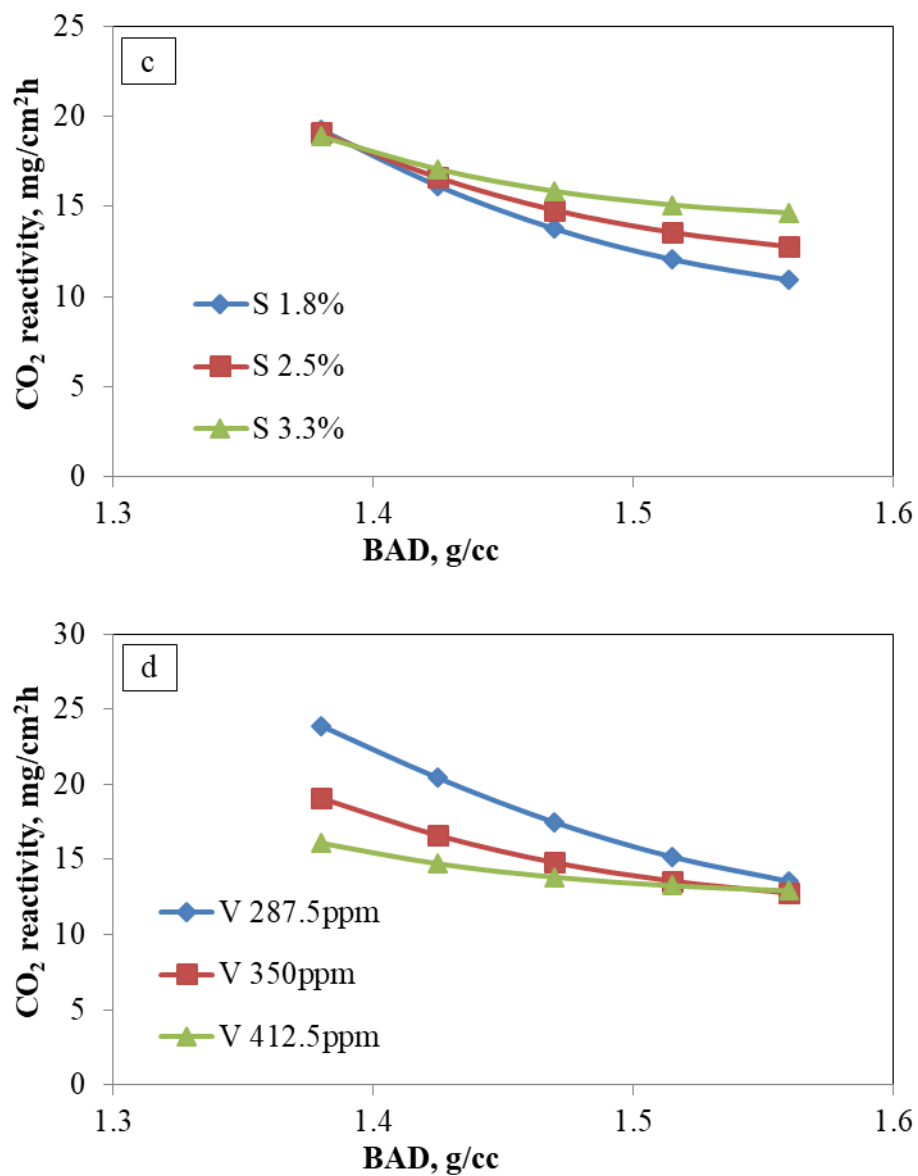


Figure A.2: The effect of BAD on CO₂ reactivity at different concentrations of (a) iron, (b) nickel, (c) sulfur, (d) vanadium (one impurity has been varied while others were maintained at their typical levels)

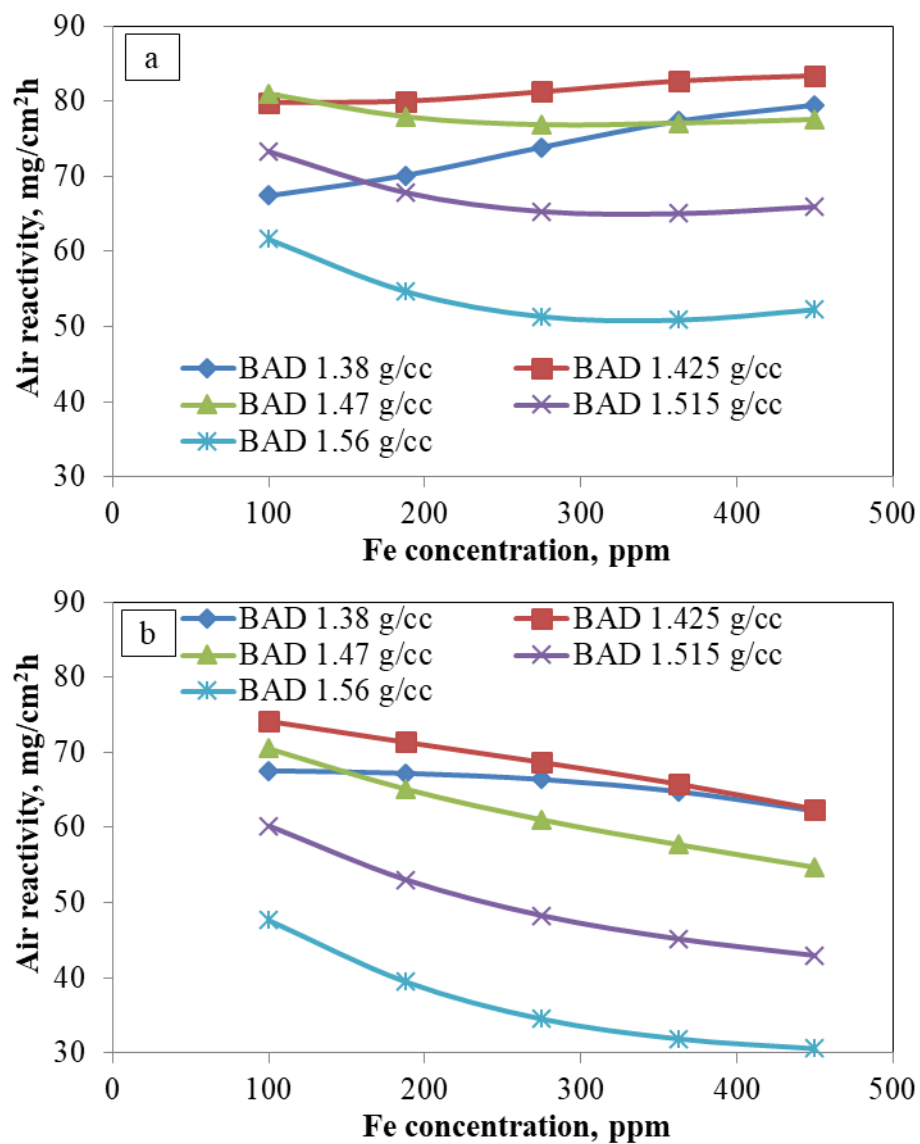


Figure A.3: The effect of the concentrations of iron on air reactivity at different BAD for (a) low and (b) high amount of nickel (other impurities, i.e., V and S, were maintained at their typical levels)

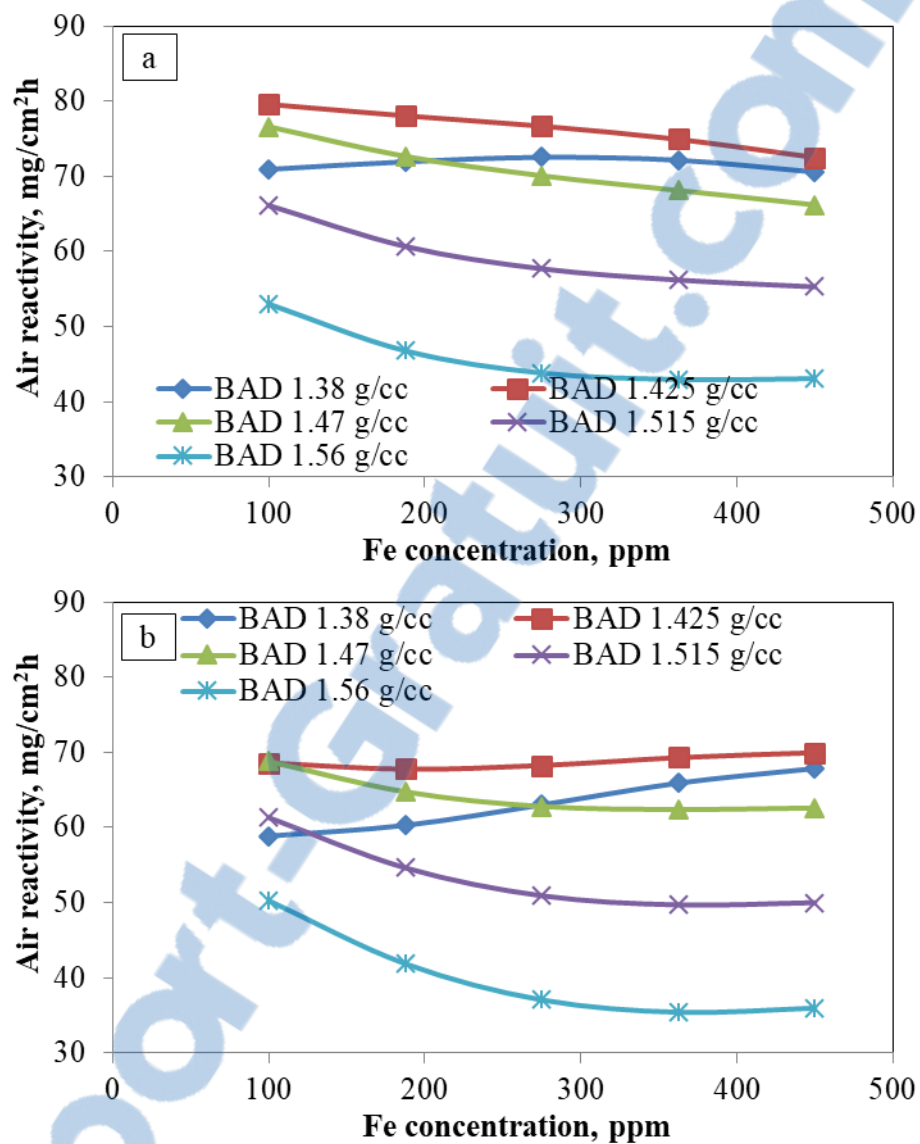


Figure A.4: The effect of concentrations of iron on air reactivity at different BAD for (a) low and (b) high amount of sulfur (other impurities, i.e., Ni and V, were maintained at their typical levels)

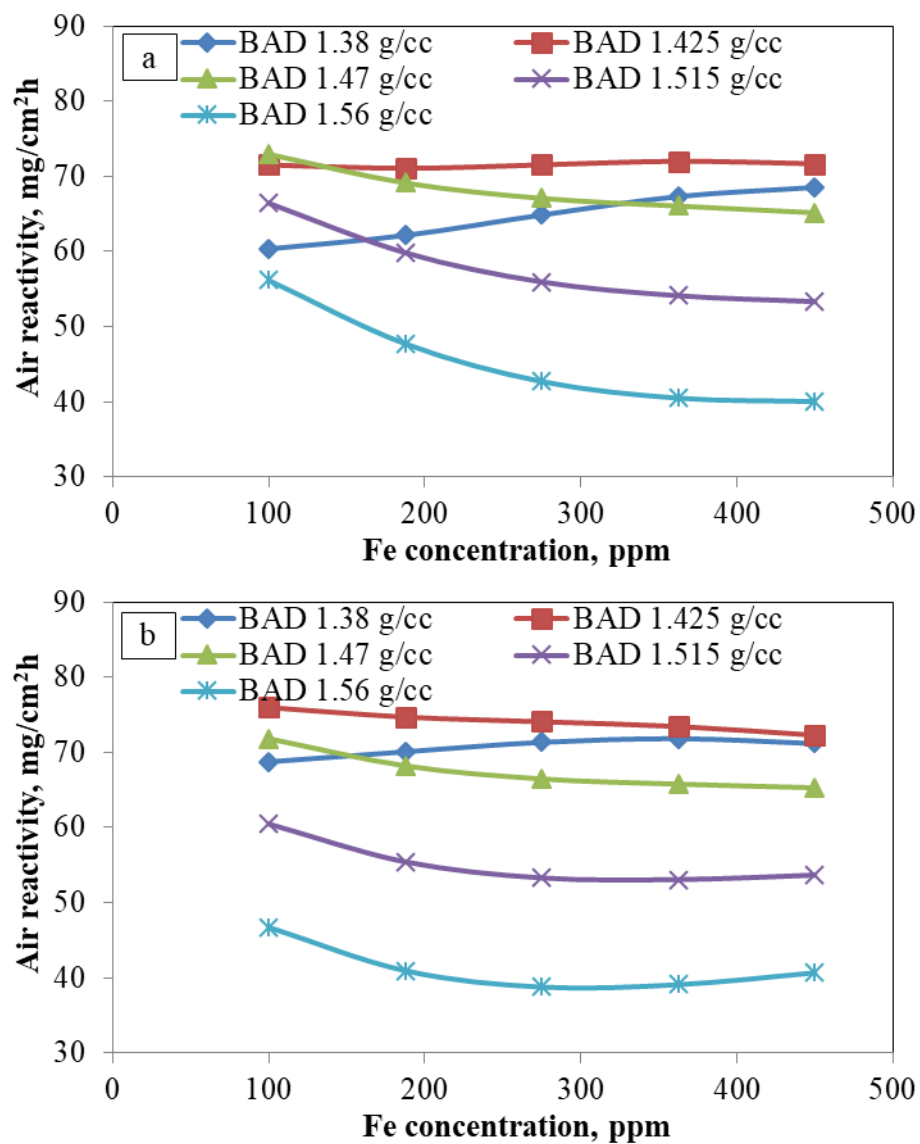


Figure A.5: The effect of concentrations of iron on air reactivity at different BAD for (a) low and (b) high amount of vanadium (other impurities, i.e., Ni and S, were maintained at their typical levels)

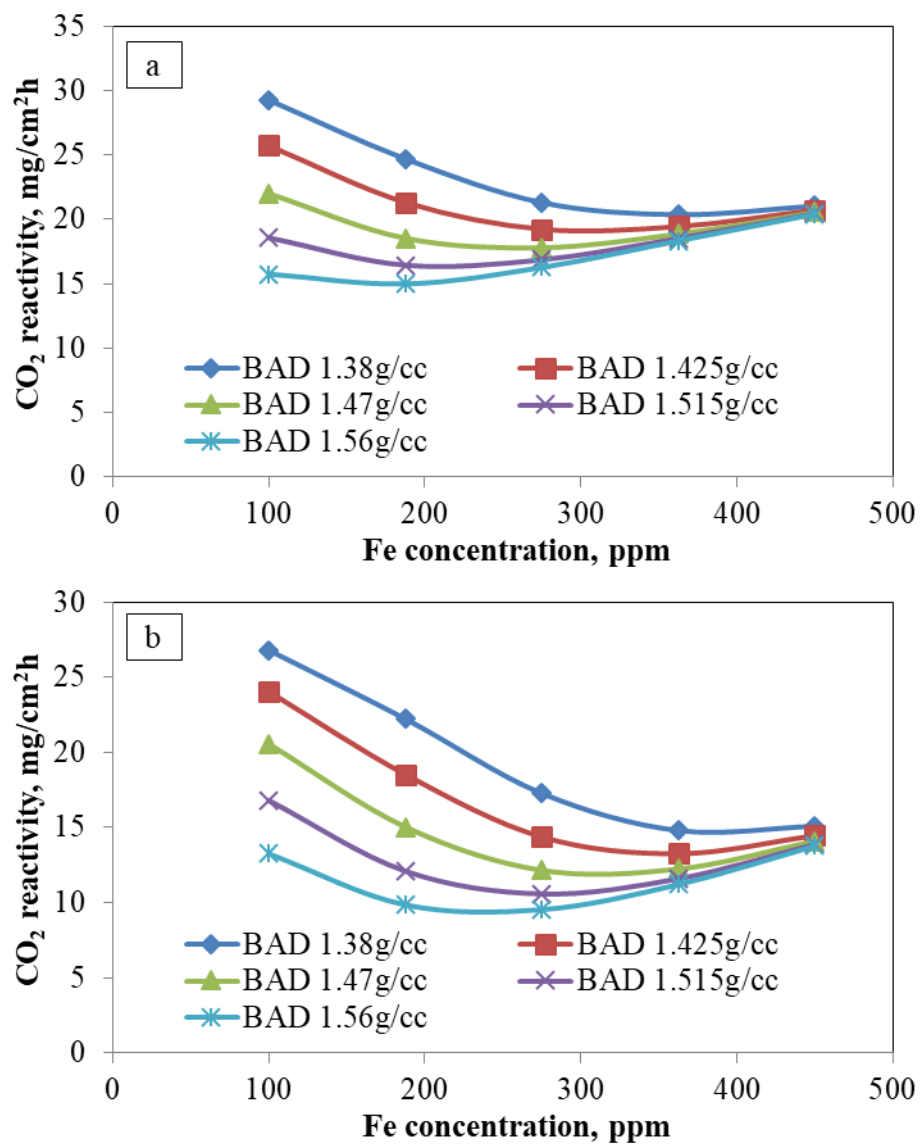


Figure A.6: The effect of concentrations of iron on CO₂ reactivity at different BAD for (a) low and (b) high amount of nickel (other impurities, i.e., V and S, were maintained at their typical levels)

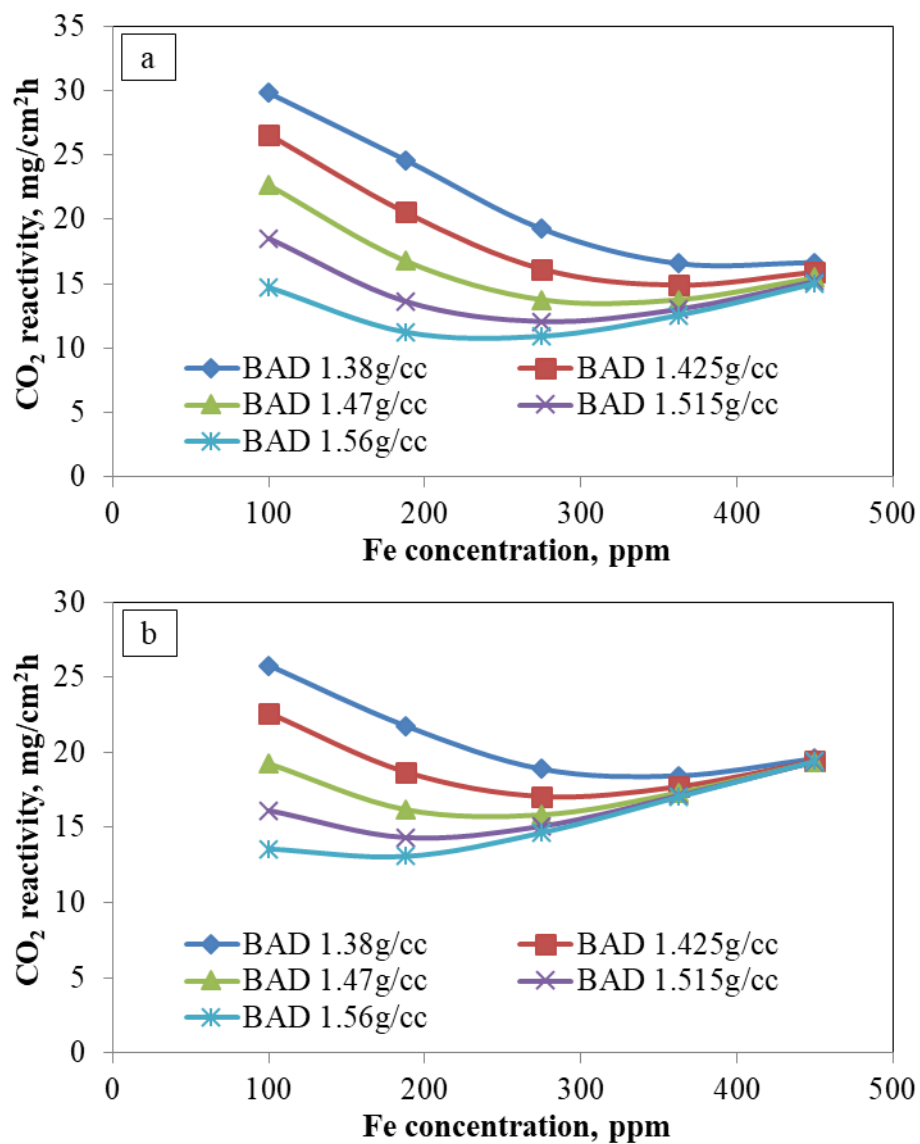


Figure A.7: The effect of concentrations of iron on CO₂ reactivity at different BAD for (a) low and (b) high amount of sulfur (other impurities, i.e., Ni and V, were maintained at their typical levels)

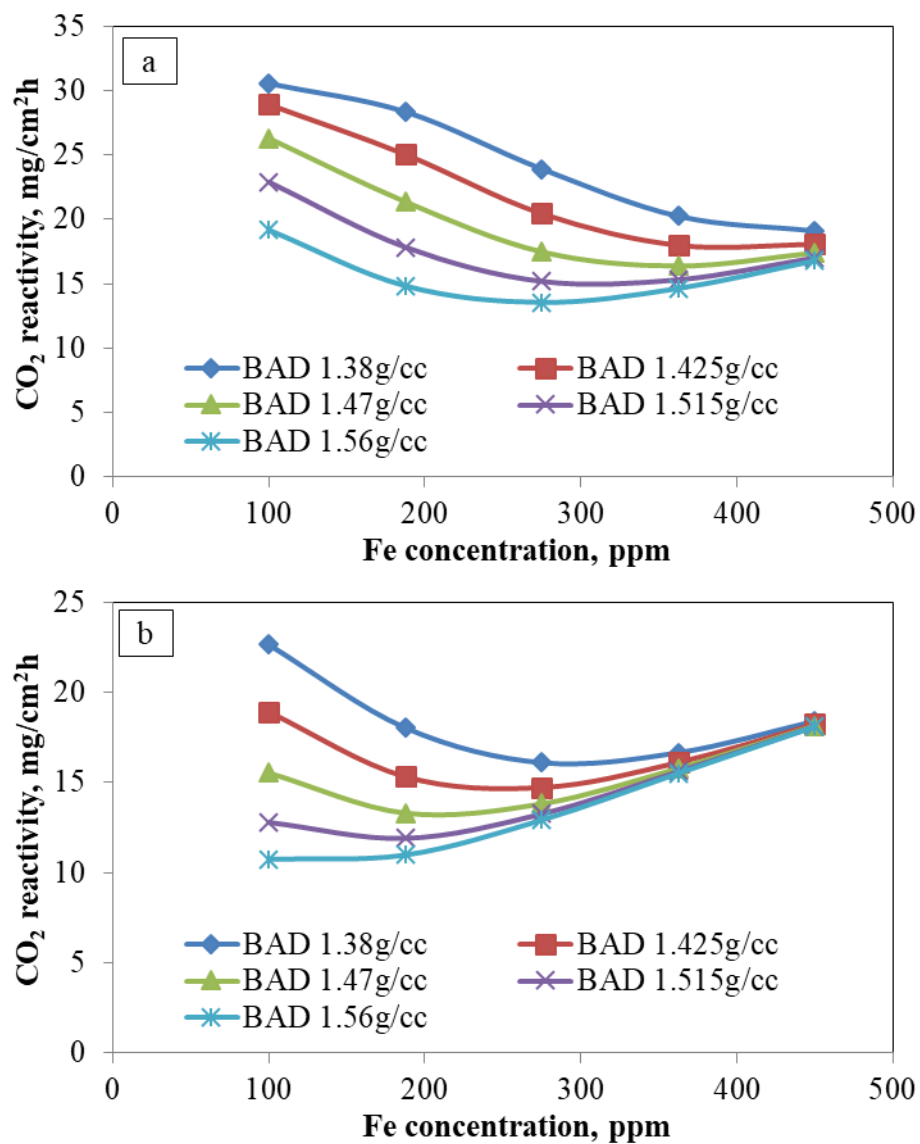


Figure A.8: The effect of concentrations of iron on CO₂ reactivity at different BAD for (a) low and (b) high amount of vanadium (other impurities, i.e., Ni and S, were maintained at their typical levels)

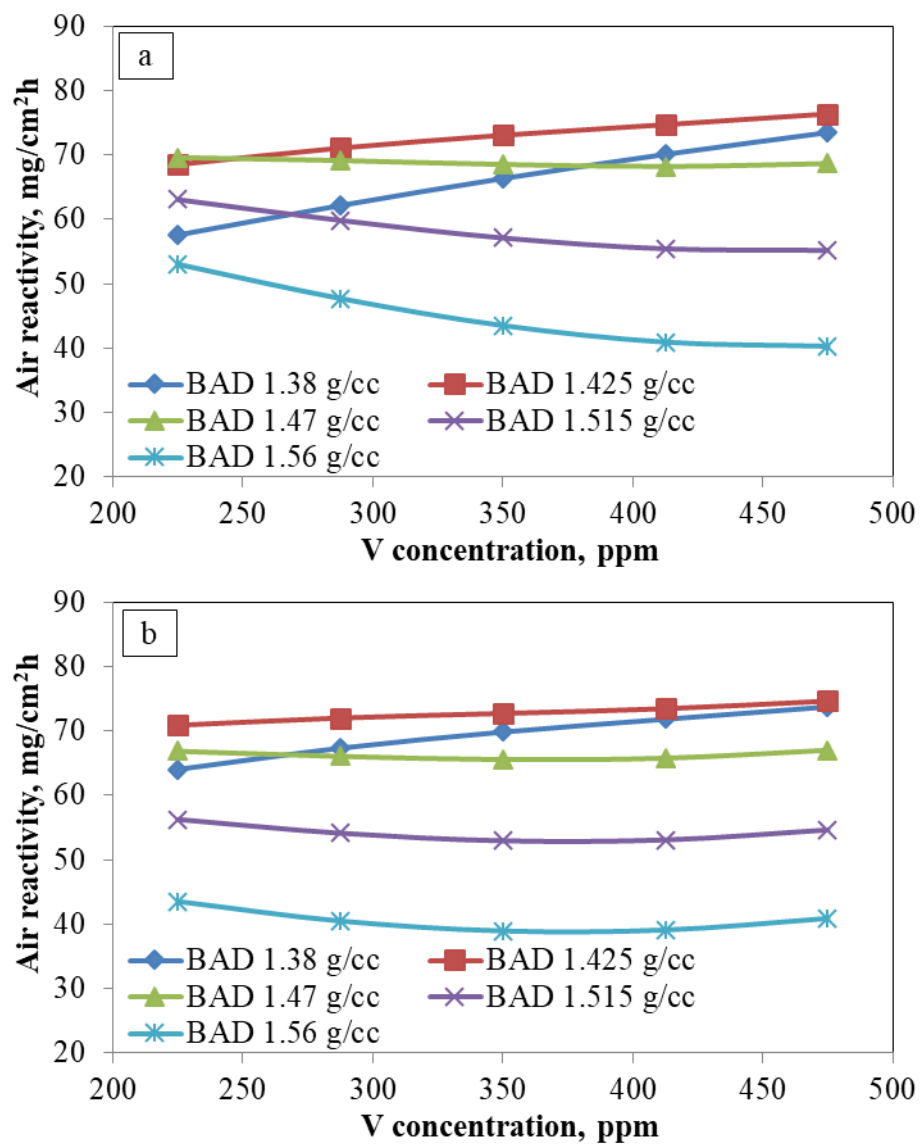


Figure A.9: The effect of concentrations of vanadium on air reactivity at different BAD for (a) low and (b) high amount of iron (other impurities, i.e., Ni and S, were maintained at their typical levels)

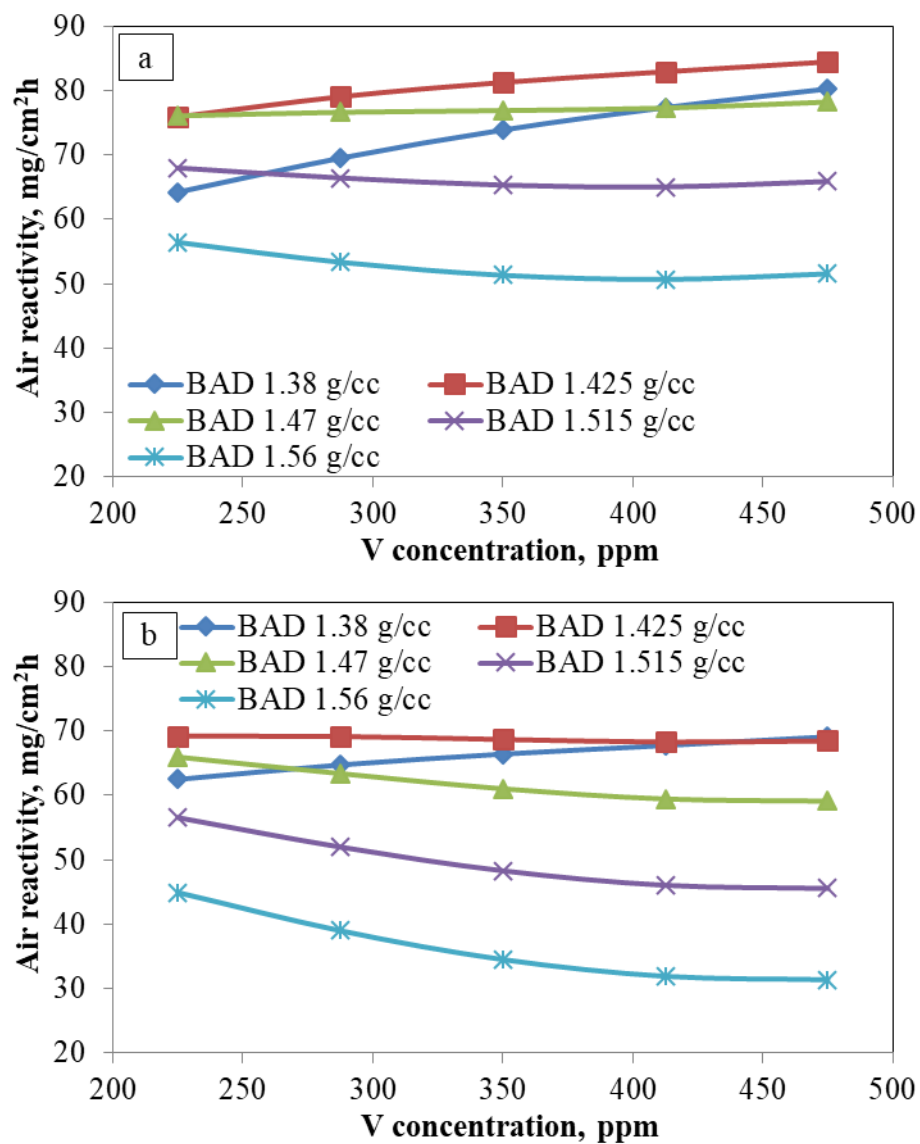


Figure A.10: The effect of concentrations of vanadium on air reactivity at different BAD for (a) low and (b) high amount of nickel (other impurities, i.e., Fe and S, were maintained at their typical levels)

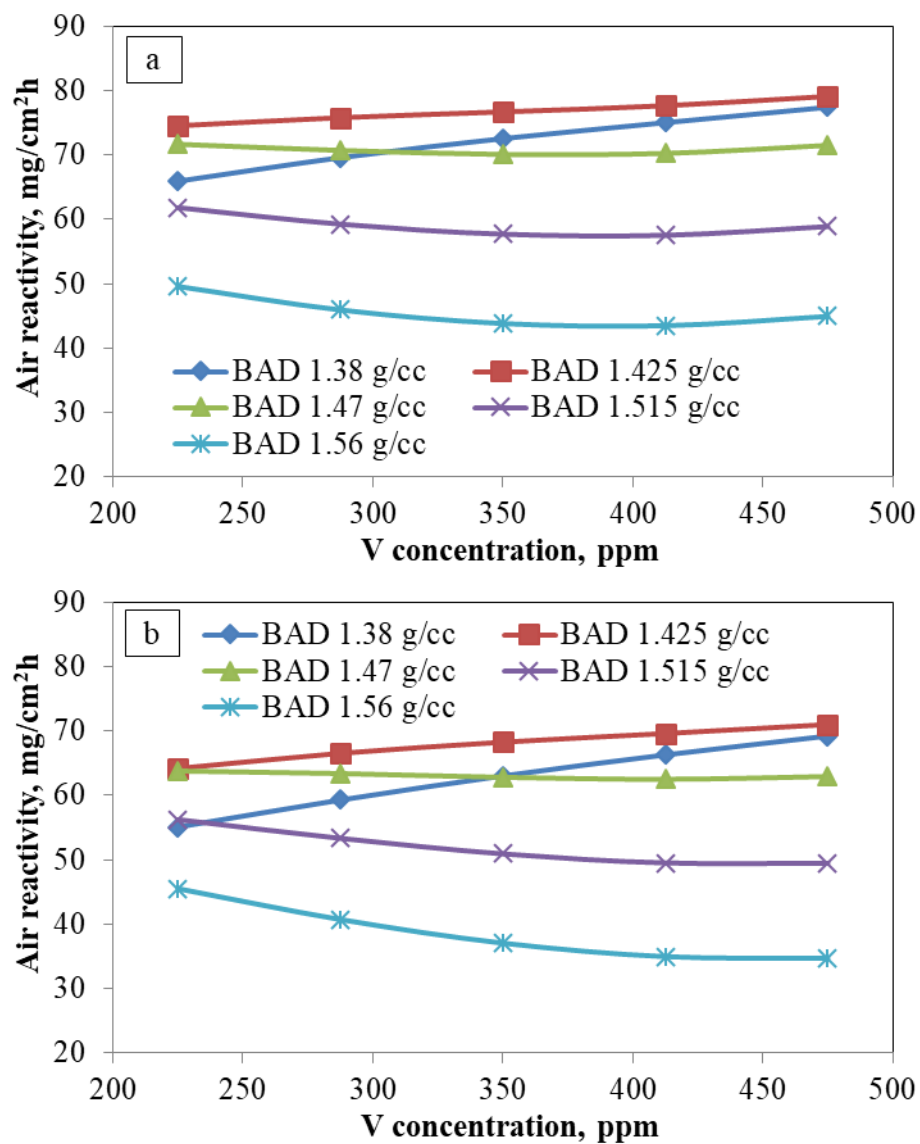


Figure A.11: The effect of concentrations of vanadium on air reactivity at different BAD for (a) low, (b) high amount of sulfur (other impurities, i.e., Fe and Ni, were maintained at their typical levels)

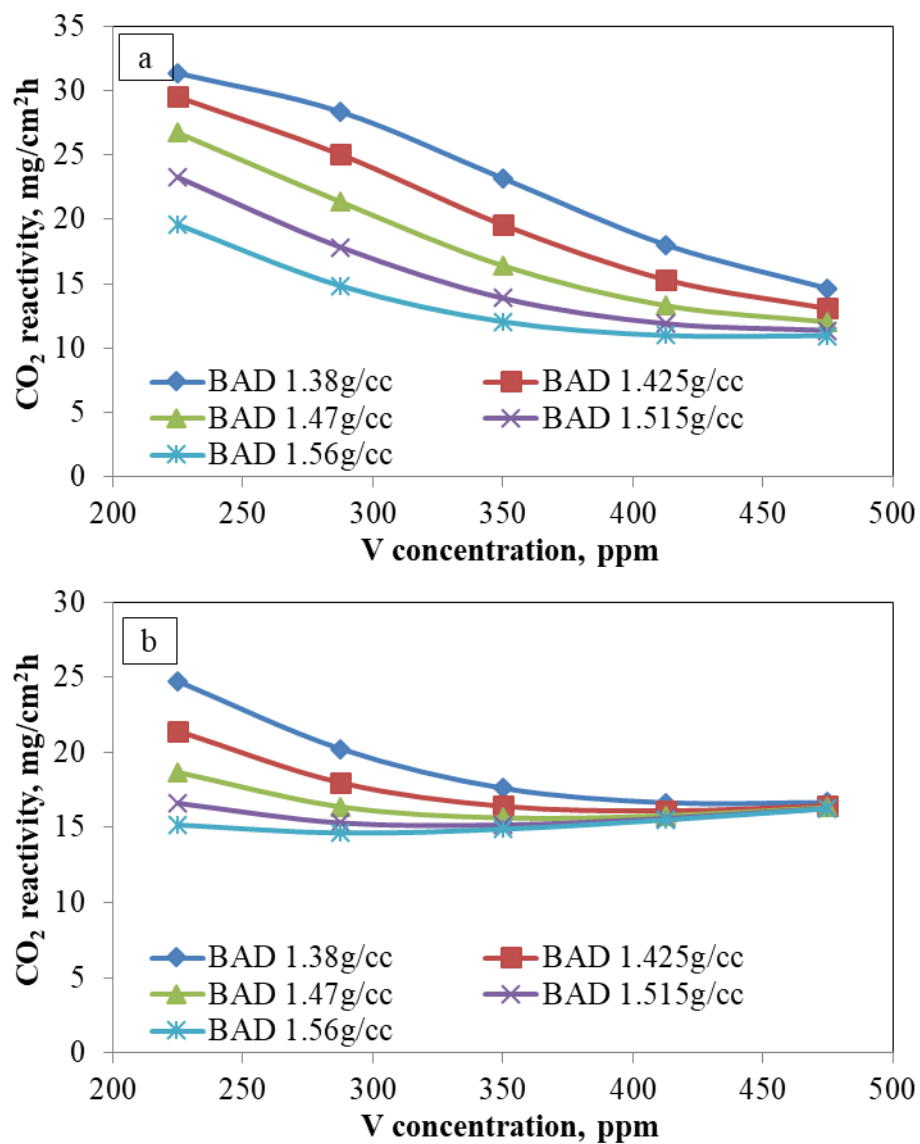


Figure A.12: The effect of concentrations of vanadium on CO₂ reactivity at different BAD for (a) low and (b) high amount of iron (other impurities, i.e., Ni and S, were maintained at their typical levels)

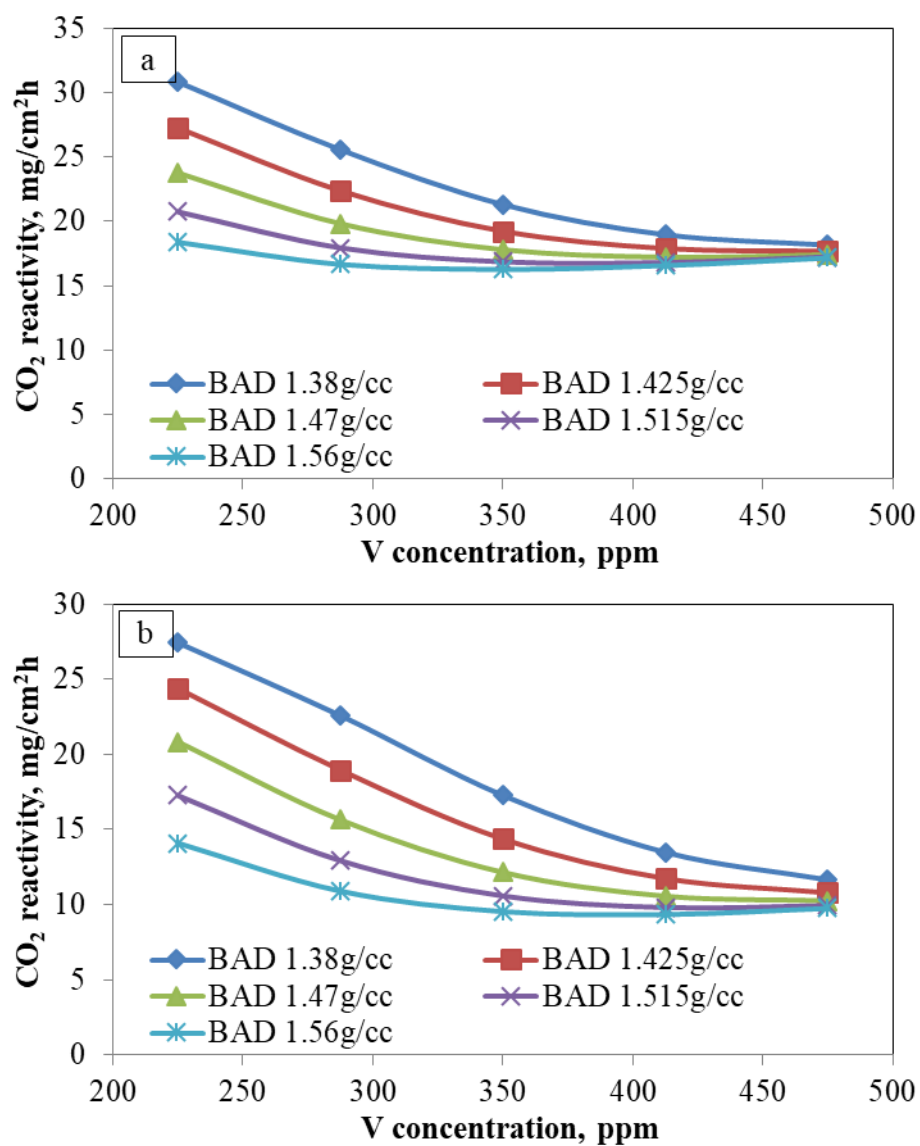


Figure A.13: The effect of concentrations of vanadium on CO₂ reactivity with different BAD for (a) low and (b) high amount of nickel (other impurities, i.e., Fe and S, were maintained at their typical levels)

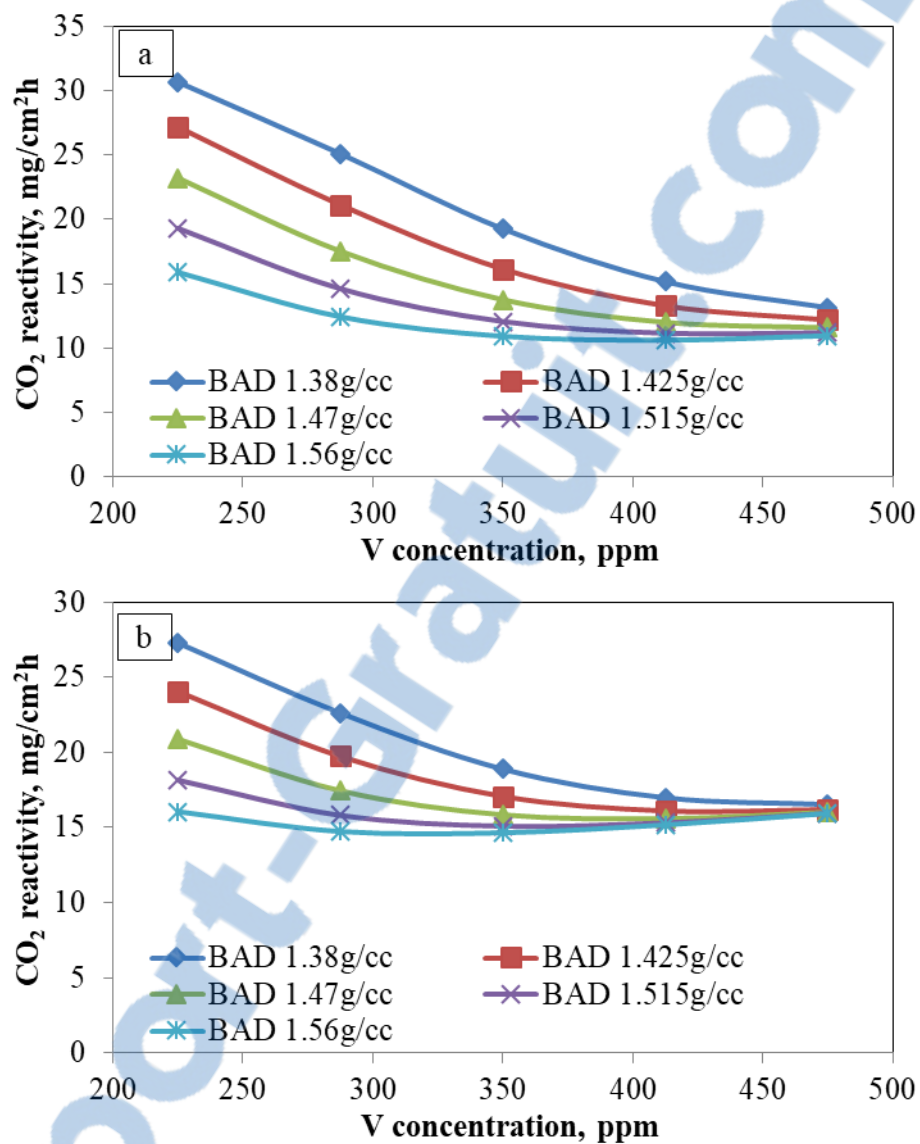


Figure A.14: The effect of concentrations of vanadium on CO₂ reactivity at different BAD for (a) low and (b) high amount of sulfur (other impurities, i.e., Fe and Ni, were maintained at their typical levels)

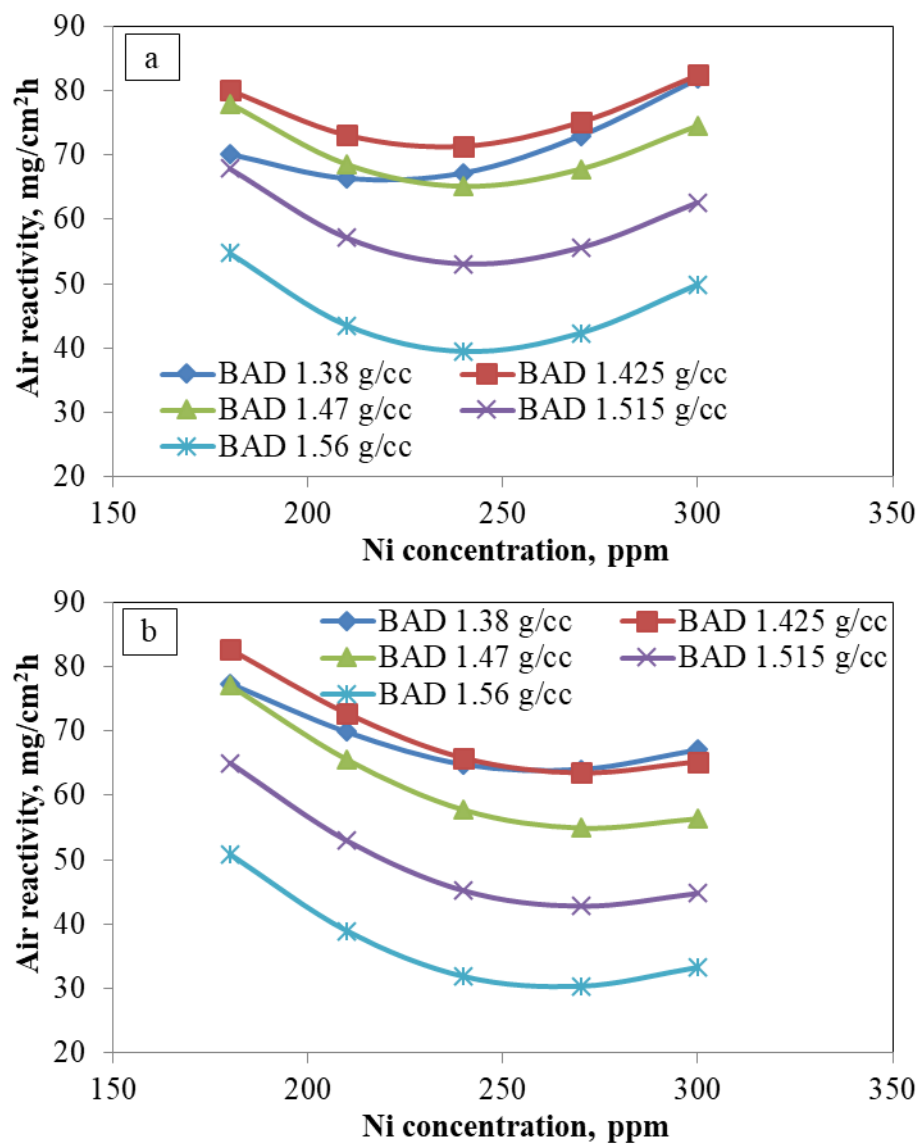


Figure A.15: The effect of concentrations of nickel on air reactivity at different BAD for (a) low and (b) high amount of iron (other impurities, i.e., V and S, were maintained at their typical levels)

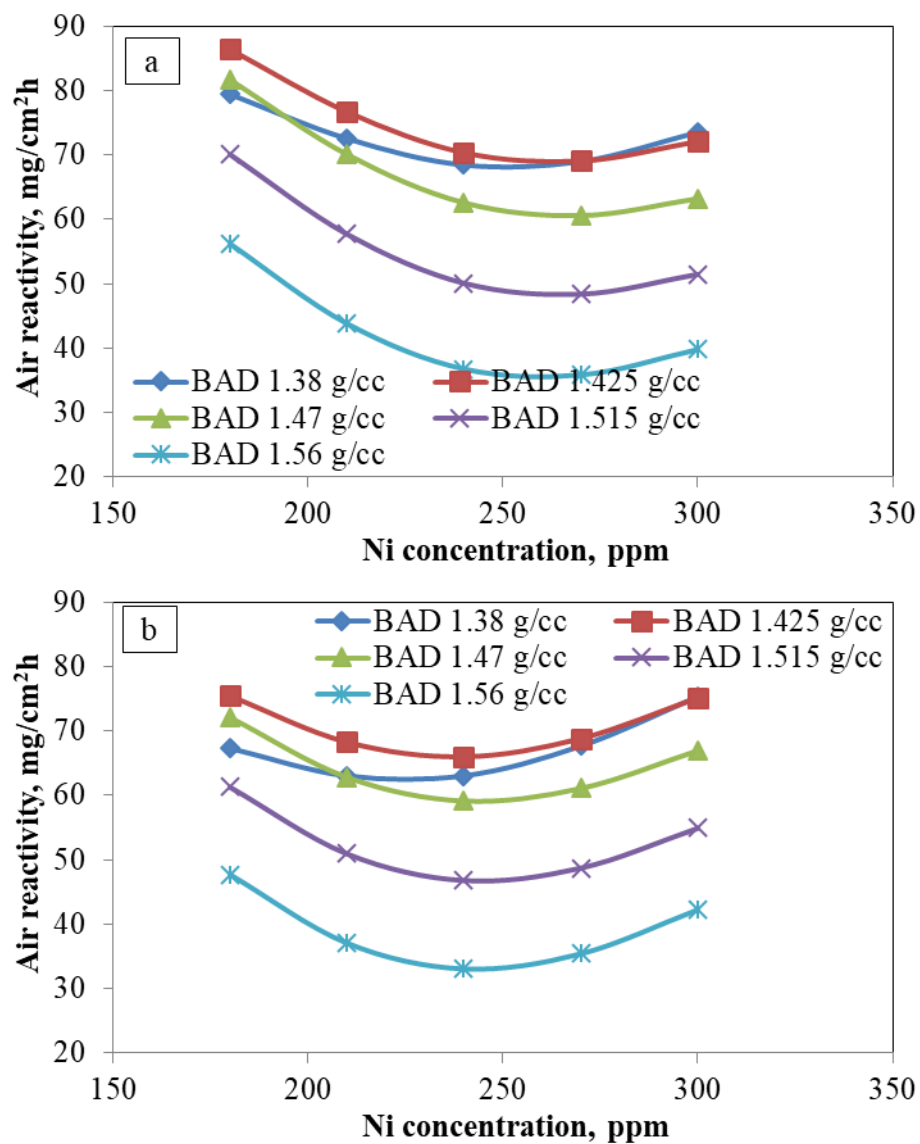


Figure A.16: The effect of concentrations of nickel on air reactivity at different BAD for (a) low and (b) high amount of sulfur (other impurities, i.e., Fe and V, were maintained at their typical levels)

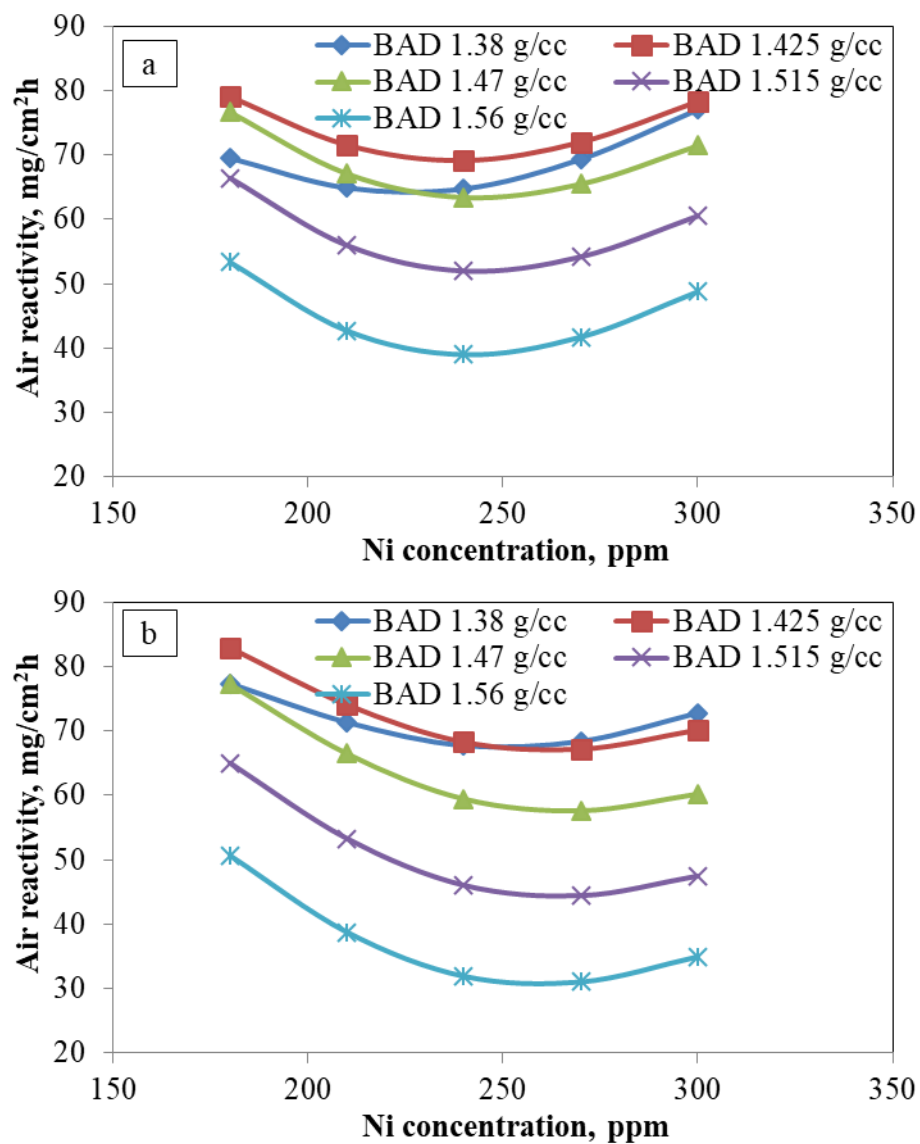


Figure A.17: The effect of concentrations of nickel on air reactivity at different BAD for (a) low and (b) high amount of vanadium (other impurities, i.e., Fe and S, were maintained at their typical levels)

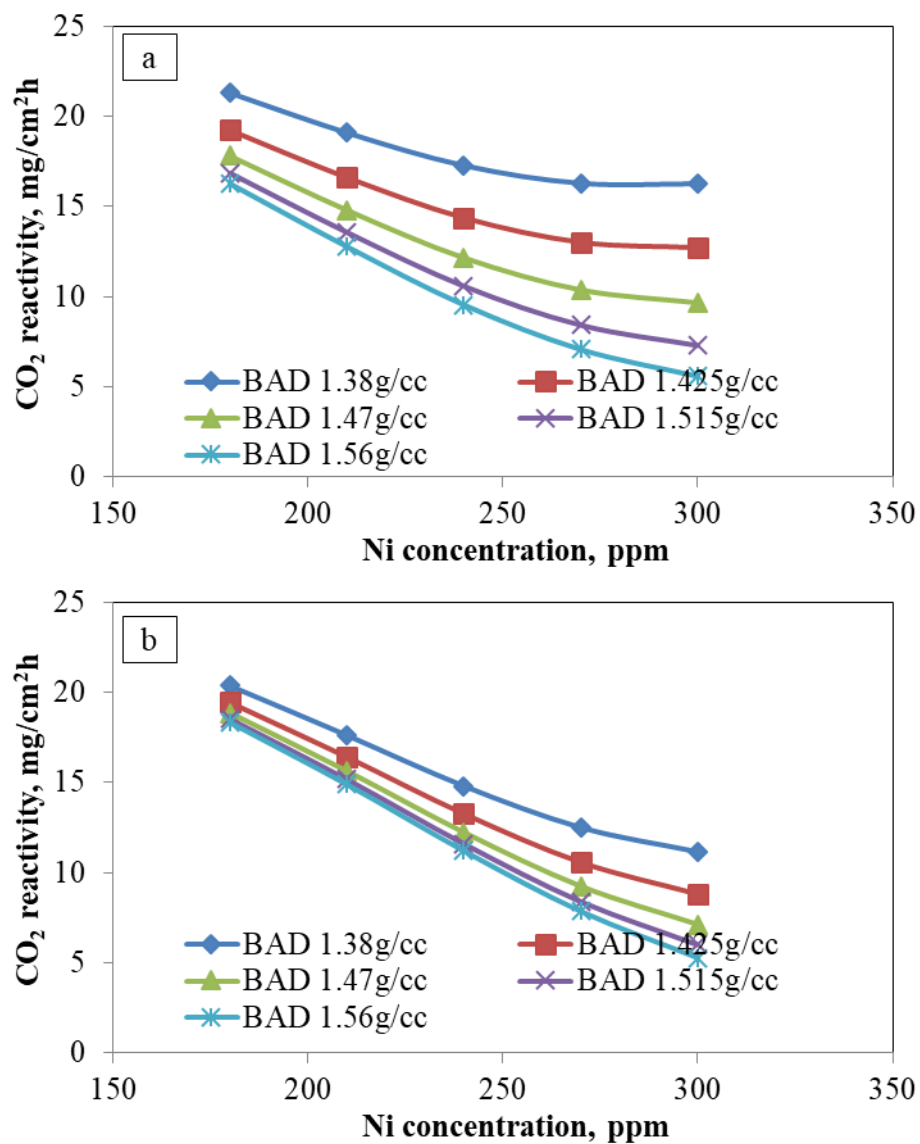


Figure A.18: The effect of concentrations of nickel on CO₂ reactivity at different BAD for (a) low and (b) high amount of iron (other impurities, i.e., V and S, were maintained at their typical levels)

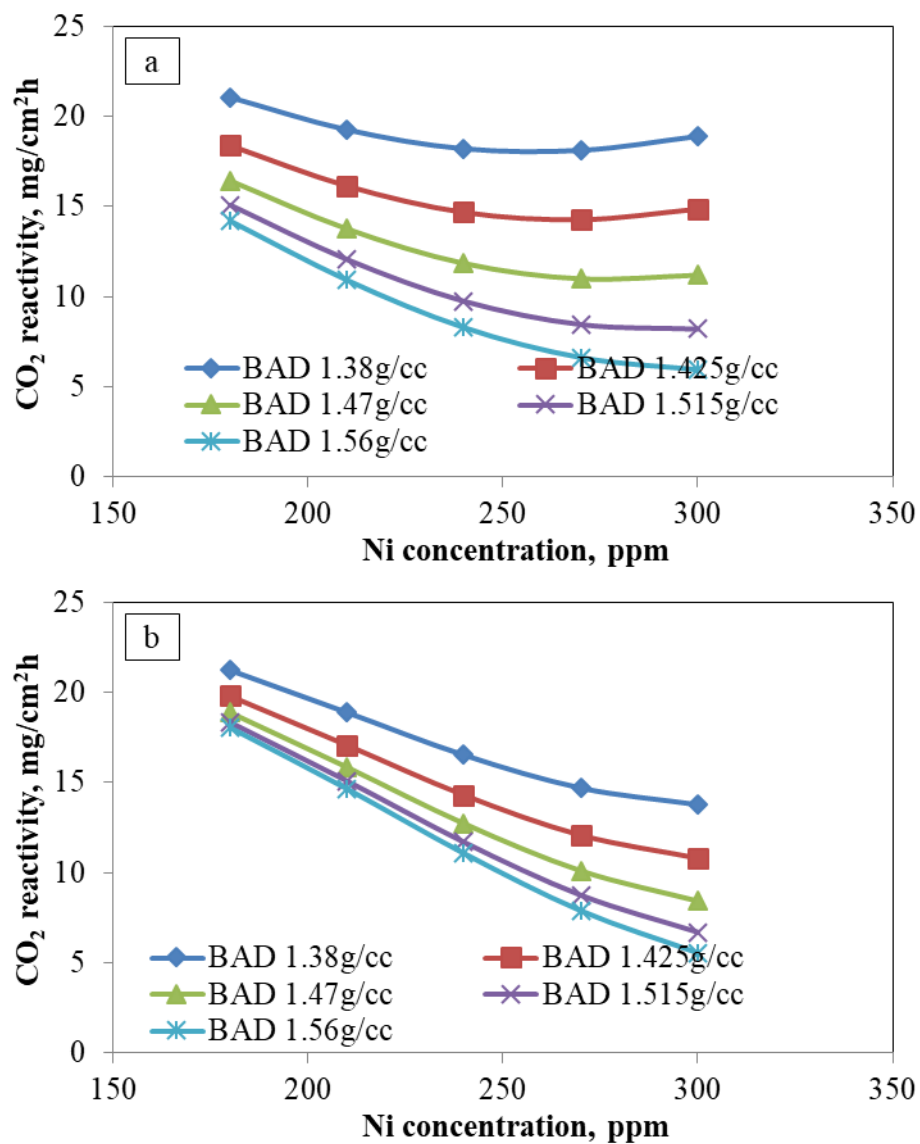


Figure A.19: The effect of concentrations of nickel on CO₂ reactivity at different BAD for (a) low and (b) high amount of sulfur (other impurities, i.e., Fe and V, were maintained at their typical levels)

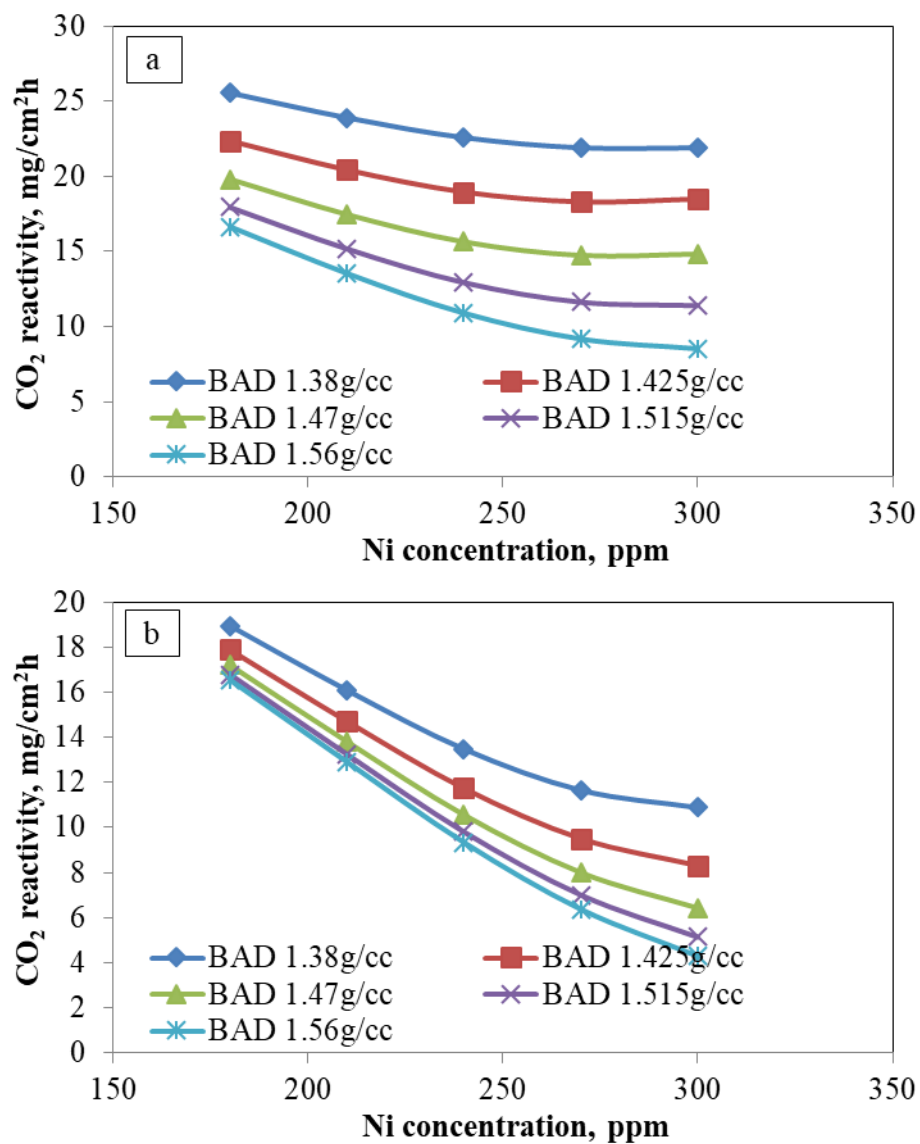


Figure A.20: The effect of concentrations of nickel on CO₂ reactivity at different BAD for (a) low and (b) high amount of vanadium (other impurities, i.e., Fe and S, were maintained at their typical levels)

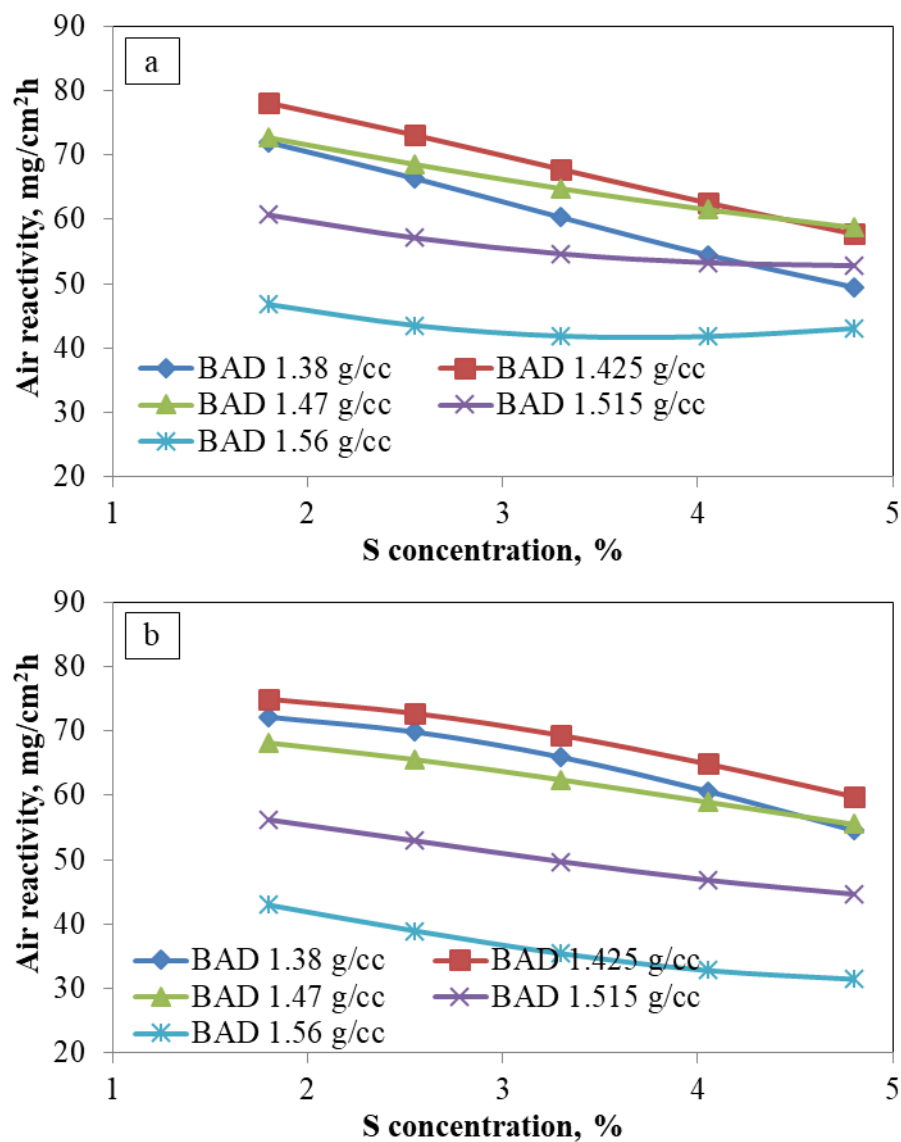


Figure A.21: The effect of concentrations of sulfur on air reactivity at different BAD for (a) low and (b) high amount of iron (other impurities, i.e., V and Ni, were maintained at their typical levels)

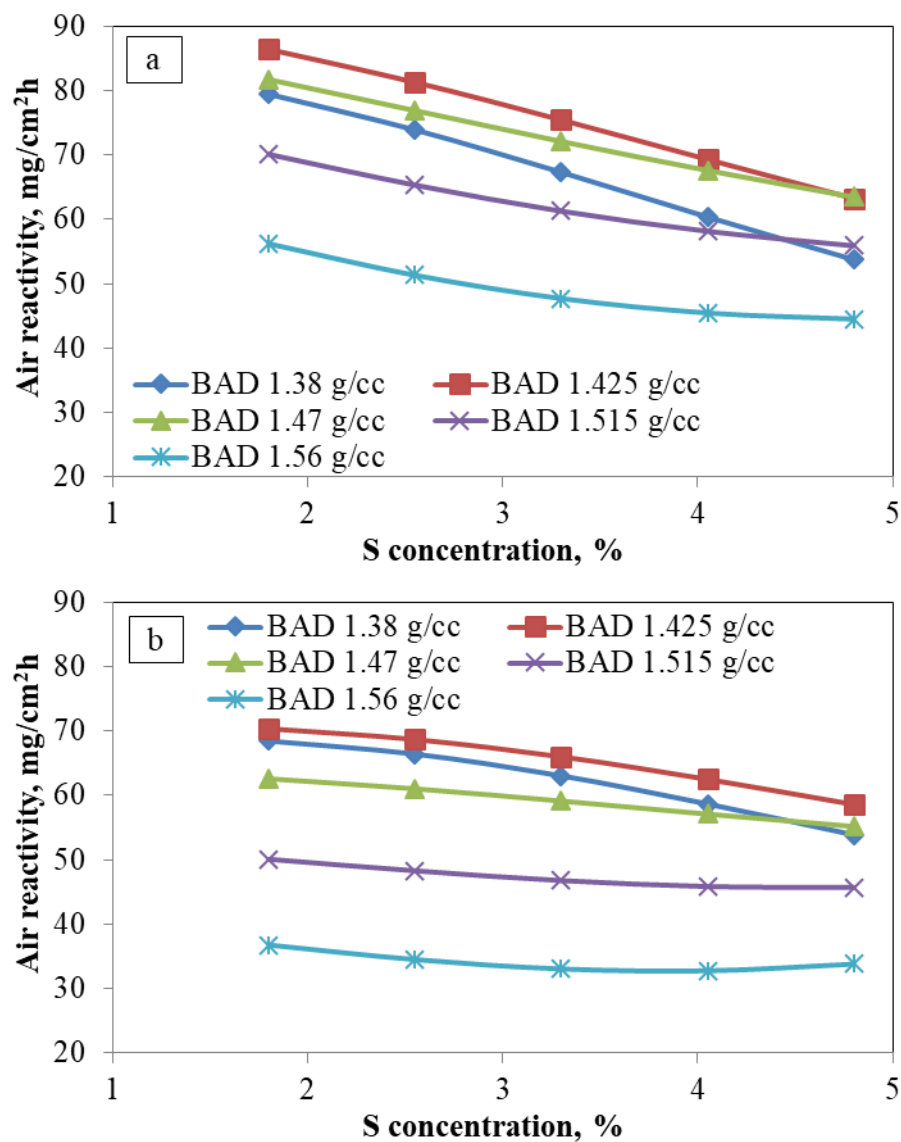


Figure A.22: The effect of concentrations of sulfur on air reactivity at different BAD for (a) low and (b) high amount of nickel (other impurities, i.e., Fe and V, were maintained at their typical levels)

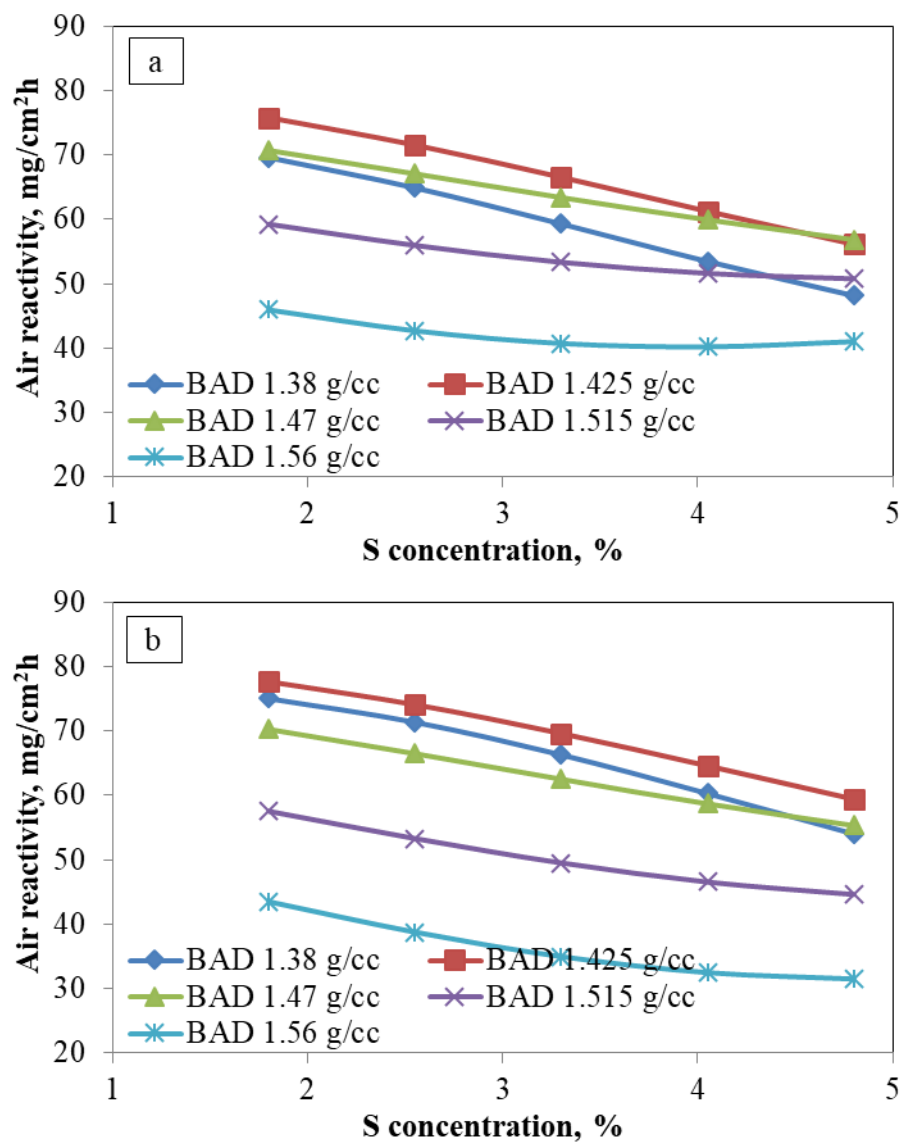


Figure A.23: The effect of concentrations of sulfur on air reactivity at different BAD for (a) low and (b) high amount of vanadium (other impurities, i.e., Fe and Ni, were maintained at their typical levels)

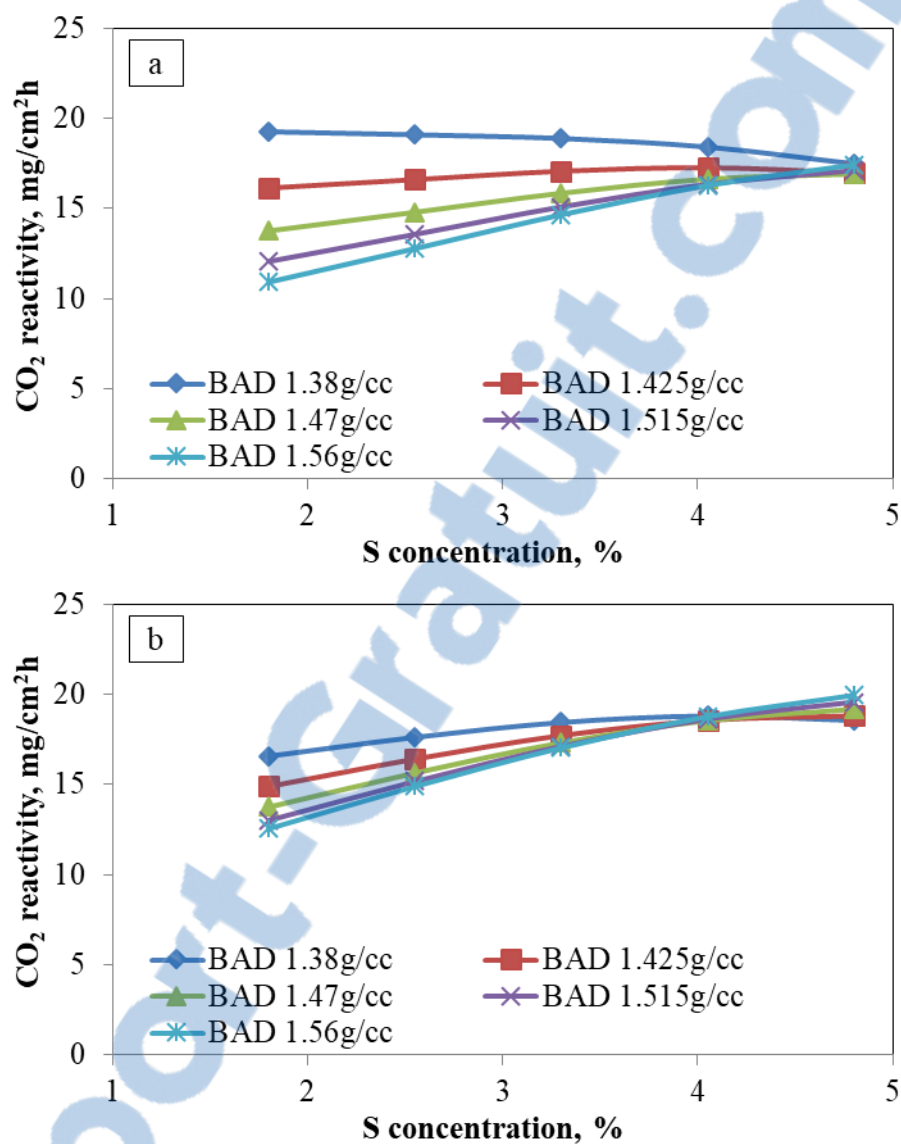


Figure A24: The effect of concentrations of sulfur on CO₂ reactivity at different BAD for (a) low and (b) high amount of iron (other impurities, i.e., V and Ni, were maintained at their typical levels)

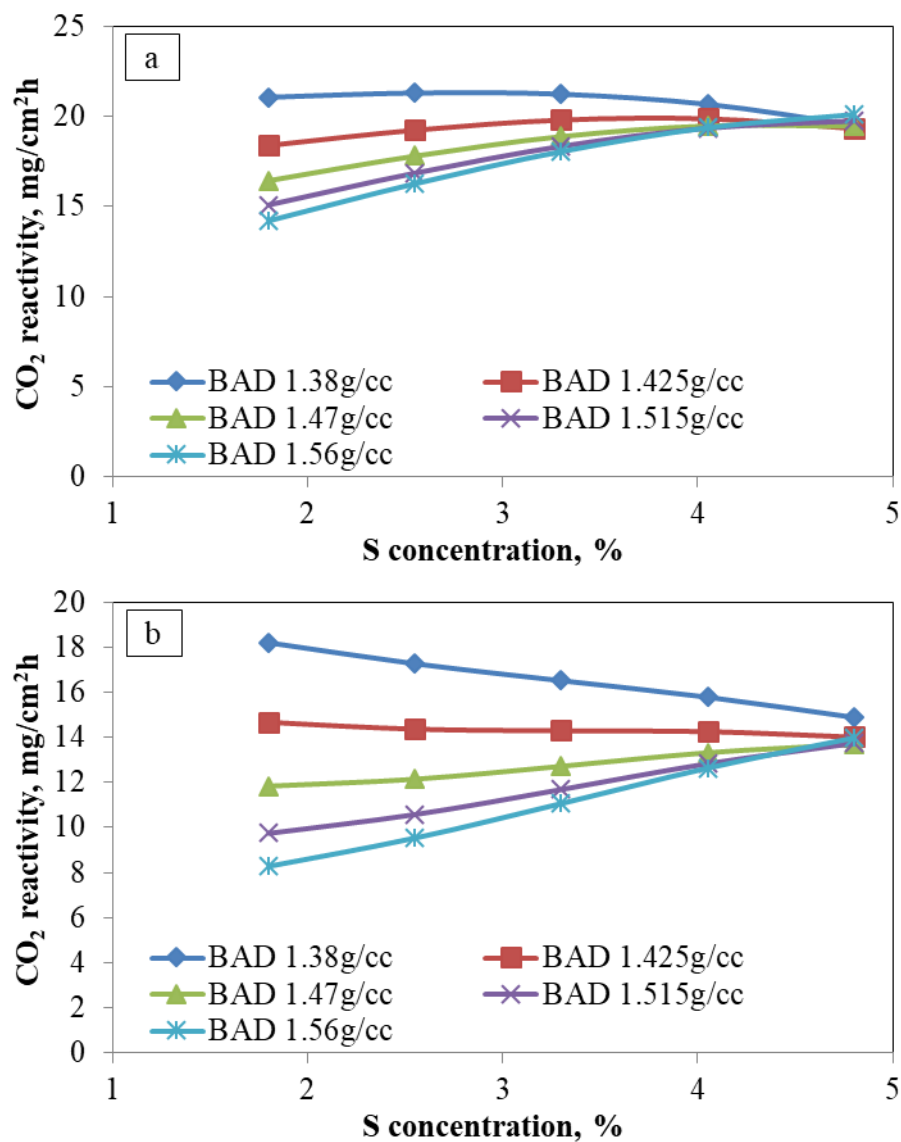


Figure A.25: The effect of concentrations of sulfur on CO₂ reactivity at different BAD for (a) low and (b) high amount of nickel (other impurities, i.e., Fe and V, were maintained at their typical levels)

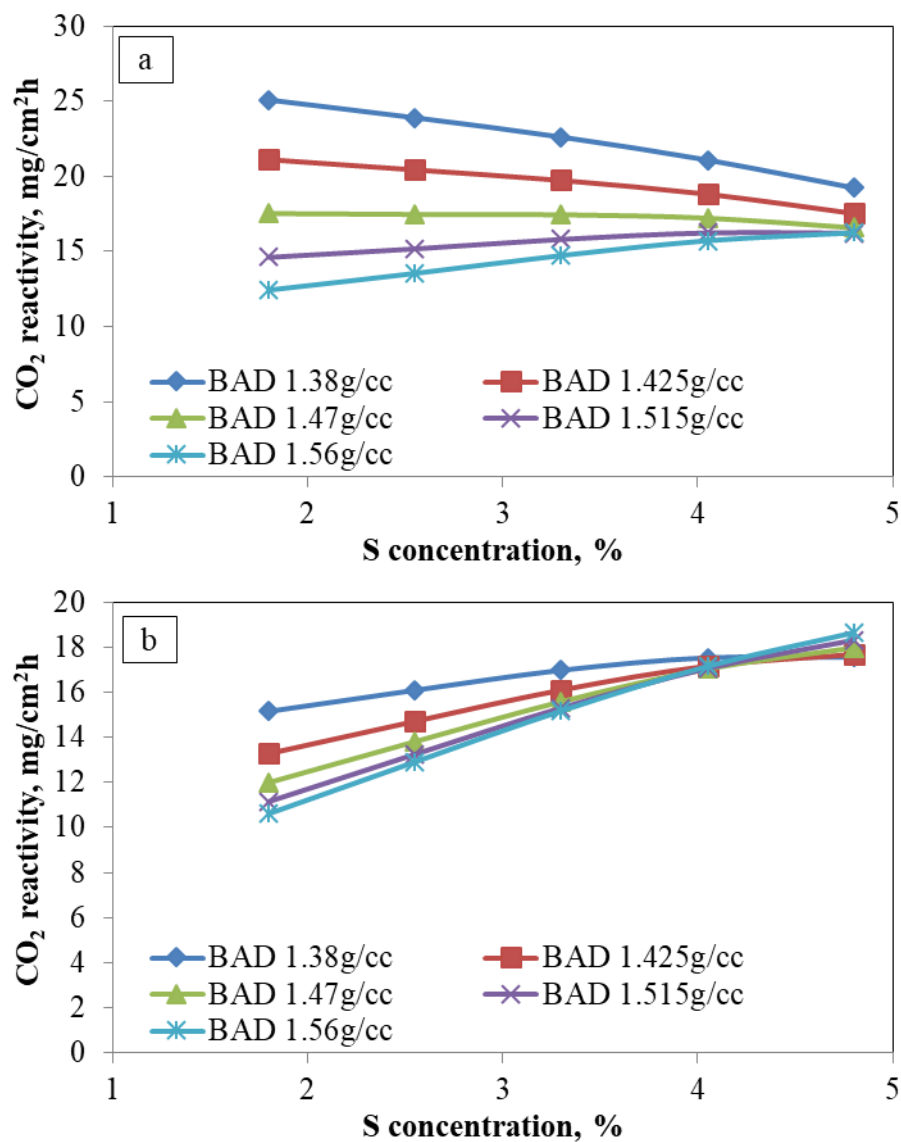


Figure A.26: The effect of concentrations of sulfur on CO₂ reactivity at different BAD for (a) low and (b) high amount of vanadium (other impurities, i.e., Fe and Ni, were maintained at their typical levels)